Stem Cells International

Neurogenesis, Neurodegeneration and Modeling Neurological Disease with Stem Cells

Lead Guest Editor: Huseyin Sumer
Guest Editors: Jun Liu and Sangho Roh

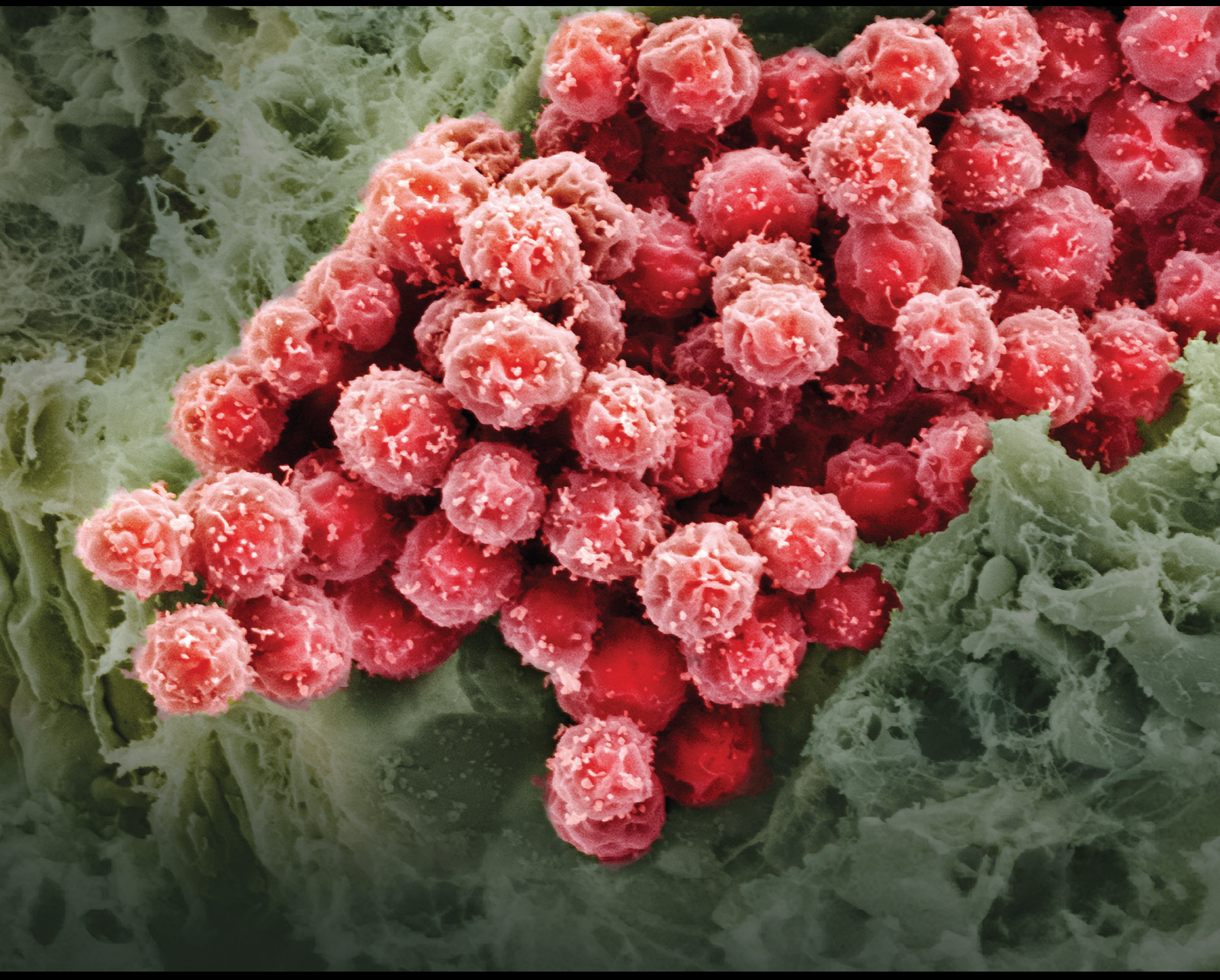

Neurogenesis, Neurodegeneration and Modeling Neurological Disease with Stem Cells

Stem Cells International

Neurogenesis, Neurodegeneration and Modeling Neurological Disease with Stem Cells

Lead Guest Editor: Huseyin Sumer
Guest Editors: Jun Liu and Sangho Roh

Contents

Hindawi
Stem Cells International
Volume 2023, Article ID 2690949, 19 pages
https://doi.org/10.1155/2023/2690949

Research Article

Bone Marrow-Derived Mesenchymal Stem Cells and γ-Secretase Inhibitor Treatments Suppress Amyloid-β25–35-Induced Cognitive Impairment in Rat Dams and Cortical Degeneration in Offspring

Asmaa Gaber,[1] **Ahlam M. Elbakry**,[1] **Rabab M. Aljarari**,[2] **Fatima A. Jaber**,[2] **Yasser A. Khadrawy**,[3] **Dina Sabry**,[4,5] **Rasha E. Abo-ELeneen**,[1] **and Osama M. Ahmed**[6]

[1]*Comparative Anatomy and Embryology Division, Department of Zoology, Faculty of Science, Beni-Suef University, P.O. Box 62521, Beni Suef, Egypt*
[2]*Department of Biology, College of Science, University of Jeddah, Jeddah 21589, Saudi Arabia*
[3]*Medical Physiology Department, Medical Branch Department, National Research Center, Giza, Egypt*
[4]*Medical Biochemistry and Molecular Biology Department, Faculty of Medicine, Badr University in Cairo, Cairo 11829, Egypt*
[5]*Medical Biochemistry and Molecular Biology Department, Faculty of Medicine, Cairo University, Cairo 11562, Egypt*
[6]*Physiology Division, Department of Zoology, Faculty of Science, Beni-Suef University, P.O. Box 62521, Beni Suef, Egypt*

Correspondence should be addressed to Asmaa Gaber; asmaa_2011@science.bsu.edu.eg

Received 27 October 2022; Revised 2 April 2023; Accepted 2 May 2023; Published 25 May 2023

Academic Editor: Huseyin Sumer

Alzheimer's disease (AD) is the most frequent cause of age-related neurodegeneration and ensuing cognitive impairment. Progressive deposition of extracellular amyloid beta (Aβ) aggregates (plaques) and intracellular hyperphosphorylated Tau protein (p-Tau) are the core pathological markers of AD but may precede clinical symptoms by many years, presenting a therapeutic window of opportunity. Females are more frequently afflicted by AD than males, necessitating evaluation of novel treatments for the female population. The current study examined the protective efficacies of intravenous bone marrow-derived mesenchymal stem cells (BM-MSCs) and oral gamma-secretase inhibitor-953 (GSI-953) during pregnancy on cognitive impairment in rat dams and neurodegeneration in offspring induced by intracerebroventricular injection of Aβ25–35 prior to pregnancy. The Aβ25–35 (AD) group exhibited significant ($P < 0.001$) impairments in the Y-maze and novel object recognition test performance prior to conception. Histological analysis of the offspring cortex revealed substantial dendritic shrinkage and activation of microglial cells, while neurochemical analysis demonstrated significant increases in the proinflammatory cytokine interleukin-1β (IL-1β) and tumor necrosis factor-α (TNF-α). In contrast, BM-MSC or GSI-953 treatment of dams following Aβ25–35 injection significantly ($P < 0.001$) reduced the number and size of activated microglial cells, markedly increased dendrite length, and reversed proinflammatory cytokine elevations in offspring. Moreover, BM-MSC or GSI-953 treatment reversed the Aβ25–35-induced amyloid precursor protein and p-Tau elevations in the offspring brain; these changes were accompanied by upregulation of the brain-derived neurotrophic factor and downregulation of glycogen synthase kinase-3β in the serum and brain. Treatment with BM-MSCs or GSI-953 also reversed Aβ25–35-induced elevations in different gene expressions in the neonatal cortex. Finally, treatment of dams with BM-MSCs or GSI-953 prevented the Aβ25–35-induced disruption of newborn brain development. Thus, BM-MSC and GSI-953 treatments have broad-spectrum effects against Aβ25–35-induced brain pathology, including the suppression of neural inflammation, restoration of developmental plasticity, and promotion of neurotrophic signaling.

1. Introduction

Alzheimer's disease (AD) is an untreatable neurodegenerative condition that accounts for 60%–80% of global dementia cases [1]. Currently, about 50 million people worldwide suffer from AD, and epidemiological analyses predict that case numbers will reach 152 million by 2050, a roughly sixfold increase since 2006 [2]. Further, the prevalence of AD is higher in females than in males. Alzheimer's pathology is characterized by progressive neuronal cell death in a wide area of the cerebral cortex, basal forebrain, and hippocampus, causing cognitive impairments, such as memory loss, impaired decision-making, and language difficulties, in addition to emotional impairments [3–6]. The pathological hallmarks of AD include the extracellular deposition of amyloid proteins in plaques, the development of intracellular neurofibrillary tangles (NFTs) containing hyperphosphorylated-(p-) Tau protein, neuroinflammation, and various changes in the synaptic structure [6–8]. Many studies have proposed that AD pathogenesis involves multiple neurodegenerative processes triggered by plaque accumulation and that all of these pathogenic mechanisms are influenced by various AD risk genes [9]. Among the most important degenerative processes is the reactive oxygen species generation by amyloid plaques, which in turn causes oxidative cell damage and triggers inflammatory cascades [10].

Neurogenesis and synaptic plasticity, two long-lasting alterations in the mother's brain, are linked to important physiological changes throughout pregnancy [11]. During normal pregnancy, amyloid beta metabolism is upregulated; consequently, the impairment in production or clearance of amyloid beta is responsible for abnormal processes of the central nervous system. Placental dysfunction and amyloid beta peptides are related, according to Lederer et al. [12]. From the prenatal to early postnatal period, epigenomic dysregulation can have a deleterious impact on health. It has been established that exposure to various settings results in illnesses, epigenetic alterations, and abnormalities in neurodevelopment [13].

It is believed that AD's pathophysiological process begins before diagnosis [14]. At the preclinical stage of AD, significant cognitive impairment may already exist [15]. In the early stages of AD, episodic memory is initially damaged by a deficit in the limbic regions of the brain, which later spreads to the cortical regions of the brain; additional cognitive symptoms arise [16]; and the dementia syndrome is seen, according to imaging-based research [17, 18]. According to the hypothesis underlying the name "preclinical AD," which was created to reflect this lengthy period of silence to support longitudinal clinical research investigations, preventive measures may be more effective in minimizing preclinical manifestation of AD dementia if applied early on [19]. Although familial AD is caused by genetic defects, the clinical manifestation of AD does not appear until middle life or later. Investigating whether beginning medication therapy while pregnant can act as a therapeutic preventative against AD pathogenesis is therefore a sensible idea [20].

Many drugs have been tested for AD treatment, but most target symptoms only, and none are able to reverse or stop disease progression. Further, only 20% of patients benefit from currently available AD drugs. Given the importance of amyloid plaque deposition and NFT formation in the early stages of AD, drug therapies that can reduce the amyloid peptide load, inhibit Tau phosphorylation, or protect vulnerable neurons against downstream pathogenic processes may prevent the associated cognitive dysfunction. Amyloid plaques are generated by the enzymatic cleavage of the transmembrane amyloid precursor protein (APP) by beta- and gamma-secretases [21]. Gamma-secretase is a multiple subunit complex that catalyzes the final step of amyloid peptide generation, so inhibition of this enzyme can prevent amyloid plaque aggregation [22, 23]. One such γ-secretase inhibitor-953 (GSI-953) is begacestat, which was found to reduce plasma amyloid peptide concentration in a phase I trial. Begacestat is 15 times more selective for the suppression of the APP cleavage as evidenced by cellular assays of Notch [24]. The same authors reported that high-dose GSI-953 substantially reduced cleaved amyloid beta 1–40 (Aβ1–40) levels in the brain, cerebrospinal fluid (CSF), and plasma, while low doses still reduced Aβ1–40 in the brain and plasma [24]. Importantly, it has been revealed that begacestat improves contextual memory impairments in Tg2576 transgenic mice [24]. Begacestat also improved contextual memory impairments in the Tg2576 transgenic mouse model of AD [24], suggesting promise as an AD treatment, although further study is required.

In addition to small-molecule drugs that inhibit AD-associated pathogenic processes, there is growing interest in stem cell therapy as a neuronal replacement and (or) protective strategy [25–27]. Indeed, stem cell therapy has shown promising results in animal models of neurodegenerative disease [28, 29]. Pluripotent stem cells (iPSCs), brain-derived neural stem cells, and bone marrow-derived mesenchymal stem cells (BM-MSCs) [30, 31] are the most widely used stem cell types in research on therapeutic applications as cells can differentiate into a wide variety of functional cells such as neural cells [32]. In comparison to conventional drug therapies, stem cell-based therapy may be more effective for AD because implanted stem cells can improve the brain microenvironment by supplying growth-promoting and growth-permissive factors for synaptogenesis and neurite repair, reduce oxidative stress by enhancing local antioxidant capacity, and trigger the sustained production of neurotrophic factors like brain-derived neurotrophic factor (BDNF) and nerve growth factor (NGF) [33].

Early AD treatment provides an opportunity to prevent or slow behavioral and synaptic dysfunction, pathogenic processes known to start long before clinical diagnosis [34]. Therefore, we evaluated the efficacies of MSCs and GSI-953 against Aβ25–35-induced cognitive dysfunction in adult females as well as against neurodegeneration in the offspring of these females.

2. Materials and Methods

2.1. Experimental Animals. Ninety Wistar rats, 60 mature females weighing 200–250 g and 30 mature males, were used in the current investigation. The animals were procured from the VACERA animal housing facility in Egypt. To

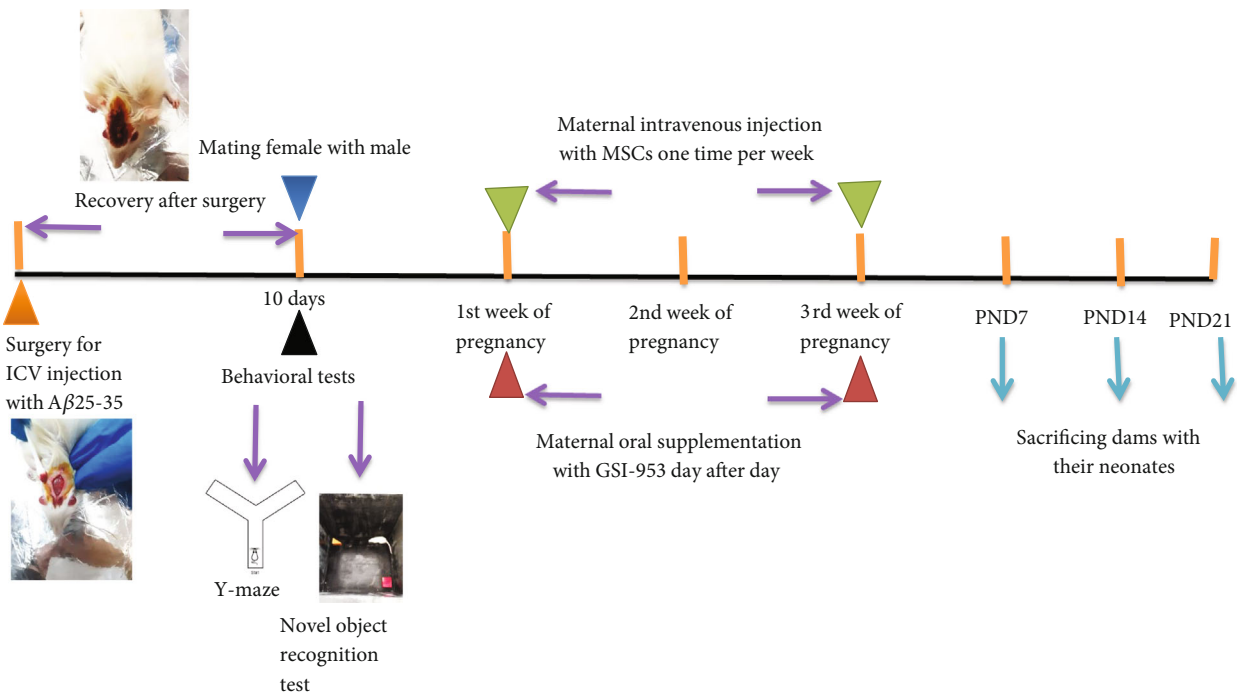

Figure 1: Design of the study: adult female albino rats were subjected to intracerebroventricular (i.c.v.) injection with Aβ25–35 and vehicle 0.9% saline before pregnancy and allowed to recover for 10 days and then subjected to behavioral testes (novel object recognition test and Y-maze test). After that, female rats were mated with males, and pregnant female rats subjected to Aβ25–35 injection were classified into the AD group, AD group that received intravenous injection of MSCs (one million/rat/week), and AD group orally treated with GSI-953 (2.5 mg/kg·b·wt). The neonates were sacrificed at different postnatal days (7, 14, and 21), and the brain cortex was subjected to histological, immunohistochemistry, qRT-PCR, and western blotting studies.

prevent infections, animals were kept under surveillance at the Department of Zoology animal house in well-ventilated stainless-steel cages under a regular daily dark/light cycle, controlled humidity (50%), and controlled air temperature (23°C). Animals were fed a conventional rat pellet meal in addition to some vegetables as a source of vitamins and had unlimited access to tap water. The animal care protocol adhered to the Beni-Suef College Animal Care and Use Committee's general recommendations (approval number 019-75).

2.2. Surgical Procedure. Surgeries were conducted as described previously [35]. Free Aβ25–35 was dissolved in 0.9% saline to 1 mg/mL and incubated for 4 days at 37°C. Rats received intraperitoneal injections of 7 mg/kg xylazine and 70 mg/kg ketamine for deep anesthesia, after which head hair was removed using surgical shears. The shaved area was then sanitized with betadine and covered with a biodegradable surgical towel. An incision was made along the median longitudinal calvaria using surgical bistouries and scissors, and the subcutaneous tissue and fascia were gently separated. Sterile dry cotton was used to stop the bleeding, and the bregma was marked with a pen. A flexible bone drill was used to make a 1 mm diameter hole at 0.8 mm posterior (P) to the bregma and 2.0 mm lateral (L) to the midline (above the lateral ventricle). The bleeding was stopped and the skull surface cleaned repeatedly with sterile cotton. A needle linked to a Hamilton microsyringe was gently inserted through the bore hole to a depth of 4.6 mm and 10 μL of Aβ25–35 slowly injected. The needle was left in place for 2 min to allow full emptying of the syringe contents into the lateral ventricle. Other rats were injected with equal-volume 0.9% saline as a control. Finally, the wound was sterilized with betadine, and the injured skin was closed using a simple suture method. One week after surgery, the rats were tested in the Y-maze and novel object recognition tests to evaluate working memory and reference memory, respectively. At the proestrus stage, the rats were mated with a male for one or two days. The first day of pregnancy was identified by checking a vaginal smear for sperm.

2.3. Animal Grouping (Figure 1). Five groups of pregnant Wistar rats were established: G1 ($n = 10$) receiving intracerebroventricular (i.c.v.) injection of 10 μL saline (0.9%) before pregnancy, G2 receiving i.c.v. Aβ25–35 before pregnancy ($n = 30$), G3 receiving intravenous (i.v.) Dulbecco's Modified Eagle Medium (DMEM) (4.5%), G4 group receiving i.v. injection BM-MSCs one time per week for three weeks during the pregnancy period starting ten days following i.c.v. injection of 10 μL Aβ25–35, and G5 receiving 2.5 mg/kg·b·wt day after day oral begacestat during the pregnancy period starting ten days after 10 μL i.c.v. Aβ25–35. The brains of the offspring were removed on postnatal days 7, 14, and 21 for histological, immunohistochemical, and neurochemical analyses.

2.4. Isolation of Bone Marrow Mesenchymal Stem Cells from Rats (Figure 2). Mesenchymal stem cells were allogeneically isolated from the rat bone marrow as described in a previous

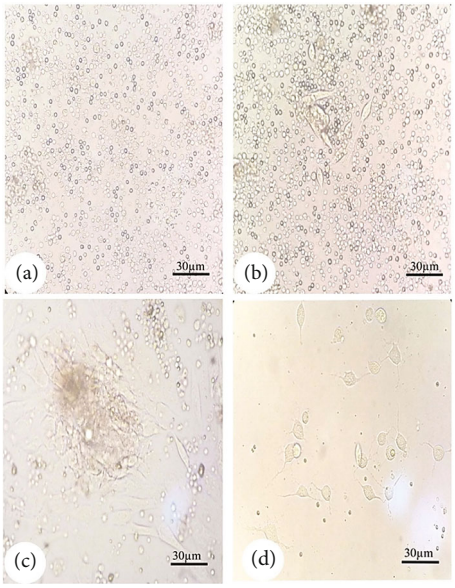

Figure 2: Morphology of isolated undifferentiated mesenchymal stem cells from bone marrow, under inverted microscopy. (a) MSCs in the culture flask at first day of isolation showed rounded cells, (b) MSCs begin to convert into a flat fibroblast-like morphology at 7 days of isolation, and (c, d) MSCs before injection at day 10 of isolation.

study [36]. Briefly, the bone marrow was flushed out of the femur using 4.5% DMEM (Life Science Group Ltd., UK) and the suspension centrifuged at 3000 rpm for 5 min. Isolated BM cells were seeded in culture flasks with complete medium composed of 4.5% DMEM, 15% fetal bovine serum (Lonza Verviers Sprl, Belgium), and 1% penicillin-streptomycin (Life Science Group Ltd., UK) and grown in an atmosphere of 5% CO_2 with 50% humidity at 37°C. The medium was exchanged after 3–4 days. When the cells reached 80%–90% confluence (7 to 10 days after seeding), they were washed twice with a phosphate-buffered saline (PBS), harvested via incubation in 0.25% trypsin/1 mM EDTA (Greiner Bio-One, Germany) for five minutes at 37°C, centrifuged, and resuspended in DMEM. Before injection, the viability was determined by combining 10 μL of the cell suspension with 10 μL of 0.4% trypan blue stain, and then, stained (dead/dying) cells were counted using a hemocytometer. Cells that demonstrated 95% viability were used for injection. Animals were injected with an estimated one million cells per week for 3 weeks. No side effect was detected during the study in response to MSC injection.

2.5. Behavioral Tests

2.5.1. Y-Maze Test (as Spatial Memory Task). The Y-maze task is used to gauge spatial working memory. The wooden Y-maze consists of three equally spaced arms (projecting 120° relative to adjacent arms), each 50 cm long, 5 cm wide at the hub, and 10 cm wide at the end, and is bounded by 20 cm high walls. Individual rats are placed on one arm and allowed to freely explore both that arm and an adjacent arm for 8 min, while the third arm is blocked by a partition. The rat is then allowed to freely explore all arms for 30 minutes. The number of entries, amount of time spent in the previously blocked (novel) arm, and amount of time spent in the two previously explored (familiar) arms were recorded. The proportion (%) of time spent in the novel arm relative to the familiar arms was calculated as an index of working memory [37].

2.5.2. Novel Object Recognition Test. The novel object recognition test is a three-day protocol for evaluating long-term memory [38]. On the first day, all animals were acclimated to a 30 × 30 × 30 cm empty wooden cage for 10 min [38, 39]. On day two, animals were placed individually in the same cage now containing two identical wooden objects placed at opposite corners 2 cm from the walls and allowed to explore freely for 10 min [40].

On the third day, one of the objects was exchanged with another of different form, size, and color, and the rat was allowed five minutes to explore. The amount of time spent examining the novel object as a fraction of the total time spent exploring both objects was calculated as the recognition index (RI) [38]. A higher RI is considered a sign of better recognition memory [41].

2.6. Histological Analysis of Newborn Cortex. The whole cortex was isolated from 3 newborns per treatment group (G1–G5), fixed in 4% paraformaldehyde for 48 h (pH 7.4) at 4°C, dehydrated in gradient ethanol, and embedded in paraffin. Sections (5 μm) were prepared and stained with hematoxylin and eosin (H&E) at room temperature for 12 min and photographed under light microscopy for evaluation of histopathological changes.

2.7. Immunohistochemistry. Newborns (four per treatment group) were anesthetized and perfused intracardially with 4% paraformaldehyde in 0.9% saline. Brain sections were cut at 5 μm, blocked with 1% bovine serum albumin (BSA) in PBS containing 0.3% Triton X-100 for 1 h, and incubated with an antibody against the microglial marker-ionized calcium-binding adapter molecule 1 (Iba-1) (1 : 1000, Abcam, Cambridge, UK) overnight at 4°C. Sections were then incubated with a corresponding secondary antibody (1 : 1000) for 1 h, and immunostaining was visualized using an Olympus microscope equipped with a 10x and 100x objective lens. Images were analyzed using ImageJ (NIH, Bethesda. MD, USA).

2.8. ELISA Assay. Alterations in inflammatory cytokines (IL-1β and TNFα), GSK-3β, and BDNF in the newborn serum were detected using ELISA kits of IL-1β (SEA563Ra) (Cloud-Clone Corp.), TNF-α (BioLegend), GSK-3β (Abbexa LLC, Houston, TX, USA), and BDNF (SEA011Ra) (Cloud-Clone Corp.). All the ELISA kits were used in accordance with the manufacturer's instructions ($n = 6$ per group); the quantity of these factors was expressed as pg/mL.

2.9. RT-PCR. Total RNA was isolated from the cortex lysate using the Direct-zol RNA Miniprep Plus kit (cat.# R2072, Zymo Research, Irvine, CA, USA) according to the manufacturer's instructions and reverse transcribed using the Superscript IV One-Step RT-PCR kit (cat.# 12594100, Thermo Fisher Scientific, Waltham, MA, USA) in accordance with

Table 1: Primer sequences of tested genes.

	Forward sequence	Reverse sequence
Caspase-3	TGGTTCATCCAGTCGCTTTGT	CAAATTCTGTTGCCACCTTTCG
TNFR	GGGATTCAGCTCCTGTCAAA	ATGAACTCCTTCCAGCGTGT
TGF-β	GTCACTGGAGTTGTACGGCA	GGGCTGATCCCGTTGATTTC
BDNF	CCGGTATCCAAAGGCCAACT	CTGCAGCCTTCCTTGGTGTA
NF-κB	TTC CCT GAA GTG GAG CTA GGA	CAT GTC GAG GAA GAC ACT GGA
β-Actin	AGG CCC CTC TGA ACC CTA AG	GGA GCG CGT AAC CCT CAT AG

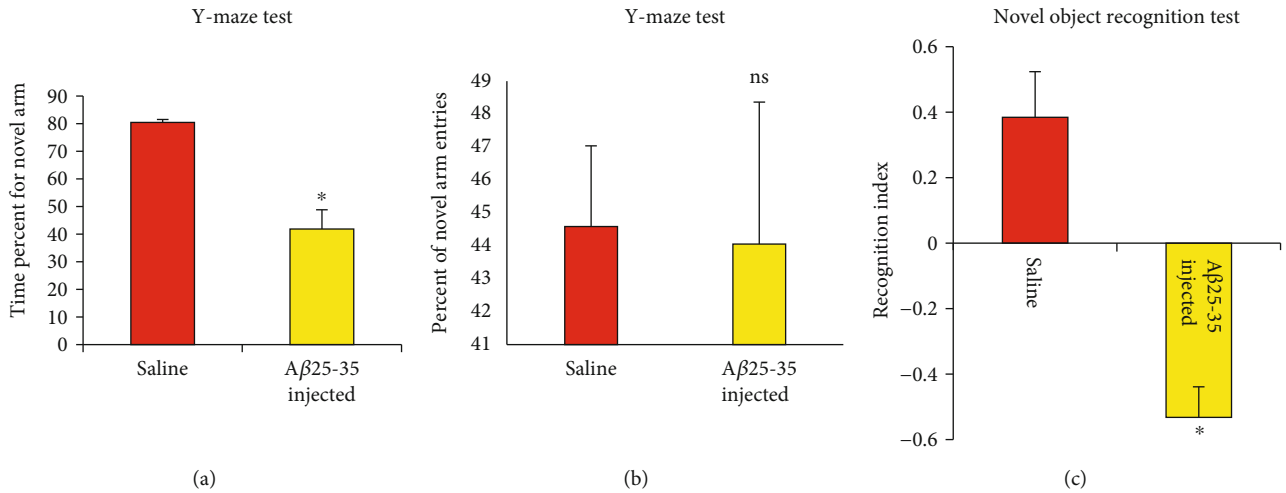

Figure 3: Effect of Aβ25–35 injection into adult female rats before pregnancy on behavioral test. (a, b) Y-maze test; (c) novel object recognition test. Data are presented as mean ± SEM. $^*P < 0.001$. ns: insignificant for the percent of novel arm entries comparing with the saline-injected group ($P > 0.05$).

the manufacturer's instructions. The product cDNA was amplified using 2x Platinum™ SuperFi™ RT-PCR Master Mix and primer pairs for the target genes (BDNF, NF-$\kappa\beta$, TNFR, TGF-β, and caspase-3) listed in Table 1. Quantitative real-time PCR (qRT-PCR) was conducted using SYBER green (StepOne, Applied Biosystem, Foster City, USA), and expression levels of target genes were calculated as the cycle threshold (Ct) relative to that of the β-actin gene using the delta-delta Ct (Ct) method.

2.10. Western Blotting. To assess brain concentrations of p-Tau and APP, the total protein was extracted from cerebral cortex samples using a total protein extraction kit (Bio-Rad cat.# 163-2086) in accordance with the manufacturer's instructions and measured via a colorimetric assay (Bio-Rad, Hercules, CA, USA, cat.# 163-2086). Equal amounts of protein were electrophoretically separated via sodium dodecyl sulfate polyacrylamide gel electrophoresis and transferred to polyvinylidene fluoride (PVDF) membranes. Membranes were incubated in a stopping buffer (tris-buffered saline with Tween 20 (TBST)) containing 3% BSA for 1 hour at room temperature and then in primary antibodies against phospho-Tau (Thr231), APP, and β-actin (as the gel-loading control) overnight at room temperature. The blot was then washed 3–5 times in TBST and immunoreactive bands visualized using chemiluminescent substrate (Clarity™ Western ECL substrate, Bio-Rad cat.# 170-5060). Target band signals were then identified using a CCD camera-based imager (ChemiDoc MP imager) and quantified relative to β-actin signals using the accompanying image analysis software.

2.11. Statistical Analysis. All statistical analyses were conducted using SPSS version 17.0 (SPSS Inc., 1989–2007; Chicago, IL, USA). Data are presented as mean ± standard error of the mean after one-way ANOVA analysis. The effects of age, therapy, and their interactions on most outcomes were examined via two-way ANOVA followed by Tukey's multiple comparison tests. Behavioral test results were evaluated via one-sample T-test. The significance was considered at three levels, $P < 0.05$, $P < 0.01$, and $P < 0.001$, while $P > 0.05$ was nonsignificant.

3. Results

3.1. Intracerebroventricular Aβ25–35 Injection Impaired Working Memory and Object Recognition Memory in Adult Female Rats. The Y-maze test (Figures 3(a) and 3(b)) revealed significant working memory impairment ($P < 0.001$) among rats injected i.c.v. with Aβ25–35 (group G2) as evidenced by the reduced time spent in the novel arm compared to rats receiving i.c.v. saline (group G1). In contrast, there were no group differences in the number of novel arm entries, suggesting no significant effects of treatment on motor activity or exploratory drive ($P > 0.05$). In

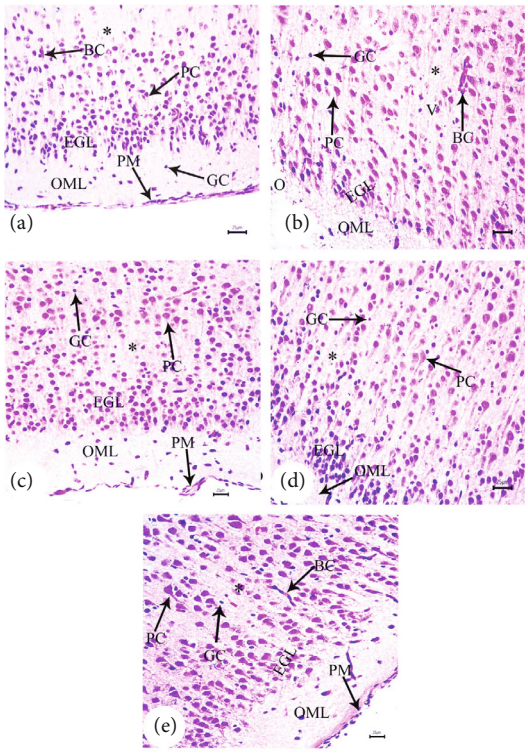

Figure 4: Photomicrograph of hematoxylin-and-eosin- (H&E-) stained sections of the neonatal cerebral cortex at PND7 of the following groups: (a) saline-injected group that illustrates that the normal organization of cells of the prefrontal cortex displays the external layers of the cortex that have the outer molecular layer (OML) underneath the regular attached pia mater (PM); both the external granular (EGL) and pyramidal layers exhibit small neuronal cell bodies having rounded open face nuclei (PC) that are surrounded with a little cytoplasm, normal capillaries (BC), and normal glial cells (GC) that are seen within the acidophilic neuropil (*). (b) Aβ25–35-injected group demonstrates disrupted and fragmented attached pia mater (PM) and disorganization of cells of the prefrontal cortex with decreased external granular layer thickness (EGL), degenerated neuronal cells (dN) with pyknotic nuclei and elongated filament, marked dilated congested inflamed capillaries (BC), neuropil (*) with marked edema (O), and degenerated glial cells (GC). (c) DMEM group displayed normal cerebral cortex architecture. (d, e) AD treated with MSCs and AD treated with GSI-953 showed normally attached pia mater and normally arranged cells of the prefrontal cortex having normal cellular thickness layer, completely regenerated neuronal cells (PC), normal capillaries (BC), absence of edema, and completely regenerated glial cells (GC) (scale bar = 25 μm).

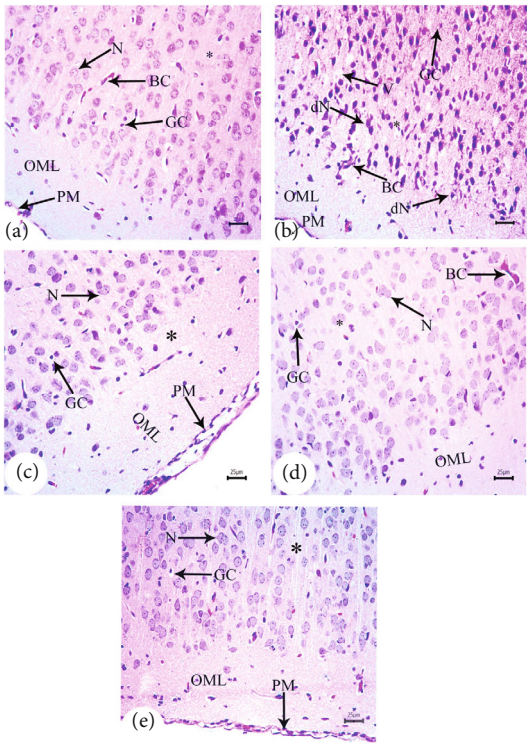

Figure 5: Photomicrograph of hematoxylin-and-eosin (H&E-) stained sections of the neonatal cerebral cortex at PND14 of the following groups: (a) saline-injected group that illustrates that the normal organization of cells of the prefrontal cortex displays the external layers of the cortex that have the outer molecular layer (OML) underneath the regular attached pia mater (PM); both the external granular (EGL) and pyramidal layers exhibit small neuronal cell bodies having rounded open face nuclei (N) that are surrounded with a little cytoplasm, normal capillaries (BC), and normal glial cells (GC) that are seen within the acidophilic neuropil (*). (b) Aβ25–35-injected group demonstrates disrupted and fragmented attached pia mater (PM) and disorganization of cells of the prefrontal cortex with decreased external granular layer thickness (EGL), degenerated neuronal cells (dN) with pyknotic nuclei, and elongated filament and pericellular haloes (PV); some of these cells had pointed ends. There were many glial cell nuclei in a vacuolated neuropil and dilated, crowded blood capillaries. Rarely visible were typical pyramidal cell bodies, marked dilated congested inflamed capillaries (BC), neuropil (*) with marked vacuoles (V), and degenerated glial cells (GC). (c) DMEM group displayed a normal histological structure of cerebral cortex. (d, e) AD treated with MSCs and AD treated with GSI-953 showed normally attached pia mater and normally arranged cells of the prefrontal cortex having a normal cellular thickness layer, completely regenerated neuronal cells (N), normal capillaries (BC), absence of edema, and completely regenerated glial cells (GC) (scale bar = 25 μm).

addition, G2 rats demonstrated a significant ($P < 0.001$) reference memory impairment compared to G1 rats as evidenced by the reduced novel object exploration during the test phase of the novel object recognition task (Figure 3(c)).

3.2. Intracerebroventricular Aβ25–35 Injection in Dam Disrupted Cortical Development in Offspring, an Effect Reversed by BM-MSC and GSI-953 Treatments. H&E-stained parasagittal slices of the prefrontal cortex (PFC) from the PND7 offspring of saline-injected (G1) dams (Figure 4(a)) exhibited an intact pia mater layer, regular arrangements of neurons in each cortical layer, and normal cellular structures. The pia mater layer was acidophilic and contained abundant blood capillaries as well as neuronal and glial cell processes. The neuronal cell bodies in inner cortical layers exhibited large nucleoli and rounded open face nuclei encircled by the basophilic cytoplasm. Inner-layer neurons were interspersed with neuroglial cell nuclei. Pyramidal cells in the cerebral cortex changed in size and shape from PND7 to PND21, consistent with the normal cortical development (Figures 5(a) and 6(a)).

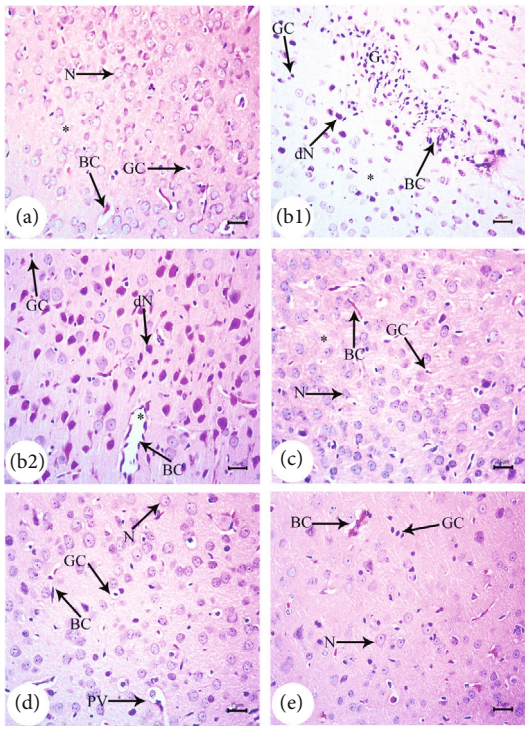

Figure 6: Photomicrograph of hematoxylin-and-eosin- (H&E-) stained sections of the neonatal cerebral cortex at PND21 of the following groups: (a) saline-injected group that illustrates that the normal pyramidal layers exhibit small neuronal cell bodies that have rounded open face nuclei (N) that are surrounded with a little cytoplasm, normal capillaries (BC), and normal glial cells (GC) that are seen within the acidophilic neuropil (*). (b1, b2) Aβ25–35-injected group demonstrates degenerated neuronal cells (dN) with pyknotic nuclei and elongated filament and pericellular haloes (PV); some of these cells had pointed ends. There were many glial cell nuclei with marked gliosis (G) in a vacuolated neuropil and dilated, crowded blood capillaries. Rarely visible were typical pyramidal cell bodies, marked dilated congested inflamed capillaries (BC), neuropil (*) with marked vacuoles (V), and degenerated glial cells (GC). (c) DMEM group displayed normal cerebral cortex architecture. (d, e) AD treated with MSCs and AD treated with GSI-953 showed completely regenerated neuronal cells (N), normal capillaries (BC), absence of edema, and completely regenerated glial cells (GC) (scale bar = 25 μm).

In contrast, the arrangement of cells in cortical slices from G2 offspring at PND7 (Figure 4(b)) was disturbed, and the external granular layer thickness was significantly ($P < 0.001$) reduced throughout all tested periods (Figure 7(b)). Neuronal cells (dN) of the granular layer exhibited pyknotic nuclei and elongated filaments interspersed with dilated and congested blood capillaries (BC), regions of marked edema (O), and degraded glial cells (GC). Similarly, parasagittal slices of the PND14 and PND21 prefrontal cortex showed evident disturbances in the cortical layer arrangement with dilated BC (Figures 5(b), 6(b1), and 6(b2)). The PFC of offspring from G2 dams also exhibited darkly stained and shrunken neuronal cell bodies with intensely stained pyknotic nuclei (dN) and pericellular vacuoles (PV) (Figures 5(b), 6(b1), and 6(b2)). Some of these cells had pointed ends. The neuropil was also dilated and vacuolated with many glial cell nuclei interspersed among closely spaced, dilated capillaries (Figures 6(b1) and 6(b2)). Moreover, few typical pyramidal cell bodies were visible. From PND7 to PND21, the cerebral cortex exhibited a significant ($P < 0.001$) rise in degenerating neurons, and pronounced gliosis was observed at PND21 (Figures 6(b1) and 7(a)). This Aβ-induced degeneration was markedly reversed via BM-MSC and GSI-963 treatments as shown in Figures 4(d), 4(e), 5(d), 5(e), 6(d), and 6(e), as slices from the G4 and G5 offspring exhibited a fully intact pia mater layer and normal cellular organization within cortical layers as well as regenerated neuronal cells (N), mildly dilated and inflamed congested capillaries (BC), mild edema (O), and regenerated glial cells at PND7–PND21. The offspring's cortexes from the DMEM group showed a normal histological structure relative to those from the saline-injected group (Figures 4(c), 5(c), and 6(c)).

3.3. BM-MSC and GSI-953 Treatments Restored near Normal Microglial Cell Counts, Soma Size, and Processes Length in the Cortex of Offspring from Aβ25–35-Injected Dams. Amyloid-β deposition causes excessive activation of microglial cells and significantly accelerates AD development. Therefore, we quantified activated microglial cell numbers in the neonatal cortex via Iba-1 immunostaining (Figures 8, 9, and 10). In the Aβ25–35-injected group (G2), the number of Iba-1-positive cells was significantly enhanced, microglial soma size significantly greater, and processes length significantly reduced (all $P < 0.001$) from PND7 to PND21 compared to age-matched neonates of saline-injected dams (G1) (Figures 11(a)–11(c)). Consistent with qualitative histological analyses, BM-MSC and GSI-953 treatments significantly ($P < 0.001$) restored microglial number and soma size as well as processes length at PND7, PND14, and PND21. In addition to these main effects, two-way ANOVA showed a significant ($P < 0.001$) interaction between the treatment group and neonatal age, suggesting restoration of the normal cortical development.

Also, there was a significant main effect of the treatment group ($F_{4,75} = 652.437$, $P < 0.001$) and neonatal age ($F_{2,75} = 4.758$, $P < 0.05$) on serum TNF-α as well as a significant treatment group × age interaction ($F_{8,75} = 78.646$, $P < 0.001$).

3.4. BM-MSC and GSI-953 Treatments Restored Normal Serum Proinflammatory, Prodegenerative, and Neuroprotective Factor Concentrations in Offspring of Aβ25–35-Injected Dams

3.4.1. Effects on Serum Neuroinflammatory Cytokine Concentrations. To evaluate the efficacies of BM-MSCs and GSI-953 against Aβ25–35-induced neuroinflammation, we measure serum IL-1β and TNF-α in G2 newborns at different PNDs. Both IL-1β and TNF-α concentrations were significantly ($P < 0.001$) elevated in the G2 group relative to the saline-injected group (G1) at all PNDs examined (Figures 12(a) and 12(b)), while BM-MSC and GSI-953 treatment of dams significantly ($P < 0.001$) diminished both serum IL-1β and TNF-α levels at all tested PNDs.

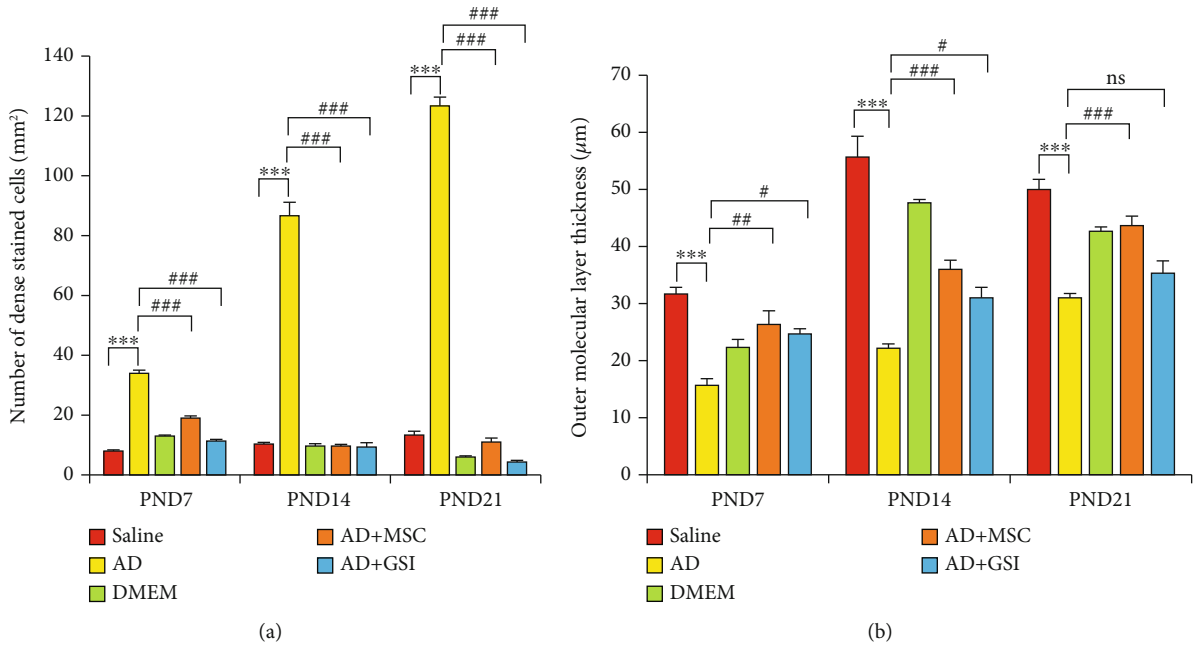

Figure 7: Effect of treatment with MSCs and GSI-953 on (a) number of degenerated neural cells/mm, (b) outer molecular layer thickness (μm) in the newborn cortex of Aβ25–35-induced Alzheimer's disease dams. Data were analyzed via two-way ANOVA followed by Tukey's multiple comparison test. Data are expressed as mean ± SEM. $^{*}P < 0.05$, $^{**}P < 0.01$, and $^{***}P < 0.001$ vs. the saline-injected group. $^{\#}P < 0.05$, $^{\#\#}P < 0.01$, and $^{\#\#\#}P < 0.001$ vs. the AD group. $^{ns}P > 0.05$ no significant.

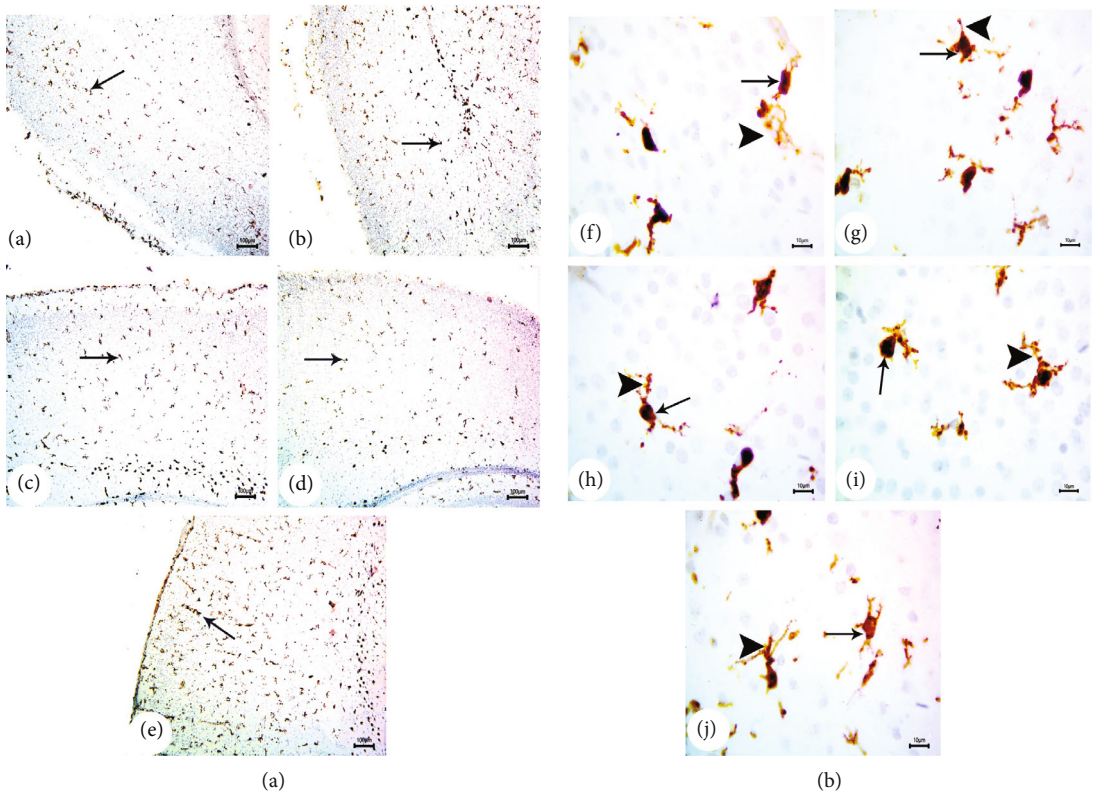

Figure 8: Photomicrographs (a) of immunohistochemical study for neonatal cortex using Iba-1 to illustrate the microglial cell reactivity at PND7: (a) saline-injected group, (b) Aβ25–35 group, (c) DMEM group, (d) AD+MSC group, and (e) AD+GSI. Scale bar 100 μm (10x). Photomicrographs (b) of immunohistochemical study for the neonatal cortex using Iba-1 to illustrate the microglial cell reactivity at PND7: (f) saline-injected group, (g) Aβ25–35 group, (h) DMEM group, (i) AD+MSC group, and (j) AD+GSI. Scale bar 10 μm (100x). Arrows refer to the cell soma size; arrowheads refer to the length, thickness, and number of dendrites.

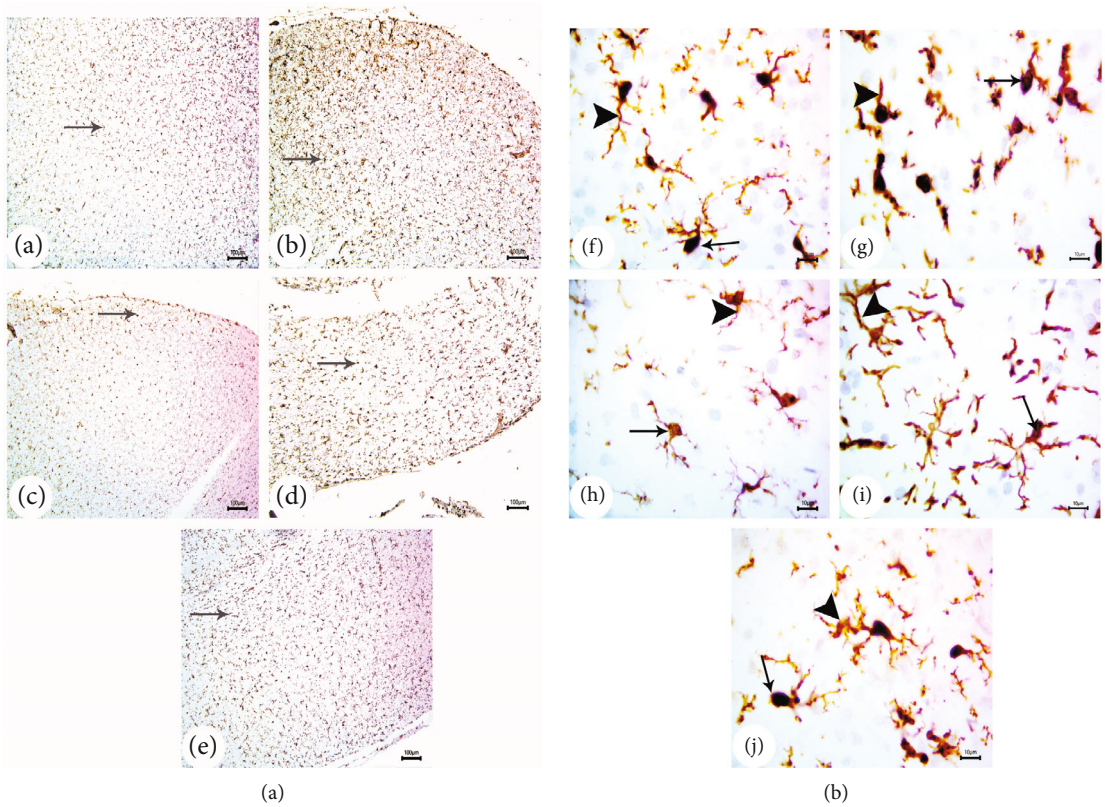

Figure 9: Photomicrographs (a) of the immunohistochemistry study for the neonatal cortex using Iba-1 to illustrate the microglial cell reactivity at PND14: (a) saline-injected group, (b) Aβ25–35 group, (c) DMEM group, (d) AD+MSC group, and (e) AD+GSI. Scale bar 100 μm (10x). Photomicrographs (b) of the immunohistochemistry study for the neonatal cortex using Iba-1 to illustrate the microglial cell reactivity at PND14: (f) saline-injected group, (g) Aβ25–35 group, (h) DMEM group, (i) AD+MSC group, and (j) AD+GSI. Scale bar 10 μm (100x). Arrows refer to the cell soma size; arrowheads refer to the length, thickness, and number of dendrites.

Specifically, the concentrations of IL-1β and TNF-α were significantly elevated in G2 offspring ($P < 0.001$) from PND7 to PND21. Two-way ANOVA revealed a significant main effect of the treatment on serum IL-1β among groups ($F_{4,75} = 624.956$, $P < 0.001$) and PNDs ($F_{2,75} = 39.079$, $P < 0.001$) as well as a significant group × age interaction ($F_{8,75} = 86.077$, $P < 0.001$).

3.4.2. Effects on Serum GSK-3β and BDNF Concentrations. To assess the neuroprotective efficacies of MSCs and GSI-953 against i.c.v. Aβ25–35-induced neurodegeneration and Tau hyperphosphorylation, we measured the serum GSK-3β level and BDNF concentration in newborns (Figures 13(a) and 13(b)). Serum GSK-3β was significantly elevated while the BDNF concentration was significantly reduced in the serum of G2 newborns compared to G1 newborns at all tested PNDs (all $P < 0.001$), while both BM-MSC and GSI treatments significantly reversed these changes at all postnatal ages (all $P < 0.001$ vs. G2). Further, the serum GSK-3β level was significantly greater and the BDNF concentration significantly lower (both $P < 0.001$) at PND21 compared to younger ages, indicating a progressive degenerative process, while the two-way ANOVA revealed a significant main effect of the treatment group on serum GSK-3β ($F_{4,75} = 699.489$, $P < 0.001$), a significant main effect of the postnatal age on serum GSK-3β ($F_{2,75} = 3.429$, $P < 0.05$), and a significant group × time interaction ($F_{8,75} = 36.289$, $P < 0.001$). Similarly, there was a significant main effect of the treatment group on serum BDNF ($F_{4,75} = 1594.494$, $P < 0.001$), a significant main effect of the postnatal age on serum BDNF ($F_{2,75} = 212.523$, $P < 0.001$), and a significant group × time interaction ($F_{8,75} = 89.763$, $P < 0.001$).

3.5. BM-MSC and GSI-953 Treatments Restore Normal Expression Levels of Neuroprotective and Proapoptotic Genes in the Cortex of Offspring from Aβ25–35-Injected Dams

3.5.1. Effects on BDNF, Caspase-3, TGF-β, NF-κB, and TNFR Gene Expression in the Neonatal Cortex. Expression levels of BDNF, caspase-3, TGF-β, NF-κB, and TNFR genes were measured in the cerebral cortex of rat offspring via qRT-PCR (Figures 14(a)–14(e)). The expression level of BDNF mRNA was significantly ($P < 0.001$) reduced in G2 offspring at all tested ages compared to G1 offspring, consistent with serum protein measurements, while BM-MSC and GSI-953 treatments significantly reversed this effect ($P < 0.001$). Further, the two-way ANOVA revealed a significant ($P < 0.001$) main effect of the treatment group, a significant main effect of the neonatal age, and a significant treatment group × age interaction. Further, mRNA expression levels of caspase-3,

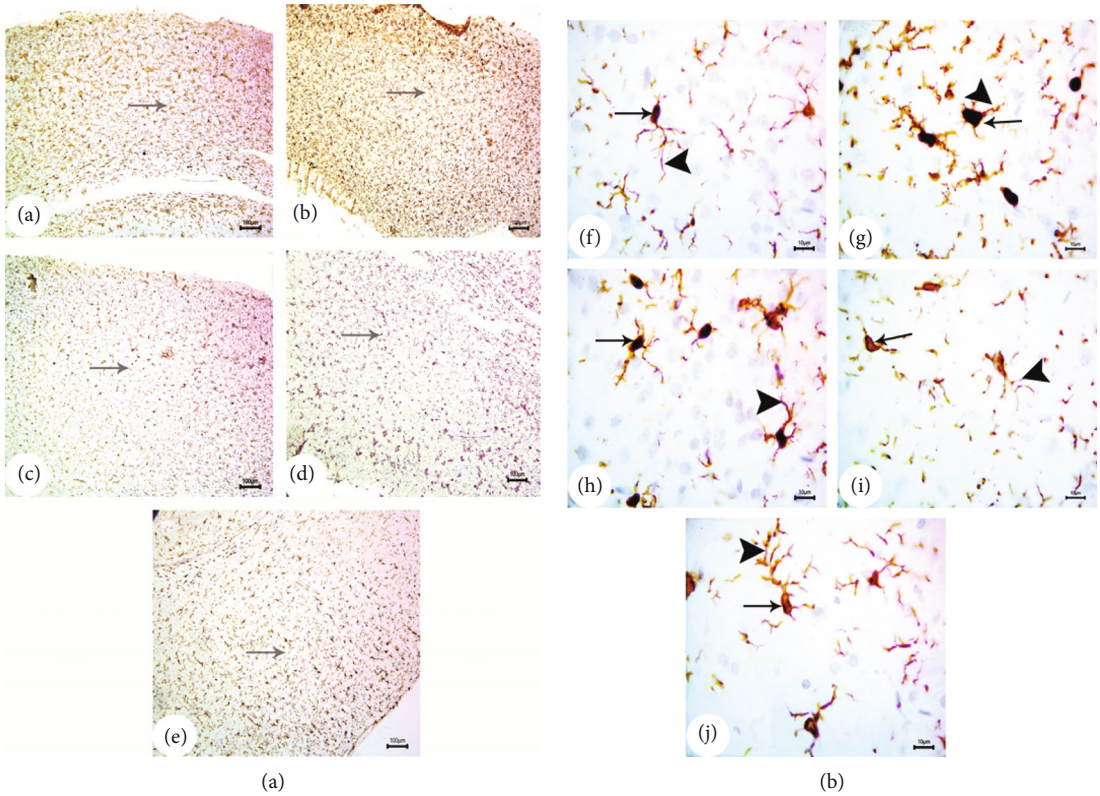

Figure 10: Photomicrographs (a) of the immunohistochemistry study for the neonatal cortex using Iba-1 to illustrate the microglial cell reactivity at PND21: (a) saline-injected group, (b) Aβ25–35 group, (c) DMEM group, (d) AD+MSC group, and (e) AD+GSI. Scale bar 100 μm (10x). Photomicrographs (b) of the immunohistochemistry study for the neonatal cortex using Iba-1 to illustrate the microglial cell reactivity at PND21: (f) saline-injected group, (g) Aβ25–35 group, (h) DMEM group, (i) AD+MSC group, and (j) AD+GSI. Scale bar 10 μm (100x). Arrows refer to the cell soma size; arrowheads refer to the length, thickness, and number of dendrites.

TGF-β, NF-κB, and TNFR were significantly ($P < 0.001$) elevated in the G2 neonatal cortex compared to the G1 neonatal cortex.

Offspring of Aβ25–35-injected dams that received BM-MSC or GSI-953 treatment showed significant ($P < 0.001$) downregulation of caspase-3, TGF-β, NF-κB, and TNFR genes relative to neonates of Aβ25–35-injected dams at all postnatal ages. Expression levels of caspase-3 ($P < 0.001$), TGF-β ($P < 0.01$), NF-κB ($P < 0.01$), and TNFR ($P < 0.05$) increased with the neonatal age, and there was a significant ($P < 0.001$) main effect of the group at all tested ages according to the two-way ANOVA.

3.5.2. Effects on p-Tau and APP Protein Concentration in the Neonatal Cortex. Phosphorylated- (p-) Tau is a core pathological hallmark of AD and contributes to disease progression. We detected a significant elevation in the cortical p-Tau protein among the newborns of G2 dams compared to the offspring of G1 dams, while BM-MSC and GSI-953 treatments significantly ($P < 0.001$) reduced p-Tau in the cerebral cortex compared to the offspring of G2 dams at all ages examined.

The two-way ANOVA showed a significant main effect of the treatment group ($P < 0.001$) and group × age interaction ($P < 0.001$). Similarly, the APP protein concentration was significantly ($P < 0.001$) elevated in the cortex of the G2 offspring compared to the G1 offspring, while MSC and GSI-953 treatments significantly reversed ($P < 0.001$) this elevation at all neonatal ages examined (Figure 15). The two-way ANOVA also revealed a significant main effect of the treatment group and a group × age interaction (both $P < 0.001$).

4. Discussion

The prevalence of AD is expected to rise substantially due to gains in human longevity, which could place an insurmountable burden on healthcare systems [42] unless effective treatments are developed [43]. The main challenge for effective AD treatment is that the pathological processes begin long before the emergence of clinical symptoms, by which time much of the disease-associated damage may be irreversible. Therefore, the development of safe but effective preventative treatments may be the best strategy to reduce the disease burden. For this purpose, investigation of treatments effective against Aβ toxicity in the young adult and developing brain may be a fruitful approach [44].

Formation of the rat neural tube is completed by gestational day E10.5–11, while the mouse neural tube is completely formed by E9.5–10 [45]. Moreover, the cerebral cortex reaches adult weight by postnatal day 20. This rapid development may be particularly advantageous for the study

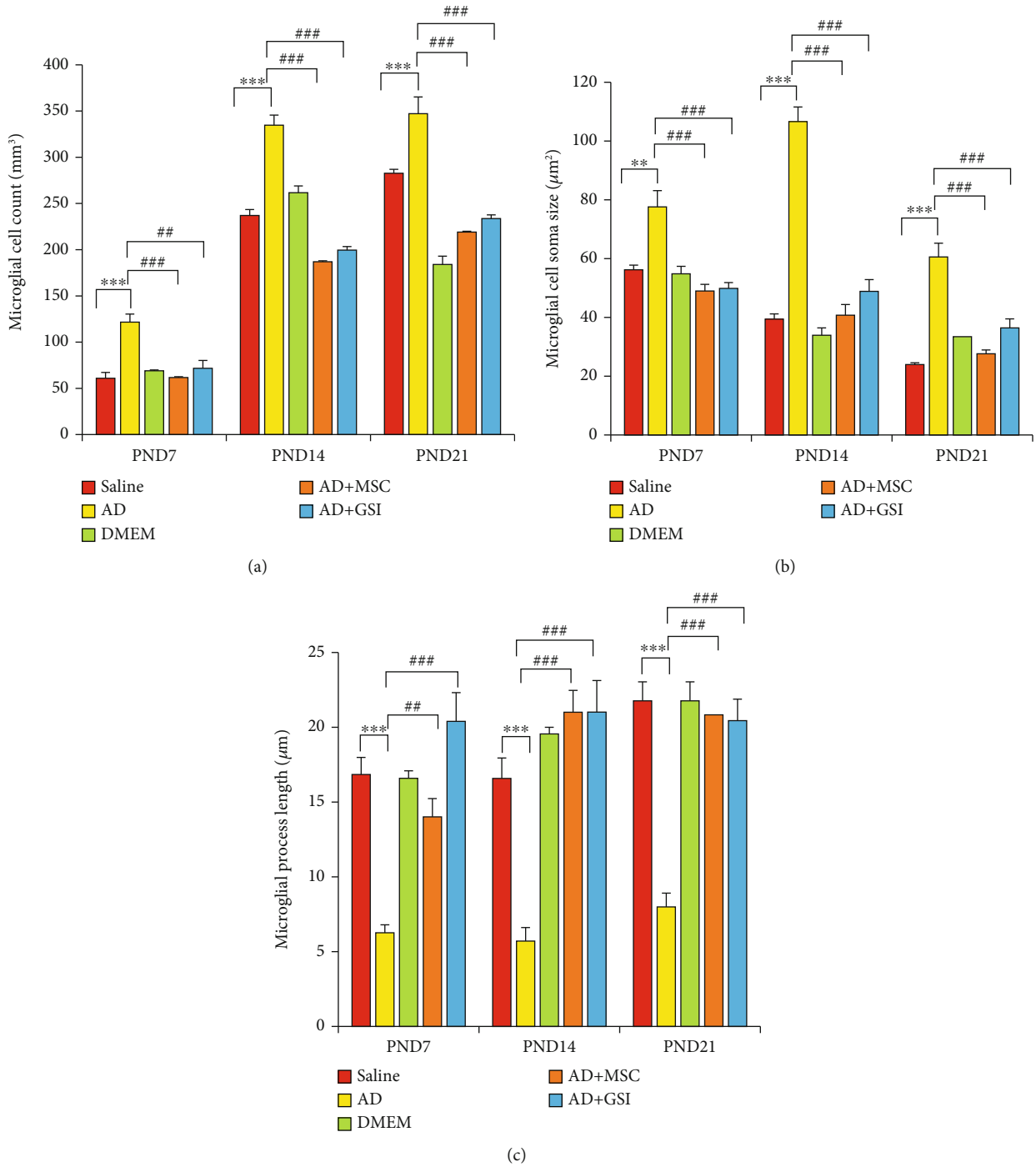

Figure 11: Effect of treatment with MSCs and GSI-953 on (a) microglial cell count/mm^3, (b) cell soma size, (c) processes length in the newborn cortex of Aβ25–35-induced Alzheimer's disease dams. Data were analyzed via two-way ANOVA followed by Tukey's multiple comparison test. Data are expressed as mean ± SEM. $^{*}P < 0.05$, $^{**}P < 0.01$, and $^{***}P < 0.001$ vs. the saline-injected group. $^{\#}P < 0.05$, $^{\#\#}P < 0.01$, and $^{\#\#\#}P < 0.001$ vs. the AD group. ns: nonsignificant ($P > 0.05$).

of preventative AD treatments, and indeed, we demonstrate that BM-MSC injection or oral GSI-953 can protect against brain maldevelopment from the maternal Aβ25–35 injection. To elucidate the protective mechanisms of BM-MSC and GSI-953, we examined effects on neuroinflammatory signaling, microglial activation, cortical cell migration, neuronal development, neurotrophic factor signaling, and apoptosis. Several research papers demonstrated that Alzheimer's disease during pregnancy causes cognitive impairment in the neonates, and possible treatment starting early from prenatal to early postnatal periods may prevent cognitive deficits, reduce Tau and amyloid pathologies, and decrease postsynaptic deficits and neuroinflammation in the brain at the adult stage in 3xTg-AD mice [44].

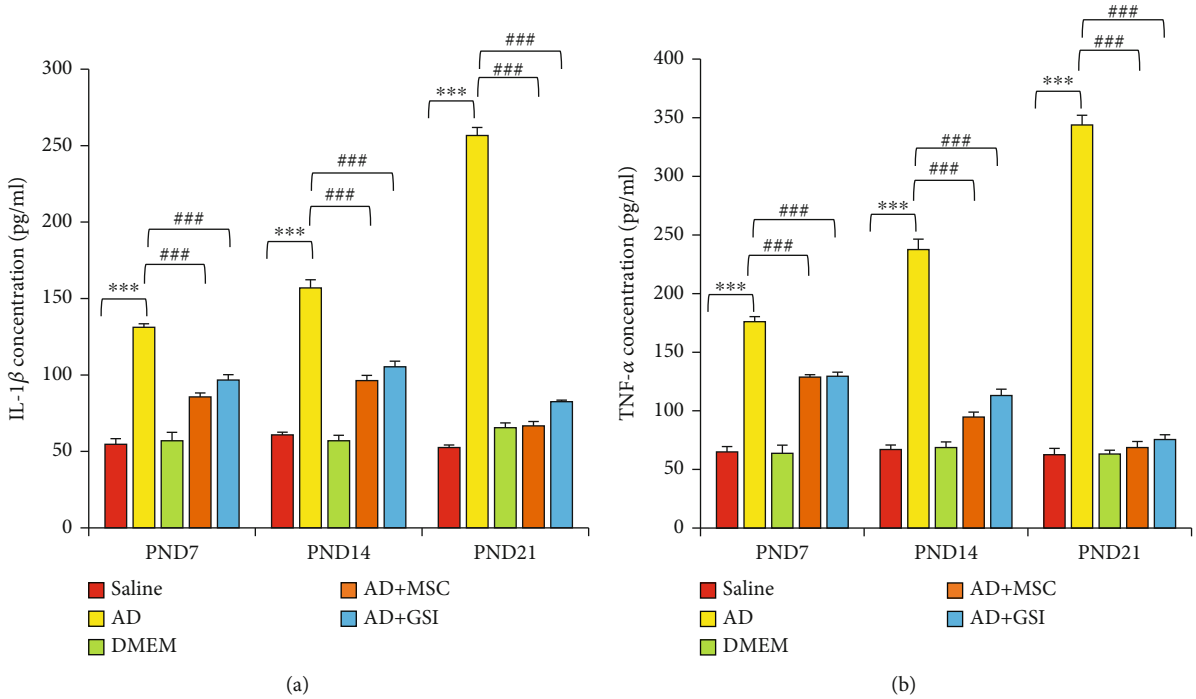

Figure 12: Effect of treatment with MSCs and GSI-953 on the neuroinflammatory cytokine concentration (pg/mg). (a) IL-1β and (b) TNF-α in the newborn cerebral cortex of Aβ25–35-induced Alzheimer's disease dams. Data were analyzed via two-way ANOVA followed by Tukey's multiple comparison test. Data are expressed as mean ± SEM. $^{*}P < 0.05$, $^{**}P < 0.01$, and $^{***}P < 0.001$ vs. the saline-injected group. $^{\#}P < 0.05$, $^{\#\#}P < 0.01$, and $^{\#\#\#}P < 0.001$ vs. AD group. ns: nonsignificant ($P > 0.05$).

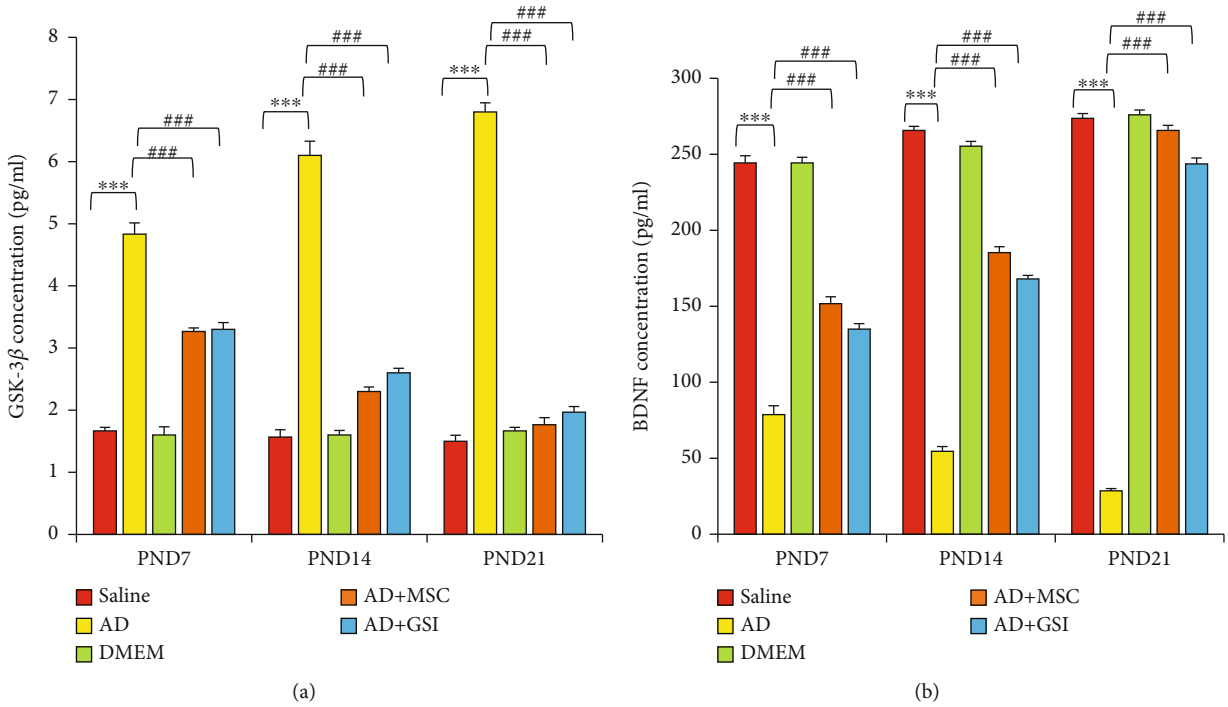

Figure 13: Effect of treatment with MSCs and GSI-953 on (a) GSK-3β and (b) BDNF concentration in newborn sera of Aβ25–35-induced Alzheimer's disease dams. Data were analyzed via two-way ANOVA followed by Tukey's multiple comparison test. Data are expressed as mean ± SEM. $^{*}P < 0.05$, $^{**}P < 0.01$, and $^{***}P < 0.001$ vs. the saline-injected group. $^{\#}P < 0.05$, $^{\#\#}P < 0.01$, and $^{\#\#\#}P < 0.001$ vs. the AD group. ns: nonsignificant ($P > 0.05$).

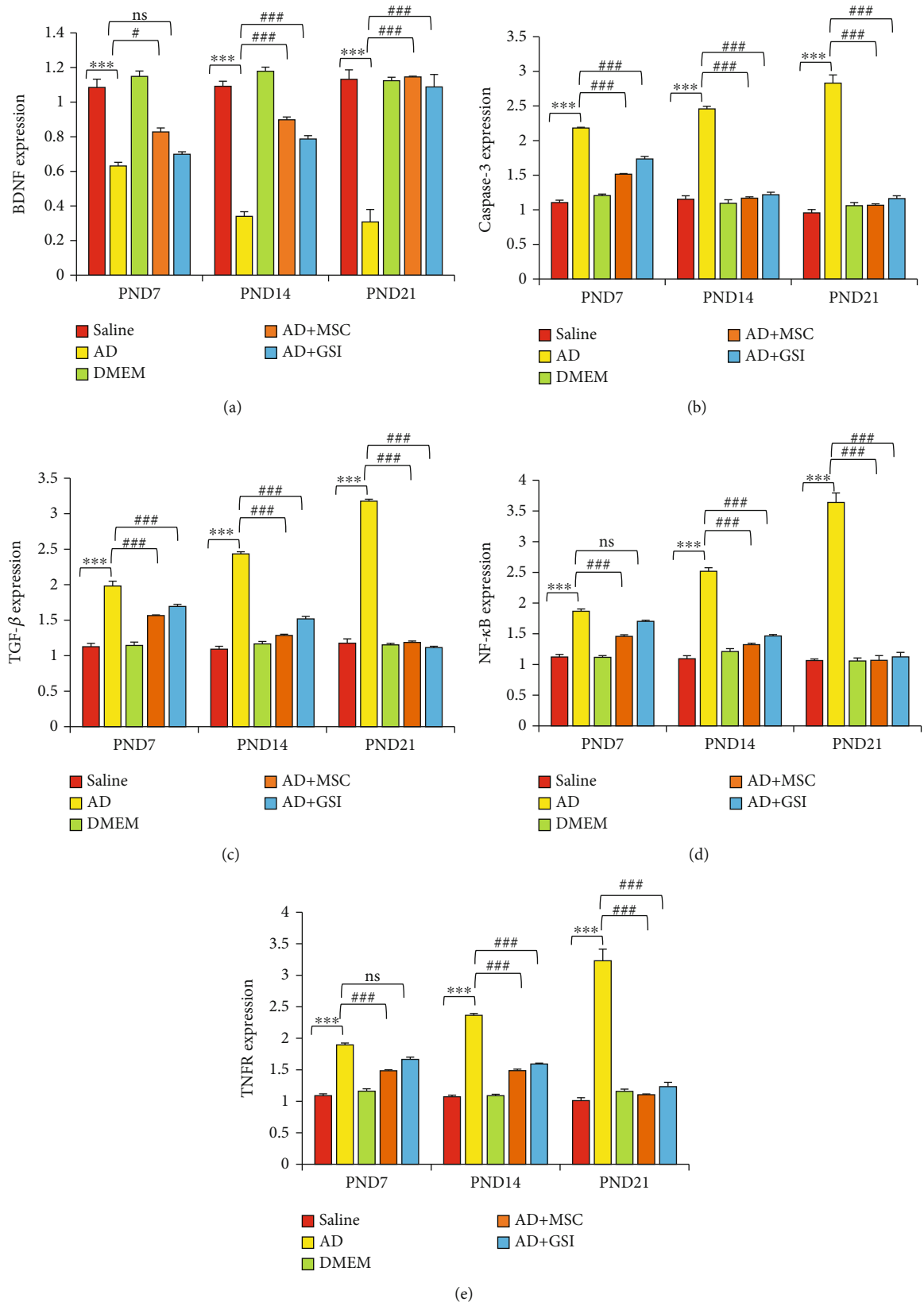

Figure 14: Effect of treatment with MSCs and GSI-953 on the gene expression of (a) BDNF, (b) cleaved caspase-3, (c) TGF-β, (d) NF-κB, and (e) TNFR in the newborn cortex of Aβ25–35-induced Alzheimer's disease dams evaluated via qRT-PCR. Data were analyzed via two-way ANOVA followed by Tukey's multiple comparison test. Data are expressed as mean ± SEM. $^{*}P < 0.05$, $^{**}P < 0.01$, and $^{***}P < 0.001$ vs. the saline-injected group. $^{\#}P < 0.05$, $^{\#\#}P < 0.01$, and $^{\#\#\#}P < 0.001$ vs. the AD group. ns: nonsignificant ($P > 0.05$).

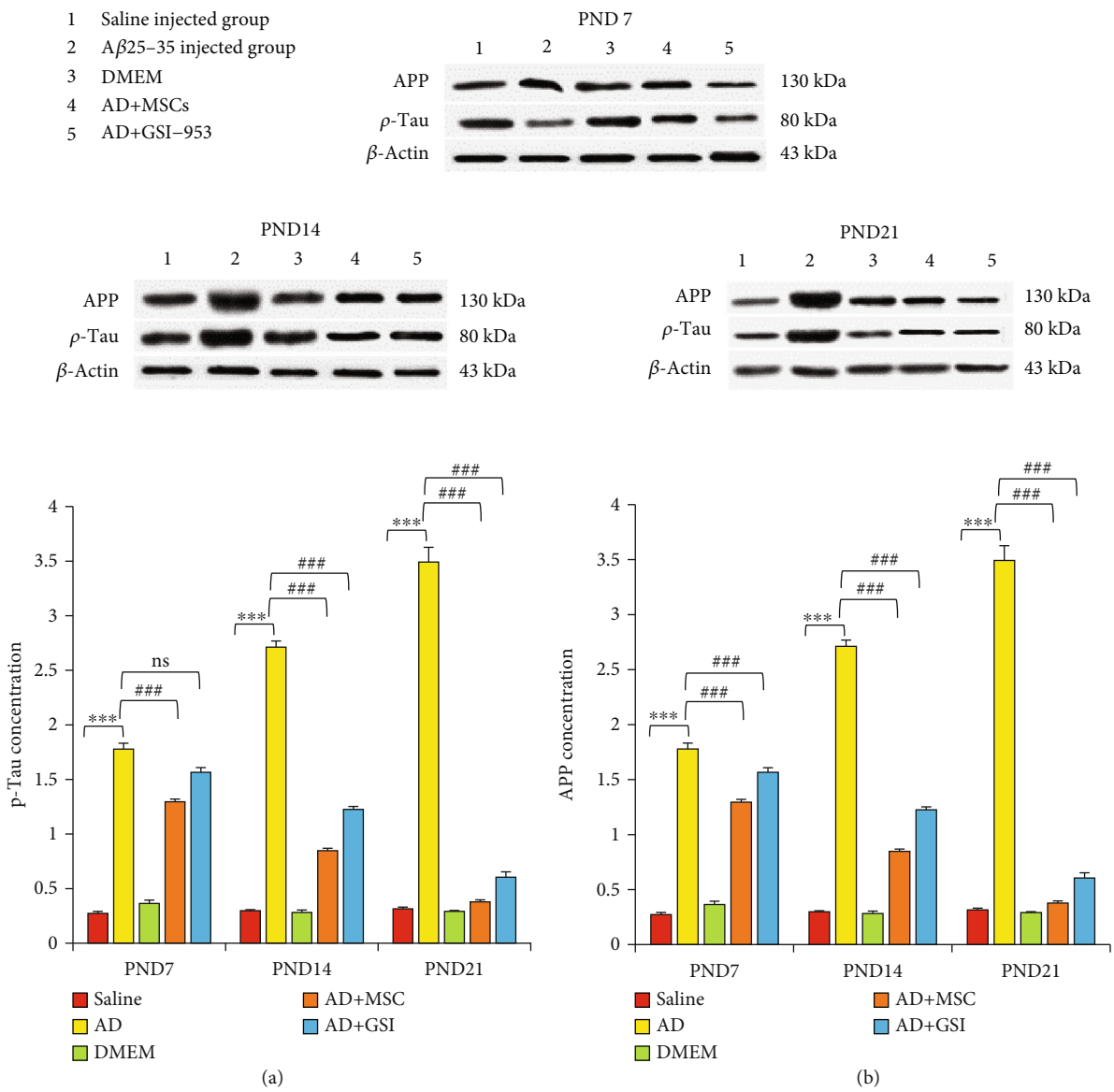

Figure 15: Effect of the treatment with MSCs and GSI-953 on (a) p-Tau and (b) APP protein concentration in the newborn cortex of Aβ25–35-induced Alzheimer's disease dams using the Western blotting technique. Data are expressed as mean ± SEM. $^{*}P < 0.05$, $^{**}P < 0.01$, and $^{***}P < 0.001$ vs. the saline-injected group. $^{\#}P < 0.05$, $^{\#\#}P < 0.01$, and $^{\#\#\#}P < 0.001$ vs. the AD group. ns: nonsignificant ($P > 0.05$).

In the current investigation, we elucidated potential underlying mechanisms of action for BM-MSCs and GSI-953 as treatments for Alzheimer's disease brought on by a single intracerebroventricular injection of the Aβ25–35 rat model (Figure 16).

The first clinical manifestation of AD is memory impairment [46]. In animal models, i.c.v. Aβ25–35 injection is one of the most popular methods for induction of AD-like pathology as Aβ25–35 is converted into a fibril sheet that mimics the toxicity of Aβ1–40 [46, 47]. In the present study, the single i.c.v. injection of Aβ25–35 into adult female rats caused significant impairments in working memory and long-term memory as evidenced by poor Y-maze and novel object recognition test performance, respectively, consistent with previous reports [48, 49]. In addition, Aβ25–35 injection induced remarkable histopathological changes in the neonatal cerebral cortex, including distortion and disorganization of cortical layers, thinning of the external granular layer, and dilatation of blood vessels. These pathological signs progressed in severity from PND7 to PND21, consistent with a previous study demonstrating thinning of the cortex in patients with mild cognitive impairment, which is considered a precursor to clinical AD [50]. These histopathological changes were reversed via maternal BM-MSC and GSI-953 treatments. The protective effect of MSCs may be explained by metabolic compensation for dysfunctional mitochondria [51, 52], while GSI-953 may suppress the plaque burden, thereby reducing downstream inflammation and other harmful processes.

In addition to the accumulation of amyloid plaques and NFTs, AD pathology involves synaptic failure, oxidative stress, neuroinflammation, and mitochondrial dysfunction

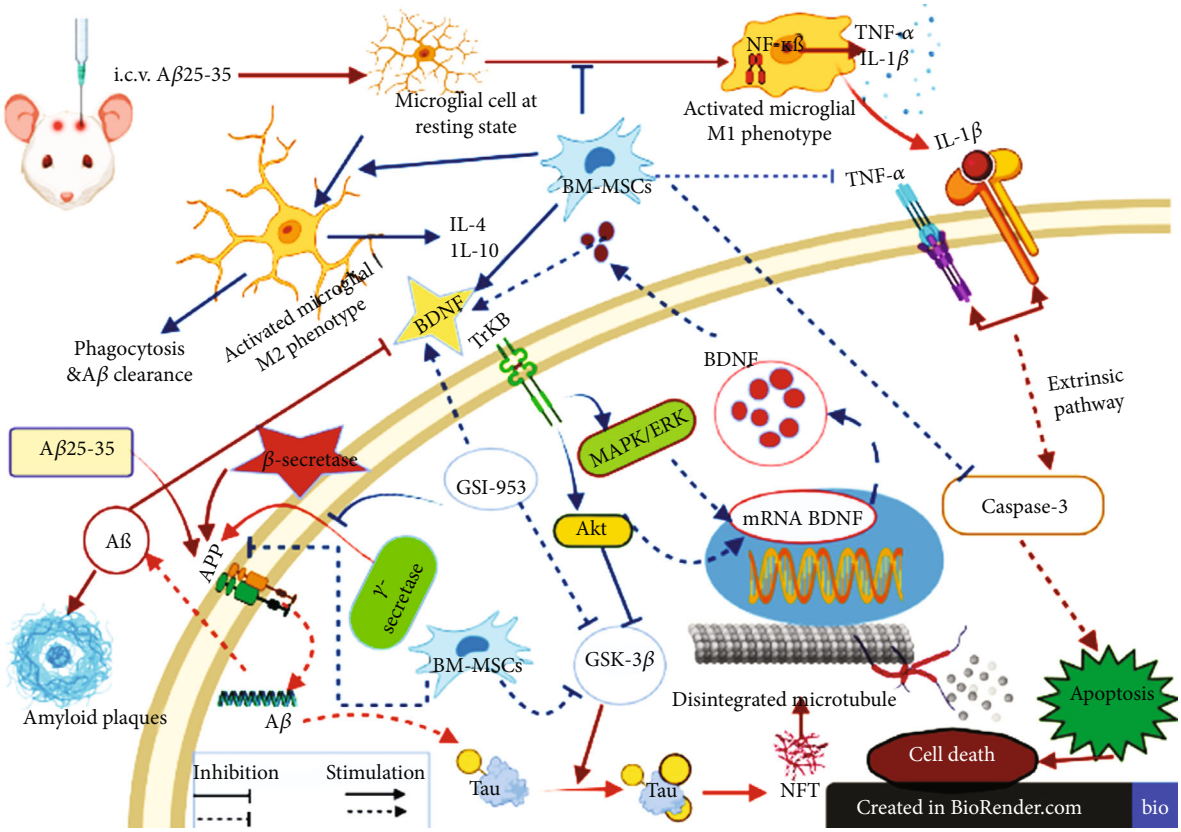

Figure 16: Pathways of MSCs and GSI-953 against the Aβ25–35-induced Alzheimer's disease in neonates. The figure was created with BioRender.com.

[42, 53]. Microglial cells are the resident macrophages of the central nervous system [42], and the pathological insult induces microglial cell activation, a state that triggers local inflammatory signaling and the recruitment of exogenous inflammatory cells [54]. Moreover, Aβ-induced microglial activation and downstream inflammatory responses further accelerate Aβ deposition [55], resulting in a self-sustaining neurogenerative condition. Injection of Aβ25–35 into the dam lateral ventricle significantly increased the number of activated microglial cells in the neonatal cortex, consistent with previous reports [47, 48], and this response was reversed by BM-MSC injection, again in accordance with previous findings [1, 56]. Panchenko et al. [57] found that intravenously injected MSCs pass through the blood-brain barrier and reach the temporal cortex and hippocampal dentate gyrus, possibly promoted by the phagocytic activity of activated microglial cells around Aβ deposits [58, 59]. In addition, we show for the first time that oral GSI-953 administration can also quell microglial cell activation in response to i.c.v. Aβ25–35 injection, possibly by reducing APP to Aβ conversion [24] through inhibition of γ-secretase activity.

The Aβ peptide is generated from APP through cleavage via β-secretase and γ-secretase [21]. The APP concentration was significantly elevated in the neonatal cortex of Aβ25–35-injected dams relative to saline-injected dams, while maternal BM-MSC and GSI-953 treatments during pregnancy reversed this rise. These findings are in agreement with Martone et al. [24], who reported that GSI-953 inhibits cleavage of APP and reduces Aβ production both *in vitro* and in a transgenic mouse model.

Tau is a microtubule-associated protein responsible for supporting the neuronal structure and synaptic function [60]. Amyloid-β deposition causes hyperphosphorylation of Tau kinases by activating GSK-3β [61, 62]. Injection of Aβ25–35 upregulated the expression of GSK-3β and increased the p-Tau concentration in the neonatal cortex, consistent with previous studies reporting a sustained rise in the p-Tau concentration within the frontal cortex following Aβ25–35 injection [48, 63]. Hyperphosphorylation reduces the affinity of Tau for microtubules, resulting in a reduced axonal transport and synaptic dysfunction [64, 65]. Maternal treatment with BM-MSCs or GSI-953 reversed this increase in p-Tau concentration, possibly by reducing GSK-3β activity [61, 66].

BDNF promotes neuronal differentiation and survival by suppressing proapoptotic proteins and upregulating neurofunctional proteins through the cyclic adenosine monophosphate response element binding protein transcription pathway [67, 68]. BDNF passes through the placenta *in vivo* and is also delivered via breast milk [44, 69]. Maternal Aβ25–35 injection significantly decreased the BDNF gene expression in the neonatal cortex (Figure 16) and reduced the serum concentration of the BDNF protein compared to offspring of saline-injected dams. Similarly, pro-BDNF, mature BDNF, and the corresponding mRNAs were reduced in the parietal cortex and hippocampus via Aβ25–

35 injection [44]. On the contrary, maternal treatment with BM-MSCs and GSI-953 reversed this BDNF downregulation, possibly due to compensatory release from transplanted BM-MSCs [70] and (or) by the GSI-953-induced suppression of the GSK-3β activity.

Amyloid-β deposition stimulates the inflammatory response by increasing the cortical levels of TNF-α, IL-1β, and NF-κB [71], which in turn increase the expression of APP and upregulate γ-secretase activity, causing a further rise in Aβ levels [72] (Figure 16). Activated microglial cells release the proinflammatory cytokines TNF-α and IL-1β in response to Aβ25–35 injection. Inactive NF-κB is retained in the cytoplasm by binding to inhibitory $\kappa\beta$ (I$\kappa\beta$). In response to various forms of stimulation, particularly those associated with stress, I$\kappa\beta$ is phosphorylated and degraded, allowing NF-κBp^{65} migration into the nucleus where it enhances the expression of proinflammatory cytokines [73]. Maternal treatment with BM-MSCs or GSI-953 reduced the upregulation of proinflammatory signals induced by Aβ25–35 injection, possibly through inhibition of NF-$\kappa\beta$ signaling [61]. In accordance with this notion, MSC transplantation into AD model mice suppressed the release of proinflammatory cytokines, such as TNF-α, IL-1β, and IL-6, from activated microglia and astrocytes [44, 59] and shifted microglial polarization from the proinflammatory M1 phenotype to the immunomodulatory M2 phenotype [33] (Figure 16). Moreover, MSCs can directly secret anti-inflammatory cytokines (IL-4 and IL-10) and neurotrophic factors (BDNF, IGF-1, and NGF) [70] as well as fibrogenic factors (TGF-β) [70].

Granulocyte macrophage colony-stimulating factor (GM-CSF) recruits peripheral monocytes that are further stimulated by Aβ deposits and accelerates the clearance of Aβ, while TGF-β participates in several pathways that modulate amyloid metabolism, immunoregulation, and neuroprotection [74]. There are no available data explaining the capacity of GSI-953 to modulate inflammatory responses induced by Aβ25–35 injection except via the direct reduction of Aβ deposition.

Treatment of pregnant rats with BM-MSCs or GSI-953 significantly suppressed the Aβ25–35-induced upregulation of the apoptosis effector cleaved caspase-3 in the neonatal cortex, in agreement with Zhang et al. [75] who reported that Aβ25–35 stimulates proapoptotic Bax and promotes the inhibition of antiapoptotic Bcl2, resulting in elevated caspase-3 activity and neural death. Transplanted MSCs have also been shown to attenuate apoptotic cell death via inhibition of cleaved caspase-3 activity [76] via the secretion of seldin and survivin [77], proteins that interact with caspase-3 and block the downstream death cascade [78].

5. Conclusion

Intravenous injection of BM-MSCs or oral administration of the γ-secretase inhibitor GSI-953 (begacestat) mitigated cognitive impairments induced by the intracerebroventricular injection of Aβ25–35 in adult female rats. Further, BM-MSC and GSI-953 treatments during pregnancy prevented cortical maldevelopment in the offspring. These protective effects in the neonatal rat cortex were associated with the reduced expression of the APP and p-Tau proteins, inhibition of the microglial activation, reduced expression of proinflammatory cytokines (IL-1β and TNF-α), and downregulation of brain caspase-3, NF-κB, and TGF-β (Figure 16). Furthermore, BM-MSC and GSI-953 treatments reversed the Aβ25–35-induced downregulation of the BDNF expression and upregulation of the GSK-3β activity. Therefore, these treatments could prevent Aβ25–35-induced neurodegeneration and cognitive impairment probably by reducing the Aβ plaque load, neurofibrillary tangle formation, and ensuing neuroinflammation. However, further studies using loss-of-function and/or gain-of-function mutation models are required to provide evidence for the implications of the tested mediators including IL-1β, TNF-α, TNFR, caspase-3, NF-κB, TGF-β, BDNF, and GSK-3β in the Aβ25–35-induced neurodegenerative damage and cognitive impairment and their roles in the BM-MSC- and GSI-953-induced recovery.

Abbreviations

AD:	Alzheimer's disease
Aβ:	Amyloid beta
p-Tau:	Phosphorylated Tau protein
BM-MSCs:	Bone marrow mesenchymal stem cells
GSI-953:	Gamma secretase inhibitor-953 (begacestat)
IL:	Interleukin
TNF-α:	Tumor necrosis factor-α
GSK-3β:	Glycogen synthase kinase-3β
BDNF:	Brain-derived neurotrophic factor
NFTs:	Neurofibrillary tangles
CSF:	Cerebrospinal fluid
APP:	Amyloid precursor protein
NGF:	Nerve growth factor
DMEM:	Dulbecco's modified eagle medium
BSA:	Bovine serum albumin
NF-$\kappa\beta$:	Nuclear factor kappa β
TNFR:	Tumor necrosis factor receptor
TGF-β:	Transforming growth factor β
PVDF:	Polyvinylidene fluoride
PND:	Postnatal day.

Data Availability

This published article includes all of the data analyzed during this investigation.

Ethical Approval

The ethics committee for the care and use of animals, Faculty of Science, Beni-Suef University, Egypt, provided suggestions, instructions, and guidelines that were followed throughout all experimentation methods (approval number 019-75).

Conflicts of Interest

No potential conflict of interest was reported by the authors.

Authors' Contributions

The experiments were created and planned by OMA, AME, REA, and YMK. The trials were run and the data was analyzed by AGM. At various phases of the study's completion, RMA, FAJ, and SDA assisted with experimental technical support and completion. The manuscript was drafted by AGM. The paper was edited by YMK, OMA, AME, RMA, FAJ, and REA. The manuscript's contents have the approval of all the authors. The final manuscript was read and approved by all the authors.

References

[1] A. F. Neves, C. Camargo, C. Premer, J. M. Hare, B. S. Baumel, and M. Pinto, "Intravenous administration of mesenchymal stem cells reduces Tau phosphorylation and inflammation in the 3xTg-AD mouse model of Alzheimer's disease," *Experimental Neurology*, vol. 341, article 113706, 2021.

[2] GBD 2019 Dementia Forecasting Collaborators, "Estimation of the global prevalence of dementia in 2019 and forecasted prevalence in 2050: an analysis for the global burden of disease study 2019," *The Lancet Public Health*, vol. 7, no. 2, pp. e105–e125, 2022.

[3] J. E. Young and L. S. Goldstein, "Alzheimer's disease in a dish: promises and challenges of human stem cell models," *Human Molecular Genetics*, vol. 21, no. R1, pp. R82–R89, 2012.

[4] S. Wu, X. Liu, R. Jiang, X. Yan, and Z. Ling, "Roles and mechanisms of gut microbiota in patients with Alzheimer's disease," *Frontiers in Aging Neuroscience*, vol. 13, article 650047, 2021.

[5] F. Chakari-Khiavi, S. Dolati, A. Chakari-Khiavi et al., "Prospects for the application of mesenchymal stem cells in Alzheimer's disease treatment," *Life Sciences*, vol. 231, article 116564, 2019.

[6] Z. Si and X. Wang, "Stem cell therapies in Alzheimer's disease: applications for disease modeling," *Journal of Pharmacology and Experimental Therapeutics*, vol. 377, no. 2, pp. 207–217, 2021.

[7] S. A. Kent, T. L. Spires-Jones, and C. S. Durrant, "The physiological roles of Tau and Aβ: implications for Alzheimer's disease pathology and therapeutics," *Acta Neuropathologica*, vol. 140, no. 4, pp. 417–447, 2020.

[8] K. Scearce-Levie, P. E. Sanchez, and J. W. Lewcock, "Leveraging preclinical models for the development of Alzheimer disease therapeutics," *Nature Reviews Drug Discovery*, vol. 19, no. 7, pp. 447–462, 2020.

[9] H. S. Park, Q. Q. Pang, Y. S. Kim, J. H. Kim, and E. J. Cho, "Neuroprotective effect of membrane-free stem cell extract against amyloid beta 25–35-induced neurotoxicity in SH-SY5Y cells," *Applied Sciences*, vol. 11, no. 5, p. 2219, 2021.

[10] Z. Cai, B. Zhao, and A. Ratka, "Oxidative stress and β-amyloid protein in Alzheimer's disease," *Neuromolecular Medicine*, vol. 13, no. 4, pp. 223–250, 2011.

[11] E. Hoekzema, E. Barba-Müller, C. Pozzobon et al., "Pregnancy leads to long-lasting changes in human brain structure," *Nature Neuroscience*, vol. 20, no. 2, pp. 287–296, 2017.

[12] W. Lederer, H. Schaffenrath, C. Alomar-Dominguez et al., "Cerebrospinal beta-amyloid peptides(1-40) and (1-42) in severe preeclampsia and HELLP syndrome - a pilot study," *Scientific Reports*, vol. 10, no. 1, p. 5783, 2020.

[13] F. Perera and J. Herbstman, "Prenatal environmental exposures, epigenetics, and disease," *Reproductive Toxicology*, vol. 31, no. 3, pp. 363–373, 2011.

[14] R. A. Sperling, P. S. Aisen, L. A. Beckett et al., "Toward defining the preclinical stages of Alzheimer's disease: recommendations from the National Institute on Aging-Alzheimer's Association workgroups on diagnostic guidelines for Alzheimer's disease," *Alzheimer's & Dementia*, vol. 7, no. 3, pp. 280–292, 2011.

[15] K. B. Rajan, R. S. Wilson, J. Weuve, L. L. Barnes, and D. A. Evans, "Cognitive impairment 18 years before clinical diagnosis of Alzheimer disease dementia," *Neurology*, vol. 85, no. 10, pp. 898–904, 2015.

[16] H. Braak and E. Braak, "Neuropathological stageing of Alzheimer-related changes," *Acta Neuropathologica*, vol. 82, no. 4, pp. 239–259, 1991.

[17] C. R. Jack, R. C. Petersen, Y. C. Xu et al., "Medial temporal atrophy on MRI in normal aging and very mild Alzheimer's disease," *Neurology*, vol. 49, no. 3, pp. 786–794, 1997.

[18] H. Braak and E. Braak, "Development of Alzheimer-related neurofibrillary changes in the neocortex inversely recapitulates cortical myelogenesis," *Acta Neuropathologica*, vol. 92, no. 2, pp. 197–201, 1996.

[19] C. R. Jack Jr, M. S. Albert, D. S. Knopman et al., "Introduction to the recommendations from the National Institute on Aging-Alzheimer's Association workgroups on diagnostic guidelines for Alzheimer's disease," *Alzheimer's & Dementia*, vol. 7, no. 3, pp. 257–262, 2011.

[20] W. Wei, Y. Liu, C. L. Dai et al., "Neurotrophic treatment initiated during early postnatal development prevents the Alzheimer-like behavior and synaptic dysfunction," *Journal of Alzheimer's Disease*, vol. 82, no. 2, pp. 631–646, 2021.

[21] H. W. Querfurth and F. M. LaFerla, "Alzheimer's disease," *The New England Journal of Medicine*, vol. 362, no. 4, pp. 329–344, 2010.

[22] M. A. Kostylev, A. C. Kaufman, H. B. Nygaard et al., "Prion-protein-interacting amyloid-β oligomers of high molecular weight are tightly correlated with memory impairment in multiple Alzheimer mouse models," *Journal of Biological Chemistry*, vol. 290, no. 28, pp. 17415–17438, 2015.

[23] J. Wen, D. Liu, and L. Zhao, "Small molecules targeting γ-secretase and their potential biological applications," *European Journal of Medicinal Chemistry*, vol. 232, article 114169, 2022.

[24] R. L. Martone, H. Zhou, K. Atchison et al., "Begacestat (GSI-953): a novel, selective thiophene sulfonamide inhibitor of amyloid precursor protein γ-secretase for the treatment of Alzheimer's disease," *Journal of Pharmacology and Experimental Therapeutics*, vol. 331, no. 2, pp. 598–608, 2009.

[25] R. Mancuso, J. van den Daele, N. Fattorelli et al., "Stem-cell-derived human microglia transplanted in mouse brain to study human disease," *Nature Neuroscience*, vol. 22, no. 12, pp. 2111–2116, 2019.

[26] C. Lee, S. M. Willerth, and H. B. Nygaard, "The use of patient-derived induced pluripotent stem cells for Alzheimer's disease modeling," *Progress in Neurobiology*, vol. 192, article 101804, 2020.

[27] X. Xu, D. Gu, B. Xu, C. Yang, and L. Wang, "Circular RNA circ_0005835 promotes promoted neural stem cells proliferation and differentiate to neuron and inhibits inflammatory cytokines levels through miR-576-3p in Alzheimer's disease," *Environmental Science and Pollution Research*, vol. 29, no. 24, pp. 35934–35943, 2022.

[28] F. Han and P. Lu, "Introduction for stem cell–based therapy for neurodegenerative diseases," in *Stem Cell-Based Therapy for Neurodegenerative Diseases*, pp. 1–8, Springer, 2020.

[29] Z. Feng and F. Gao, "Stem cell challenges in the treatment of neurodegenerative disease," *CNS Neuroscience & Therapeutics*, vol. 18, no. 2, pp. 142–148, 2012.

[30] H. Yang, Z. H. Xie, L. F. Wei et al., "Human umbilical cord mesenchymal stem cell-derived neuron-like cells rescue memory deficits and reduce amyloid-beta deposition in an AβPP/PS1 transgenic mouse model," *Stem Cell Research & Therapy*, vol. 4, no. 4, pp. 1–14, 2013.

[31] J. Penney, W. T. Ralvenius, and L.-H. Tsai, "Modeling Alzheimer's disease with iPSC-derived brain cells," *Molecular Psychiatry*, vol. 25, no. 1, pp. 148–167, 2020.

[32] T. L. Spitzer, A. Rojas, Z. Zelenko et al., "Perivascular human endometrial mesenchymal stem cells express pathways relevant to self-renewal, lineage specification, and functional phenotype," *Biology of Reproduction*, vol. 86, no. 2, pp. 1–16, 2012.

[33] C. Qin, Y. Li, and K. Wang, "Functional mechanism of bone marrow-derived mesenchymal stem cells in the treatment of animal models with Alzheimer's disease: inhibition of neuroinflammation," *Journal of Inflammation Research*, vol. Volume 14, pp. 4761–4775, 2021.

[34] R. J. Bateman, C. Xiong, T. L. Benzinger et al., "Clinical and biomarker changes in dominantly inherited Alzheimer's disease," *The New England Journal of Medicine*, vol. 367, no. 9, pp. 795–804, 2012.

[35] H. Y. Kim, D. K. Lee, B. R. Chung, H. V. Kim, and Y. S. Kim, "Intracerebroventricular injection of Amyloid-β peptides in normal mice to acutely induce Alzheimer-like cognitive deficits," *Journal of Visualized Experiments*, vol. 109, no. 109, article e53308, 2016.

[36] R. H. Ahmed, S. R. Galaly, N. Moustafa et al., "Curcumin and mesenchymal stem cells ameliorate ankle, testis, and ovary deleterious histological changes in arthritic rats *via* suppression of oxidative stress and inflammation," *Stem Cells International*, vol. 2021, Article ID 3516834, 20 pages, 2021.

[37] T. Sumathi, D. Asha, G. Nagarajan, A. Sreenivas, and R. Nivedha, "L-Theanine alleviates the neuropathological changes induced by PCB (Aroclor 1254) via inhibiting upregulation of inflammatory cytokines and oxidative stress in rat brain," *Environmental Toxicology and Pharmacology*, vol. 42, pp. 99–117, 2016.

[38] N. N. Nalivaeva, N. D. Belyaev, D. I. Lewis et al., "Effect of sodium valproate administration on brain neprilysin expression and memory in rats," *Journal of Molecular Neuroscience*, vol. 46, no. 3, pp. 569–577, 2012.

[39] P. H. Botton, M. S. Costa, A. P. Ardais et al., "Caffeine prevents disruption of memory consolidation in the inhibitory avoidance and novel object recognition tasks by scopolamine in adult mice," *Behavioural Brain Research*, vol. 214, no. 2, pp. 254–259, 2010.

[40] S. J. Cohen and R. W. Stackman Jr., "Assessing rodent hippocampal involvement in the novel object recognition task. A review," *Behavioural Brain Research*, vol. 285, pp. 105–117, 2015.

[41] M. F. Iulita, S. Allard, L. Richter et al., "Intracellular Aβ pathology and early cognitive impairments in a transgenic rat overexpressing human amyloid precursor protein: a multidimensional study," *Acta Neuropathologica Communications*, vol. 2, no. 1, pp. 1–17, 2014.

[42] M. M. Rahman and C. Lendel, "Extracellular protein components of amyloid plaques and their roles in Alzheimer's disease pathology," *Molecular Neurodegeneration*, vol. 16, no. 1, pp. 1–30, 2021.

[43] X. Yue, Y. Zhou, M. Qiao et al., "Intermittent hypoxia treatment alleviates memory impairment in the 6-month-old APPswe/PS1dE9 mice and reduces amyloid beta accumulation and inflammation in the brain," *Alzheimer's Research & Therapy*, vol. 13, no. 1, pp. 1–16, 2021.

[44] W. Wei, Y. Wang, Y. Liu et al., "Prenatal to early postnatal neurotrophic treatment prevents Alzheimer-like behavior and pathology in mice," *Alzheimer's Research & Therapy*, vol. 12, no. 1, pp. 1–18, 2020.

[45] B. D. Semple, K. Blomgren, K. Gimlin, D. M. Ferriero, and L. J. Noble-Haeusslein, "Brain development in rodents and humans: identifying benchmarks of maturation and vulnerability to injury across species," *Progress in Neurobiology*, vol. 106-107, pp. 1–16, 2013.

[46] H. Jahn, "Memory loss in Alzheimer's disease," *Dialogues in Clinical Neuroscience*, vol. 15, no. 4, pp. 445–454, 2013.

[47] B. Cao, M. Zeng, Q. Zhang et al., "Amentoflavone ameliorates memory deficits and abnormal autophagy in Aβ25–35-induced mice by mTOR signaling," *Neurochemical Research*, vol. 46, no. 4, pp. 921–934, 2021.

[48] C. Zussy, A. Brureau, E. Keller et al., "Alzheimer's disease related markers, cellular toxicity and behavioral deficits induced six weeks after oligomeric amyloid-β peptide injection in rats," *PLoS One*, vol. 8, no. 1, article e53117, 2013.

[49] L. Zhu, F. Lu, X. Jia, Q. Yan, X. Zhang, and P. Mu, "Amyloid-β (25-35) regulates neuronal damage and memory loss via SIRT1/Nrf2 in the cortex of mice," *Journal of Chemical Neuroanatomy*, vol. 114, article 101945, 2021.

[50] A. M. Kälin, M. T. Park, M. M. Chakravarty et al., "Subcortical shape changes, hippocampal atrophy and cortical thinning in future Alzheimer's disease patients," *Frontiers in Aging Neuroscience*, vol. 9, p. 38, 2017.

[51] X. Wei, X. Yang, Z. P. Han, F. F. Qu, L. Shao, and Y. F. Shi, "Mesenchymal stem cells: a new trend for cell therapy," *Acta Pharmacologica Sinica*, vol. 34, no. 6, pp. 747–754, 2013.

[52] J. D. Glenn and K. A. Whartenby, "Mesenchymal stem cells: emerging mechanisms of immunomodulation and therapy," *World Journal of Stem Cells*, vol. 6, no. 5, pp. 526–539, 2014.

[53] B. Mandal, S. Niyogi, K. Sarkar, and R. Das, *Structure Based Virtual Screening of Rivastigmine Derivatives as Cholinesterase Inhibitors*, Research Square, 2022.

[54] T. Ma, K. Gong, Q. Ao et al., "Intracerebral transplantation of adipose-derived mesenchymal stem cells alternatively activates microglia and ameliorates neuropathological deficits in Alzheimer's disease mice," *Cell Transplantation*, vol. 22, 1_suppl, pp. 113–S126, 2013.

[55] S. Hong, V. F. Beja-Glasser, B. M. Nfonoyim et al., "Complement and microglia mediate early synapse loss in Alzheimer mouse models," *Science*, vol. 352, no. 6286, pp. 712–716, 2016.

[56] O. Lykhmus, L. Koval, L. Voytenko et al., "Intravenously injected mesenchymal stem cells penetrate the brain and treat inflammation-induced brain damage and memory impairment in mice," *Frontiers in Pharmacology*, vol. 10, p. 355, 2019.

[57] M. Panchenko, R. A. Poltavtseva, N. V. Bobkova et al., "Localization and differentiation pattern of transplanted human multipotent mesenchymal stromal cells in the brain of bulbectomized mice," *Bulletin of Experimental Biology and Medicine*, vol. 158, no. 1, pp. 118–122, 2014.

[58] T. Harach, F. Jammes, C. Muller et al., "Administrations of human adult ischemia-tolerant mesenchymal stem cells and factors reduce amyloid beta pathology in a mouse model of Alzheimer's disease," *Neurobiology of Aging*, vol. 51, pp. 83–96, 2017.

[59] K.-S. Kim, H. S. Kim, J. M. Park et al., "Long-term immunomodulatory effect of amniotic stem cells in an Alzheimer's disease model," *Neurobiology of Aging*, vol. 34, no. 10, pp. 2408–2420, 2013.

[60] A. M. Pooler, W. Noble, and D. P. Hanger, "A role for Tau at the synapse in Alzheimer's disease pathogenesis," *Neuropharmacology*, vol. 76, pp. 1–8, 2014.

[61] F. D. Petry, B. P. Coelho, M. M. Gaelzer et al., "Genistein protects against amyloid-beta-induced toxicity in SH-SY5Y cells by regulation of Akt and Tau phosphorylation," *Phytotherapy Research*, vol. 34, no. 4, pp. 796–807, 2020.

[62] J. B. Hoppe, K. Coradini, R. L. Frozza et al., "Free and nanoencapsulated curcumin suppress β-amyloid-induced cognitive impairments in rats: involvement of BDNF and Akt/GSK-3β signaling pathway," *Neurobiology of Learning and Memory*, vol. 106, pp. 134–144, 2013.

[63] F. dos Santos Petry, J. B. Hoppe, C. P. Klein et al., "Genistein attenuates amyloid-beta-induced cognitive impairment in rats by modulation of hippocampal synaptotoxicity and hyperphosphorylation of Tau," *The Journal of Nutritional Biochemistry*, vol. 87, article 108525, 2021.

[64] N. N. Naseri, H. Wang, J. Guo, M. Sharma, and W. Luo, "The complexity of Tau in Alzheimer's disease," *Neuroscience Letters*, vol. 705, pp. 183–194, 2019.

[65] S. S. Khan and G. S. Bloom, "Tau: the center of a signaling nexus in Alzheimer's disease," *Frontiers in Neuroscience*, vol. 10, p. 31, 2016.

[66] B. P. Coelho, M. M. Gaelzer, F. dos Santos Petry et al., "Dual effect of doxazosin: anticancer activity on SH-SY5Y neuroblastoma cells and neuroprotection on an *in vitro* model of Alzheimer's disease," *Neuroscience*, vol. 404, pp. 314–325, 2019.

[67] C. Cunha, R. Brambilla, and K. L. Thomas, "A simple role for BDNF in learning and memory?," *Frontiers in Molecular Neuroscience*, vol. 3, p. 1, 2010.

[68] G. S. Tejeda and M. Díaz-Guerra, "Integral characterization of defective BDNF/TrkB signalling in neurological and psychiatric disorders leads the way to new therapies," *International Journal of Molecular Sciences*, vol. 18, no. 2, p. 268, 2017.

[69] S.-H. Kim, Y. J. Ko, J. Y. Kim, and Y. J. Sim, "Treadmill running improves spatial learning memory through inactivation of nuclear factor kappa B/mitogen-activated protein kinase signaling pathway in amyloid-β-induced Alzheimer disease rats," *International Neurourology Journal*, vol. 25, Suppl 1, pp. S35–S43, 2021.

[70] S. K. Sanganalmath and R. Bolli, "Cell therapy for heart failure: a comprehensive overview of experimental and clinical studies, current challenges, and future directions," *Circulation Research*, vol. 113, no. 6, pp. 810–834, 2013.

[71] S. Y. Park, M. J. Kim, Y. J. Kim et al., "Selective PCAF inhibitor ameliorates cognitive and behavioral deficits by suppressing NF-κB-mediated neuroinflammation induced by Aβ in a model of Alzheimer's disease," *International Journal of Molecular Medicine*, vol. 35, no. 4, pp. 1109–1118, 2015.

[72] I. Ling, T. E. Golde, D. R. Galasko, and E. H. Koo, "Modulation of Aβ42 in vivo by γ-secretase modulator in primates and humans," *Alzheimer's Research & Therapy*, vol. 7, no. 1, pp. 1–10, 2015.

[73] J.-H. Choi, K. S. Chung, B. R. Jin et al., "Anti-inflammatory effects of an ethanol extract of Aster glehni via inhibition of NF-κB activation in mice with DSS-induced colitis," *Food & Function*, vol. 8, no. 7, pp. 2611–2620, 2017.

[74] C. Qin, L. Bai, Y. Li, and K. Wang, "The functional mechanism of bone marrow-derived mesenchymal stem cells in the treatment of animal models with Alzheimer's disease: crosstalk between autophagy and apoptosis," *Stem Cell Research & Therapy*, vol. 13, no. 1, pp. 1–13, 2022.

[75] Q. Zhang, J. Li, C. Liu et al., "Protective effects of low molecular weight chondroitin sulfate on amyloid beta (Aβ)-induced damage *in vitro* and *in vivo*," *Neuroscience*, vol. 305, pp. 169–182, 2015.

[76] S. P. Wang, Z. H. Wang, D. Y. Peng, S. M. Li, H. Wang, and X. H. Wang, "Therapeutic effect of mesenchymal stem cells in rats with intracerebral hemorrhage: reduced apoptosis and enhanced neuroprotection," *Molecular Medicine Reports*, vol. 6, no. 4, pp. 848–854, 2012.

[77] P. Singh, S. Fukuda, L. Liu, B. R. Chitteti, and L. M. Pelus, "Survivin is required for mouse and human bone marrow mesenchymal stromal cell function," *Stem Cells*, vol. 36, no. 1, pp. 123–129, 2018.

[78] W. Roos, A. Thomas, and B. Kaina, "DNA damage and the balance between survival and death in cancer biology," *Nature Reviews Cancer*, vol. 16, no. 1, pp. 20–33, 2016.

Hindawi
Stem Cells International
Volume 2023, Article ID 7284986, 21 pages
https://doi.org/10.1155/2023/7284986

Research Article

Lama2 And Samsn1 Mediate the Effects of Brn4 on Hippocampal Neural Stem Cell Proliferation and Differentiation

Lei Zhang,[1] Xunrui Zhang,[2] Ruijie Ji,[1] Yaya Ji,[1] Yuhang Wu,[1] Xiuyu Ding,[1] Zhiying Shang,[1] Xueyuan Liu,[1] Wen Li,[1] Jingjing Guo,[1] Jue Wang,[1] Xiang Cheng,[1] Jianbing Qin,[1] Meiling Tian,[1] Guohua Jin,[1] and Xinhua Zhang[1,3]

[1]*Department of Anatomy, Institute of Neurobiology, Medical School, Co-Innovation Center of Neuroregeneration, Nantong University, Nantong, China*
[2]*Faculty of Medicine, Xinglin College, Nantong University, Nantong, China*
[3]*Central Lab, Yancheng Third People's Hospital, The Sixth Affiliated Hospital of Nantong University, Yancheng 224002, China*

Correspondence should be addressed to Xinhua Zhang; zhangxinhua@ntu.edu.cn

Received 22 October 2022; Revised 14 January 2023; Accepted 20 March 2023; Published 13 April 2023

Academic Editor: Huseyin Sumer

The transcription factor Brn4 exhibits vital roles in the embryonic development of the neural tube, inner ear, pancreas islet, and neural stem cell differentiation. Our previous studies have shown that Brn4 promotes neuronal differentiation of hippocampal neural stem cells (NSCs). However, its mechanism is still unclear. Here, starting from the overlapping genes between RNA-seq and ChIP-seq results, we explored the downstream target genes that mediate Brn4-induced hippocampal neurogenesis. There were 16 genes at the intersection of RNA-seq and ChIP-seq, among which the Lama2 and Samsn1 levels can be upregulated by Brn4, and the combination between their promoters and Brn4 was further determined using ChIP and dual luciferase reporter gene assays. EdU incorporation, cell cycle analysis, and CCK-8 assay indicated that Lama2 and Samsn1 mediated the inhibitory effect of Brn4 on the proliferation of hippocampal NSCs. Immunofluorescence staining, RT-qPCR, and Western blot suggested that Lama2 and Samsn1 mediated the promoting effect of Brn4 on the differentiation of hippocampal NSCs into neurons. In conclusion, our study demonstrates that Brn4 binds to the promoters of Lama2 and Samsn1, and they partially mediate the regulation of Brn4 on the proliferation inhibition and neuronal differentiation promotion of hippocampal NSCs.

1. Introduction

Neural stem cells (NSCs) exist in the mammalian brain throughout their life, mainly distributed in the subgranular zone (SGZ) of the hippocampal dentate gyrus and subventricular zone (SVZ) of the lateral ventricle [1]. After migration and differentiation, NSCs in SGZ eventually mature into granular cells in the dentate gyrus. On the one hand, they receive neural afferents from the entorhinal cortex. On the other hand, they can also form axons to project to pyramidal cells in the hippocampal CA3 region. This is an important part of the hippocampal "trisynaptic circuit", which is closely related to learning and memory processes [1, 2]. Therefore, the self-renewal and differentiation of NSCs in the SGZ directly affect the maintenance and repair of hippocampal function.

Alzheimer's disease (AD) is an age-related chronic degenerative disease of the central nervous system. The main pathological features in AD brain tissues are the extracellular diffuse or plaque-like abnormal deposition of β-amyloid protein and the intracellular neurofibrillary tangles caused by the hyperphosphorylation of tau protein in neurons [3]. In addition, the progression of AD is also closely related to astrocytes, microglia, vascular system, mitochondrial dysfunction, inflammation, intestinal flora, and immune system [4–6]. These factors work together to cause synaptic dysfunction and neuronal degeneration in the brain of AD patients, which trigger a series of neuropsychiatric symptoms and

eventually death [7]. However, till now, there is no effective treatment for the loss of neurons and the consequent neurological symptoms in AD patients [3]. During the progression of AD, the proliferation, migration, and differentiation of hippocampal NSCs are significantly changed, suggesting that hippocampal NSCs may be closely related to the pathogenesis of AD, like synaptic abnormalities, amyloid deposition, neuronal loss, and the changes in learning and memory ability [8–10]. Although neurogenesis seems to increase in AD patients, progressive neuron loss is still observed, which indicates that the differentiation ability of NSCs in AD brain is insufficient [8].

Since the transplantation of human fetal substantia nigra dopaminergic neurons into a rat model of Parkinson's disease significantly improved the disease behavior [11], cell replacement therapy has gradually become a research hotspot as a breakthrough to solve major nervous system diseases. Transplanted cells come from a wide range of sources, in which NSCs are the most direct source of neurons and glial cells. Other pluripotent stem cells, such as embryonic stem cells and mesenchymal stem cells, first need to be transformed into neural lineage precursor cells to differentiate into neurons, while NSCs can bypass this step and directly differentiate into required neurons or glial cells. In addition, compared with other pluripotent stem cells, NSCs also largely avoid the risk of teratogenesis after transplantation [12]. However, the proportion of NSCs differentiating into neurons is low, which cannot meet the number requirements of cell transplantation under pathological conditions [13]. Therefore, clarifying the regulation mechanism of NSC proliferation and differentiation may provide new ideas and methods not only for the brain self-repairing but also for cell replacement therapy.

The transcription factor Brn4, namely, Brain 4, also known as POU3F4, OCT9, OTF9, DFN3, and DFNX2, is named because of its first discovery in the brain and plays an important role in embryonic development, cell reprogramming, and regulation of NSC proliferation and differentiation [14]. Brn4 can promote not only the differentiation of NSCs into neurons but also the maturation of newborn neurons [15–18]. Besides, many studies have shown that Brn4 can also reprogram human or mouse fibroblasts and astrocytes into neurons or neuron precursor cells [19–22]. All these researches suggest that the role of Brn4 in the development of the central nervous system and the differentiation of NSCs should not be ignored.

The behavior experiments also showed that the learning and memory abilities of Brn4 knockout mice decreased significantly. At the same time, Brn4 not only inhibited the proliferation of hippocampal NSCs but also promoted their differentiation into neurons. These results suggest that Brn4 may have a protective effect on the brain during the progression of AD. However, the mechanism of Brn4 regulating the proliferation and differentiation of hippocampal NSCs is still unclear. RNA sequencing analysis suggested that the level of genes related to neuron development and maturation increased, while the level of genes related to the maintenance of NSC stemness decreased after Brn4 overexpression [23], indicating the existence of downstream genes mediating the function of transcription factor Brn4. In this study, we verified the intersection genes of RNA-seq and ChIP-seq results through multiple experiments to explore the downstream target genes directly bound by Brn4 and the molecular mechanism of Brn4 regulating the neurogenesis in the hippocampus. Our research reveals the downstream mechanism of the transcription factor Brn4, and it may provide new ideas for regulating the proliferation and differentiation of NSCs *in vitro* and *in vivo*, which is helpful to solve neurodegenerative diseases through self-repairing or cell replacement therapy.

2. Materials and Methods

2.1. Animals and Cell Culture. The SPF neonatal (1 day) ICR mice used for the primary culture of hippocampal NSCs were purchased from the Animal Research Center of Nantong University of China. We made great efforts to reduce the number of mice sacrificed and to minimize their pain. All animal experiments were approved by the Nursing and Use Committee of the Experimental Animal Research Center of Nantong University. The N2a cell line was obtained from the National Collection of Authenticated Cell Cultures. N2a cells were cultured in Dulbecco Modified Eagle Medium and Ham F12 (DMEM/F12, Corning) supplemented with 10% FBS (Gibco) and 100 U/mL penicillin-streptomycin (HyClone) at 37°C with 5% CO_2. The culture and differentiation of hippocampal NSCs were performed as described previously with some modifications [24, 25]. Firstly, the hippocampi were derived from the brains of neonatal (1 day) ICR mice and mechanically dissociated in DMEM/F12. After the cell suspension passed through a 200-mesh nylon filter, single cells were cultured in a 25 cm^2 flask at a density of 1×10^4 cells/mL with NSCs culture medium, which was composed of DMEM/F12, 2% B27 (Gibco), 20 ng/mL epidermal growth factor (EGF, Gibco), 20 ng/mL fibroblast growth factor 2 (bFGF, Sigma) and 100 U/mL penicillin/streptomycin (Shanghai Biotech Research Institute) at 37°C in a humidified incubator with 95% air and 5% (v/v) CO_2. Secondly, about 5-7 days later, neurospheres were formed and suspended in the medium. Using the Accutase enzyme (Sigma), we digested these spheres into single cells and continued to culture. Thirdly, after three generations, single cells at a density of 1×10^4 cells/mL were plated in 24-well plates coated with poly-L-lysine (Sigma) in advance. Some were cultured with an NSC culture medium, and others were cultured with a differentiation medium composed of DMEM/F12 and 1% fetal bovine serum (FBS, Gibco). Finally, 7 days later, in order to determine whether the cells we cultured were NSCs, immunocytochemistry was used to detect the expression of stem cell markers and various neural cell markers, respectively, to detect the characterization of the cells. So as to ensure the purity of cells, we used neurospheres of the third generation to carry out subsequent experiments.

2.2. Plasmid Transfection and Virus Infection. Lama2 CRISPR SAM coactivated plasmids (Santa Cruz) were used to activate the Lama2 expression. After being seeded onto 6-well plates with 3 mL medium for each well, cells were

transfected, respectively, with 1 ug, 2 ug, or 3 ug plasmids by Lipofectamine 3000 (Invitrogen) according to the manufacturer's protocol. The lentiviruses were directly added into the medium to infect cells. The overexpression and knockdown lentiviruses used in this study were as follows: pLenti-EF1a-EGFP-F2A-Puro-CMV-MCS (negative control) vs. pLenti-EF1a-EGFP-F2A-Puro-CMV-Brn4-HA (Genechem); pSLenti-EF1a-EGFP-F2A-Puro-CMV-MCS-3Flag (negative control) vs. pSLenti-EF1a-EGFP-F2A-Puro-CMV-Samsn1-3Flag (OBiO); pSLenti-U6-shRNA-CMV-EGFP-2A-Puro (negative control) vs. pSLenti-U6-shRNA(Lama2)-CMV-EGFP-2A-Puro (Lama2-shRNA) (OBiO); pSLenti-U6-shRNA-CMV-EGFP-2A-Puro (negative control) vs. pSLenti-U6-shRNA (Samsn1)-CMV-EGFP-2A-Puro (Samsn1-shRNA) (OBiO); and pLKD-CMV-mcherry-2A-Puro-U6-shRNA (negative control) vs. pLKD-CMV-mcherry-2A-Puro-U6-shRNA(Pou3f4) (Brn4-shRNA) (OBiO).

2.3. Establishment of Stable Lentivirus Strains. 2×10^5 N2a cells were plated onto a 6-well plate and cultured at 37°C with 5% CO_2 for 12-16 h. When the cell confluence reached approximately 40-60%, the control lentivirus (empty vector, pLenti-EF1a-EGFP-F2A-Puro-CMV-MCS) and Brn4 overexpression lentivirus (pLenti-EF1a-EGFP-F2A-Puro-CMV-Brn4-HA) were, respectively, added into the medium and cultured for 48 h. Then, the cells were selected with 2 μg/mL puromycin (YEASEN) for 7 days. RT-qPCR and Western blot were performed to detect the Brn4 overexpression efficiency.

2.4. ChIP Assay. 4×10^6 Brn4-overexpressing N2a cells were needed for each immunoprecipitation. The ChIP assay was carried out according to the manufacturer's instructions (Cell Signaling Technology). Briefly, the cells were cross-linked by 1% formaldehyde, and then the chromatin was digested to 150-900 bp DNA-protein fragments by micrococcal nuclease and ultrasonic treatment. After respective incubation with different immunoprecipitating antibodies overnight at 4°C, elution from antibody/protein G agarose beads, and reversal of cross-links, the DNA was purified using spin columns and quantified by PCR. PCR was performed with DreamTaq Green PCR Master Mix (Thermo Fisher Scientific) according to the manufacturer's protocol using the following PCR conditions: 95°C for 5 min, followed by 40 cycles of 95°C for 15 s, 55°C for 30 s, and 72°C for 40 s. The results were visualized using 1% agarose gel electrophoresis. The sequences of the primers used in the study are in Table 1.

2.5. Dual Luciferase Reporter Gene Experiment. The binding sites of Brn4 on the Lama2 and Samsn1 promoters were analyzed using the JASPAR website (http://jaspar.genereg.net/). The top three sites with the highest scores were deleted to construct the mutated dual luciferase reporter gene plasmid, respectively. 1×10^4 N2a cells were plated onto 96-well plates and cultured overnight at 37°C with 5% CO_2. 48 h after the plasmids (OBiO) transfection by Lipofectamine 3000 (Invitrogen), the dual luciferase reporter gene experiment was performed by using the Duo-Lite Luciferase Assay System (Vazyme) according to the manufacturer's protocol. The luminescence was measured using Synergy 2 multimode reader (Gene Company).

Table 1: The primer sequences used in the ChIP assay.

Gene symbols	Primers
Lama2	Forward: GCTTCCAACCAGTGGAGTGAT
	Reverse: GACTGTCCCAAGGTCATGGT
Pla2g4a-p1	Forward: CCCTAGGCAACTGATGTGCT
	Reverse: AAGCCCATTGCCTCTGTGTT
Pla2g4a-p2	Forward: GTGACTTGATCCGTGGCACT
	Reverse: GCAGGGTCTTATGTAGCCCA
Samsn1	Forward: CAGGCCATTTAACCAGAGCC
	Reverse: GTGATGCTACCGACTGCTCA

2.6. RNA Extraction and RT-qPCR. For the stable N2a lentivirus strains, RNA extraction was performed until the cell confluence reached approximately 80%. For primary hippocampal NSCs, the RNA was extracted 7 days after induced differentiation in DMEM/F-12 supplementing with 1% FBS and 100 U/mL penicillin-streptomycin 24 h after plasmid transfection or 48 h after lentivirus infection at 37°C with 5% CO_2. As described previously [26], total RNA was extracted using Total RNA Isolation Reagent (Shanghai Pufei Biotechnology), cDNA synthesis was performed with a RevertAid First Strand cDNA Synthesis kit (Thermo Fisher Scientific), and RT-qPCR was performed with Universal SYBR Green Master Mix (Roche Diagnostics) according to the manufacturer's protocol using the following PCR conditions: 95°C for 10 min, followed by 40 cycles of 95°C for 30 s, 60°C for 30 s and 72°C for 40 s, followed by a final elongation step of 10 min at 72°C. Gene expression was normalized to β-actin expression calculated using the $2^{-\Delta\Delta CT}$ method [27]. The primer sequences are shown in Table 2.

2.7. Western Blot. The cells were harvested when N2a stable lentivirus strains reached 80-90% confluence or primary hippocampal NSCs were induced to differentiate for 7 days using DMEM/F-12 supplemented with 1% FBS 24 h after plasmid transfection or 48 h after lentivirus infection at 37°C with 5% CO_2. In brief, cell monolayers were washed with PBS and harvested in Mammalian Protein Extraction Reagent (Thermo Fisher Scientific) containing Protease Inhibitor Cocktail (Thermo Fisher Scientific). Equal amounts of protein were fractionated in SDS-PAGE gels (Epizyme Biotech) and transferred onto a 0.45 μm PVDF membrane. The membranes were probed at 4°C overnight after being blocked in 5% skim milk-TBST with the following primary antibodies: anti-β-actin (Abcam), anti-Brn4 (Abcam), anti-Lama2 (Abcam), and anti-Tuj1 (Abcam) at 1 : 1,000; anti-GFAP (Abcam) at 1 : 2,000; anti-Samsn1 (Proteintech) at 1 : 3,000; anti-HA (Sigma) at 1 : 20,000. Then, incubation was performed for 2 h at room temperature (RT) with respective HRP-labeled secondary antibodies (Abcam) diluted at 1 : 5,000. The results were visualized by ChemiDoc Touch Imaging System (Bio-Rad) with Clarity Western ECL Substrate (Bio-Rad). The protein expression was normalized to β-actin bands.

Table 2: The primer sequences used in the RT-qPCR.

Gene symbols	Primers
β-Actin	Forward: CTGAGAGGGAAATCGTGCGT
	Reverse: AGGAAGGCTGGAAAAGAGCC
Brn4	Forward: GACGCCAACCTCTGATGAGT
	Reverse: TACCATACAGTGTGCCCAGC
Arhgap30	Forward: TGCAGAGTTTGTGCAAGAGT
	Reverse: TGGGAGTTCTCTGAAGTAGGC
Col5a2	Forward: GAGTGCTGTCCGGTGTGC
	Reverse: ACGACCGCGTATACCTGTTA
Ddr2	Forward: ACGAAAGTGCTACCAACGGT
	Reverse: AGTAGACAGCAGTGGGTTCC
Dock2	Forward: CATGACCGGATGGAGGAGTG
	Reverse: CTTTCTGCGGGGACTTTGCT
Efemp1	Forward: CCAGATGCTTGCAAAGGTGGA
	Reverse: CAGTGGTGGCACCTGACGAA
Efhc1	Forward: GTCTGTCATCGAGCCCGTAG
	Reverse: TCGGAAGGTTTTGCCGTACA
Fyb	Forward: GGGAGTAACCCGACAGAGGA
	Reverse: CTGCCAAGGGTGGTTTTGTG
Irx1	Forward: ACGAGCGTGATGGCGAC
	Reverse: GGCGAATCTTGAGACTTGAGTG
Lama2	Forward: GAAGTGCATCTCTCCTCGGG
	Reverse: CACTTCGATGGGCTGTTCCT
Pla2g4a	Forward: GCACTGTATGAGTCGGGGATT
	Reverse: CTCCTCGGGACCTTTCTCTG
Pros1	Forward: GTCCTTGGTGGATTCTCGCT
	Reverse: GCTGATCCGAGCACAGAGAT
Rgs9	Forward: CTTCGGTGTCTCTTGGAGGAA
	Reverse: TCCACTCGCATCTTGGTTGG
Rnf213	Forward: AAGACCTGCTAGTTCACGCC
	Reverse: CGACTGGAAGACCACAGTCC
Samsn1	Forward: AGCCAGCGACTCTATGGACA
	Reverse: GGCTGTCATCATCCAGTCGG
Tmem117	Forward: TGGGCATCCGCAATGAAAGT
	Reverse: GACAAGCACCACCACGGAAG
Trpm2	Forward: CCTTCGATGAGCCAGATGCT
	Reverse: AAGGCACCTTCTCGTTAGGC
MAP2	Forward: ATCGCCAGCCTCAGAACAAA
	Reverse: GGGAGGATGGAGGAAGGTCT
S100b	Forward: CGAGAGGGTGACAAGCACAA
	Reverse: CCATCCCCATCTTCGTCCAG

2.8. EdU Incorporation. A Cell-Light EdU Apollo567 in vitro kit (RiboBio) was used for EdU combination assay according to the manufacturer's protocol. The cells were incubated in the EdU medium for 2 h at 37°C 24 h after plasmid transfection or 48 h after lentivirus infection. After double staining with Hoechst (Beyotime) cells were analyzed under a fluorescence microscope (Zeiss AG) using x400 magnification. EdU and Hoechst-labeled cells in the 10 random fields were counted, and the percentage of EdU/Hoechst was calculated for comparison between groups.

2.9. Cell Cycle Analysis. As described [26], NSCs were harvested 24 h after plasmid transfection or 48 h after lentivirus infection and then fixed with ice-cold 75% ethanol at -20°C for at least 24 h. Next, cells were stained with Hoechst 33342 solution (BD Biosciences) and incubated for 30 min at RT, washed, and suspended in BD Pharmingen™ Stain Buffer (BD Biosciences). The results were analyzed using the BD FACSCalibur system (BD Biosciences) with ModFit LT v3.3.11 software (Verity Software House).

2.10. CCK-8 Assay. Cell Counting Kit-8 (Dalian Meilun Biology Technology) was used in the CCK-8 assay following the manufacturer's instructions. 1×10^4 NSCs were plated in poly-L-lysine-coated (Sigma) 24-well plates and cultured at 37°C for 24 h. Then, the cells were infected or transfected, respectively, with the lentiviruses or plasmids. After the infection or transfection for 0, 1, 2, 3, and 4 days, 50 μL CCK-8 reagent was added to each well and incubated at 37°C for 2 h. The optical density (OD) was examined at a wavelength of 450 nm (OD 450 nm) using the Synergy 2 multmode reader.

2.11. Immunofluorescence Staining. The primary hippocampal NSCs were induced to differentiate for 7 days using DMEM/F-12 supplemented with 1% FBS 24 h after plasmid transfection or 48 h after lentivirus infection at 37°C with 5% CO_2. Briefly, cell monolayers were washed with PBS and fixed in 4% formaldehyde for 20 min at RT. After being blocked in 10% goat serum-PBS containing 0.3% Triton X-100, the cells were in turn incubated at 4°C overnight with anti-Tuj1 antibody (Abcam), at RT for 2 h with Alexa Fluor 555-labeled secondary antibodies (Invitrogen), and at RT for 10 min with Hoechst (Beyotime). The primary antibodies were as follows: mouse anti-microtubule associated protein (MAP) 2 (1 : 200), mouse anti-Nestin (1 : 100) (both from Millipore); rabbit anti-glial fibrillary acidic protein (GFAP, 1 : 1,000), rabbit anti-β-III-tubulin (Tuj1, 1 : 1,000) (both from Abcam); rabbit anti-Ki67 (1 : 200, Sigma). The secondary antibodies were Alexa Fluor 568-conjugated goat anti-rabbit IgG (1 : 1,000) and Alexa Fluor 488-conjugated goat anti-mouse IgG (1 : 1,000) (both from Invitrogen).

2.12. Statistical Analysis. GraphPad Prism 8.0 software (GraphPad Software, La Jolla, CA, USA) was used for statistical analysis. The data were presented as the mean ± SEM based on at least three independent samples in each group. Experiments with two experimental groups were evaluated using an unpaired Student's two-tailed t-test. In experiments with more than two experimental groups, one-way analysis of variance was used. $P < 0.05$ was considered statistically significant.

3. Results

3.1. Culture and Identification of Hippocampal NSCs. The process of cell culture and differentiation was conducted as shown in the schematic in Figure 1(a). The single cells digested from the third generation of neurospheres

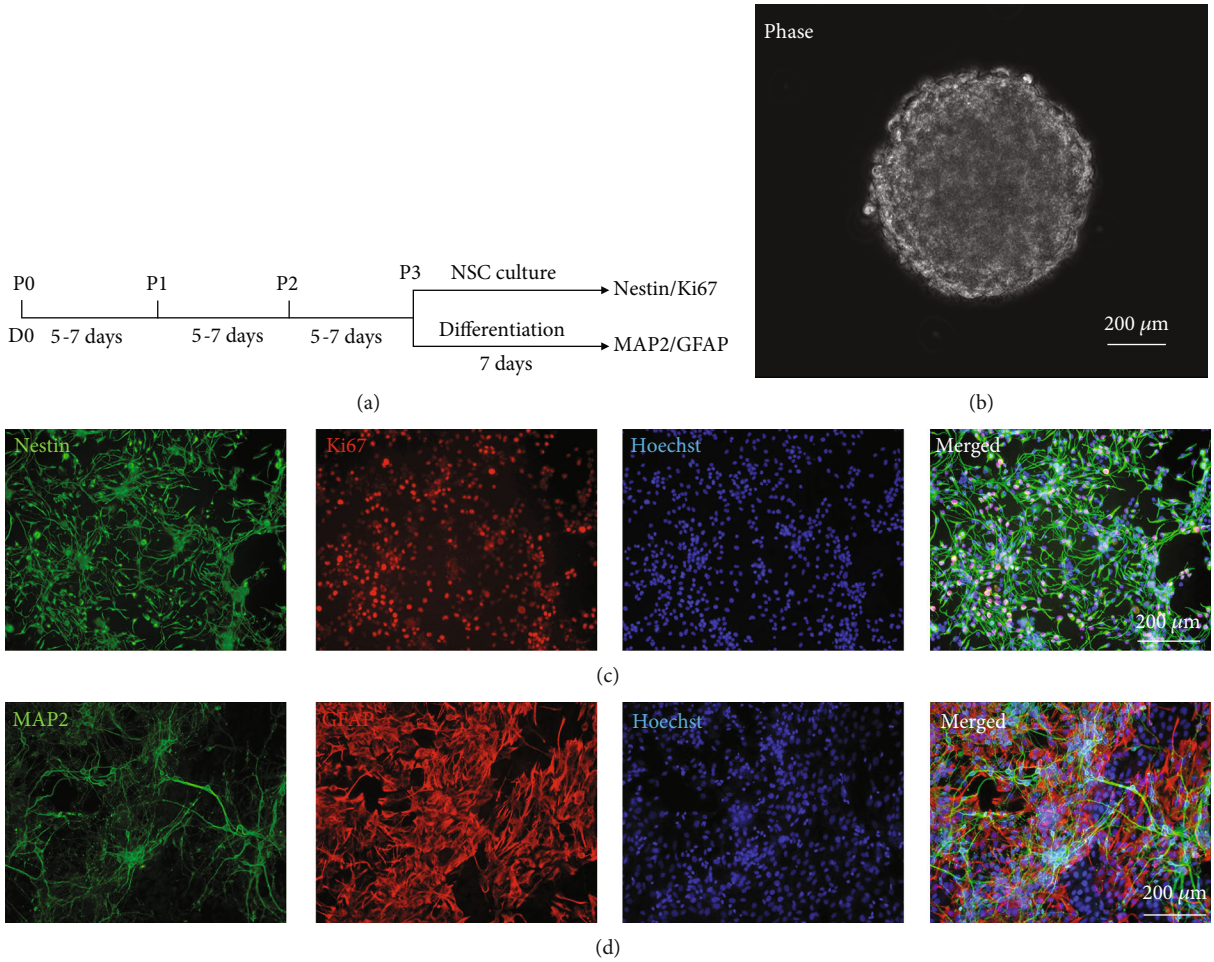

Figure 1: Culture and identification of hippocampal NSCs. (a) The schematic of the culture and differentiation of NSCs. (b) A representative image showing the morphology of the third-generation neurosphere derived from the hippocampi of the neonatal (1 day) ICR mice. (c) Immunocytochemistry staining on the third generation showed that most of the cells expressed Nestin (green). and Ki67 (red). (d) After being cultured in a differentiation medium for 7 d, immunocytochemistry analysis showed that some cells could express MAP2 (green) and GFAP (red). Nuclei were stained with Hoechst (blue). Scale bar = 200 μm.

(Figure 1(b)) were cultured in an NSC culture medium for 7 days. Immunocytochemistry analysis showed that about 95.47% of cells were Nestin-positive (Figure 1(c)), indicating that these cells were embryonic. And about 98.35% of cells were positive for Ki67 (Figure 1(c)), indicating that cells were in the state of proliferation. To further determine the multiple differentiation potential, the single cells of the third generation were cultured in the differentiation medium for 7 days. Immunocytochemistry analysis showed that some cells could express MAP2 or GFAP (Figure 1(d)), which indicated that cells had the ability to differentiate into neurons and astrocytes. Therefore, we considered that the cells we extracted from the hippocampus and purified were NSCs.

3.2. Brn4 Bound to the Promoters of Lama2 and Samsn1 and Promoted Their Expression. Previous studies have shown that transcription factor Brn4 can promote the differentiation of hippocampal NSCs into neurons [15, 16], but the specific mechanism is not clear. Therefore, we used RNA-seq and ChIP-seq to detect the changes in the gene expression level of the cells after forced Brn4 overexpression. The RNA-seq data were analyzed with FDR < 0.001 and Fold Change ≥ 2 as screening criteria, and the results showed that the transcription level of 638 genes elevated after Brn4 overexpression. The ChIP-seq data were analyzed with P value < 0.001 as the screening criteria, and the results showed that 771 genes were involved in the Brn4 binding sequence. There were totally 16 genes in the intersection of the two sequencing results (Figure 2(a)). In this study, we took the 16 genes, overlapping genes of RNA-seq and ChIP-seq, as the breakthrough to explore the exact downstream target genes bound by Brn4.

At first, we established two different stable lentivirus strains (Brn4 overexpression and an empty viral vector) in N2a cells and verified the overexpression efficiency of Brn4 using Western blot (Figures 2(b) and 2(c)) and RT-qPCR (Figure 2(d)). Then, the mRNA levels of the 16 overlapping genes were detected by RT-qPCR. The results showed that the transcription levels of three genes, Lama2, Pla2g4a, and Samsn1, were increased after Brn4 overexpression

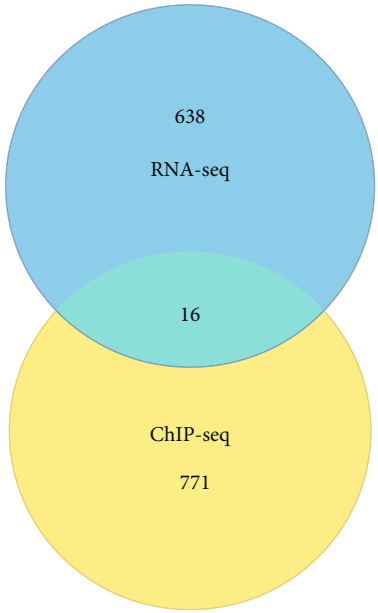

Genes	GO terms
Arhgap30	Positive regulation of GTPase activity
Col5a2	Eye morphogenesis
Ddr2	Cell adhesion
Dock2	Immunological synapse formation
Efemp1	Peptidyl-tyrosine phosphorylation
Efhc1	Cellular calcium ion homeostasis
Fyb	Mast cell activation
Irx1	Metanephros development
Lama2	Axon guidance
Pla2g4a	Positive regulation of vesicle fusion
Pros1	Positive regulation of phagocytosis
Rgs9	Positive regulation of GTPase activity
Rnf213	ATP catabolic process
Samsn1	Negative regulation of adaptive immune response
Tmem117	Biological process
Trpm2	Transmembrane transport

(a)

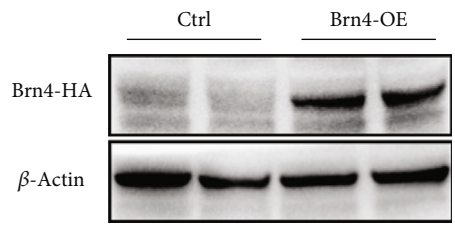

(b)

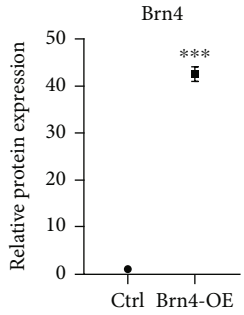

(c)

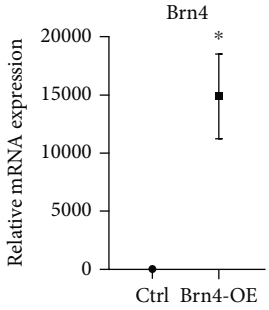

(d)

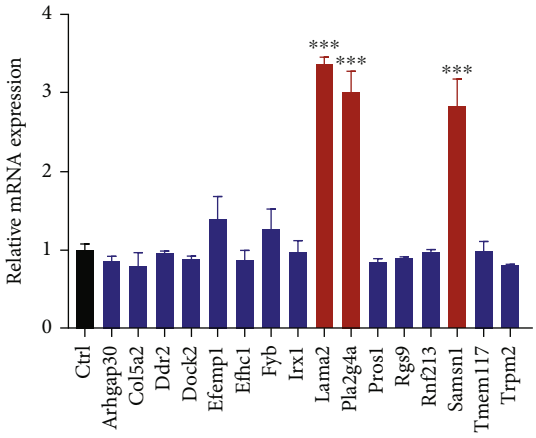

(e)

Figure 2: Continued.

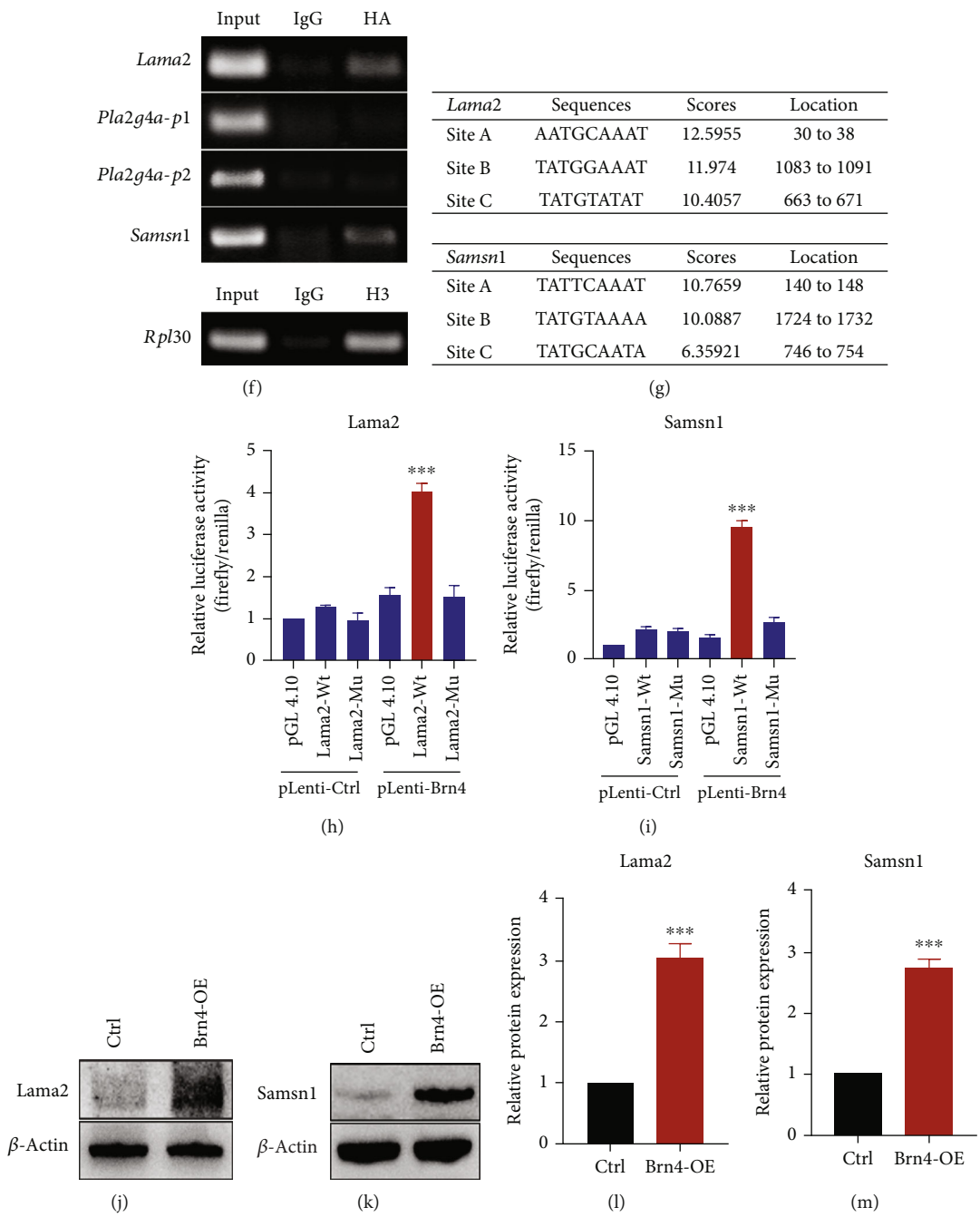

Lama2	Sequences	Scores	Location
Site A	AATGCAAAT	12.5955	30 to 38
Site B	TATGGAAAT	11.974	1083 to 1091
Site C	TATGTATAT	10.4057	663 to 671

Samsn1	Sequences	Scores	Location
Site A	TATTCAAAT	10.7659	140 to 148
Site B	TATGTAAAA	10.0887	1724 to 1732
Site C	TATGCAATA	6.35921	746 to 754

Figure 2: Brn4 binds to the promoters of Lama2 and Samsn1 and promotes their expression. (a) Overlapping genes of RNA-seq and ChIP-seq. (b, c) Representative immunoblots of Brn4-HA and β-actin in the N2a stable Brn4-overexpressed lentivirus strains (b) and quantification of Brn4-HA protein level normalized to β-actin (c). (d) Quantification of Brn4 mRNA level normalized to β-actin. (e) Quantification of mRNA levels for the overlapping genes between RNA-seq and ChIP-seq normalized to β-actin. (f) Nucleic acid electrophoresis for ChIP-PCR assay in the N2a stable Brn4-overexpressed lentivirus strains. (g) Sequences of the top three Brn4 binding sites on the Lama2 and Samsn1 promoters with the highest scores. (h, i) Dual-luciferase reporter gene experiment using N2a cells. (j–m) Representative immunoblots of Lama2, Samsn1, and β-actin in the N2a stable Brn4-overexpressed lentivirus strains (j, k) and quantification of Lama2 and Samsn1 protein levels normalized to β-actin (l, m). Error bars represent the mean ± SEM. $n = 3$. $^{*}P < 0.05$, $^{***}P < 0.001$. Abbreviations: Ctrl: control; Brn4-OE: Brn4-overexpression.

(Figure 2(e)). We constructed PCR primers using the promoter sequences of the three genes as a template. Among them, Pla2g4a has two transcripts with completely different promoters, so we designed different primers for the two promoters to analyze independently. ChIP assay was performed on the Brn4 overexpressing stable strain. The results indicated that Brn4 bound to the promoters of Lama2 and Samsn1, while there was no obvious Brn4 binding site in

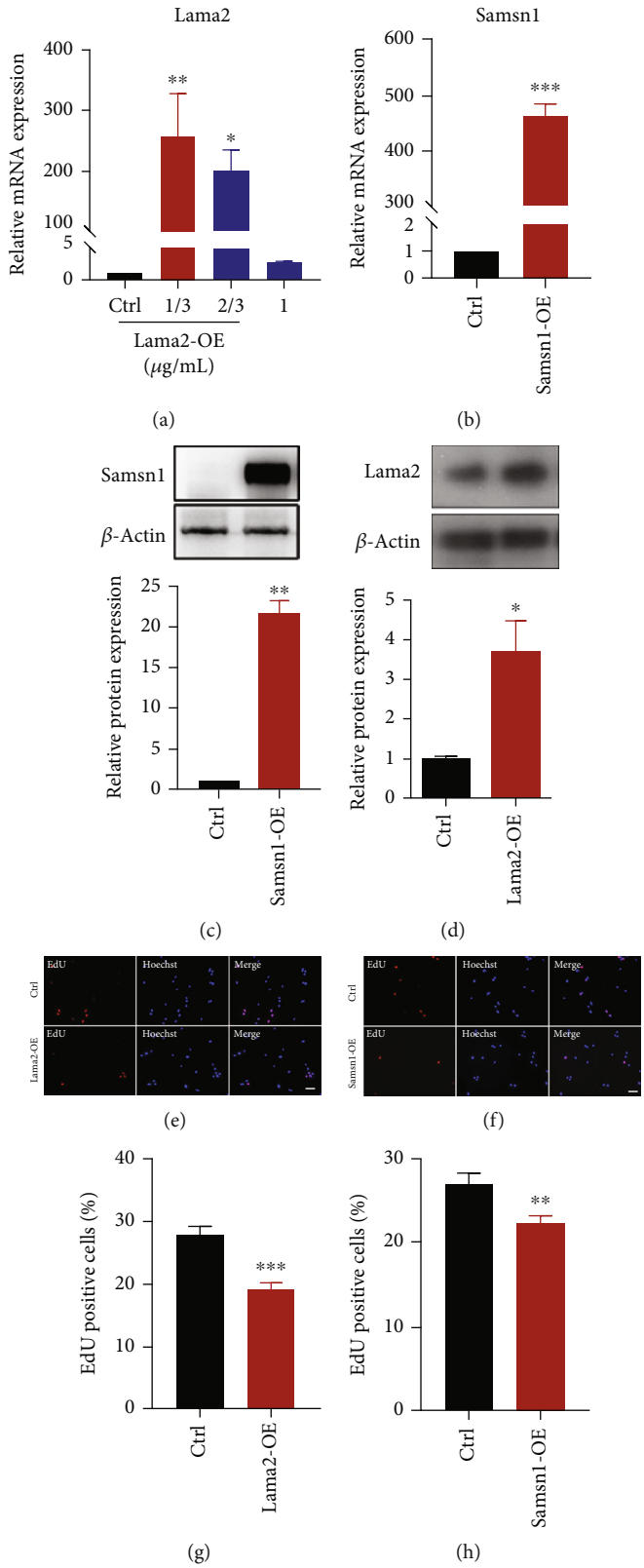

Figure 3: Continued.

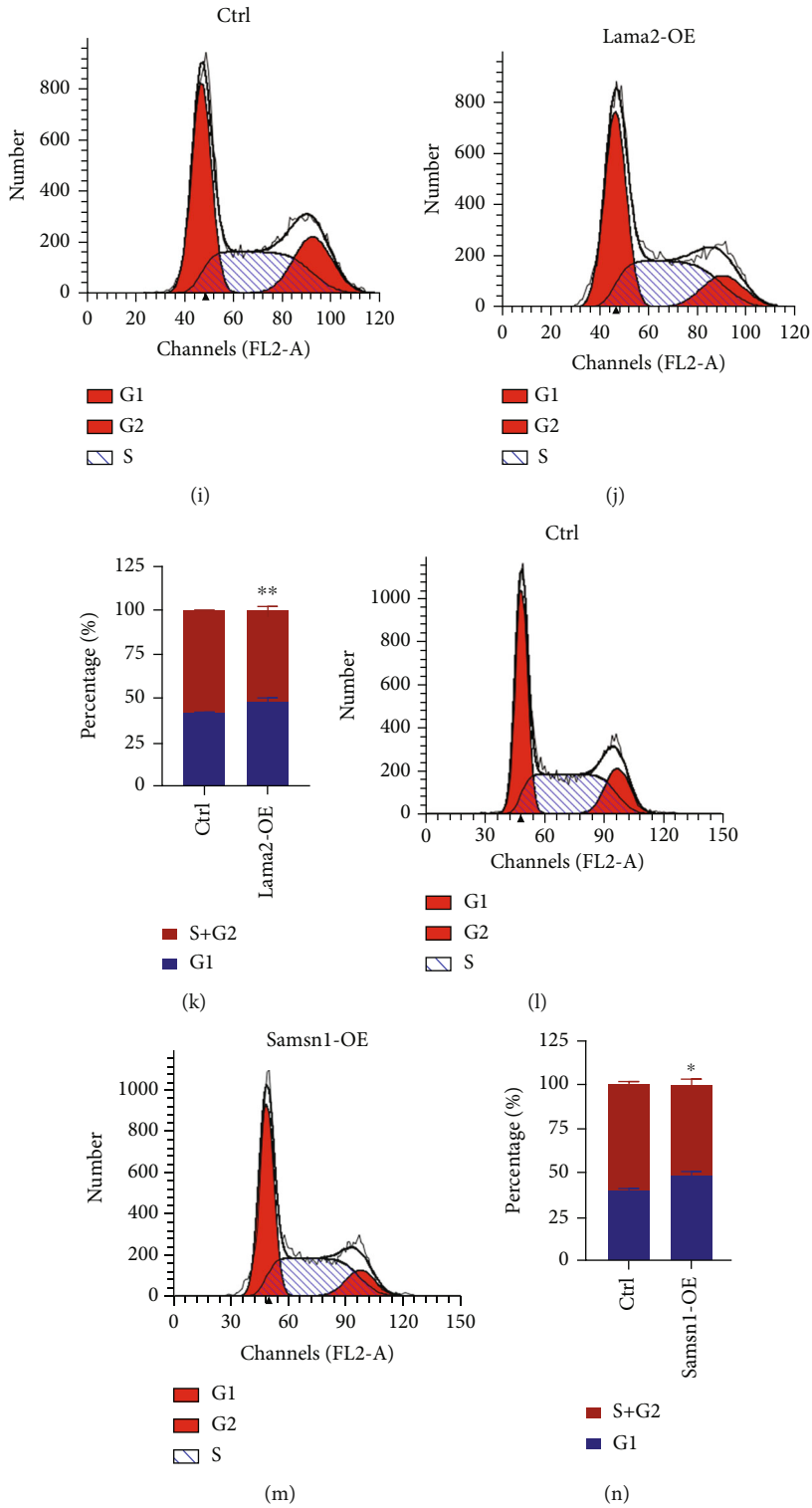

Figure 3: Continued.

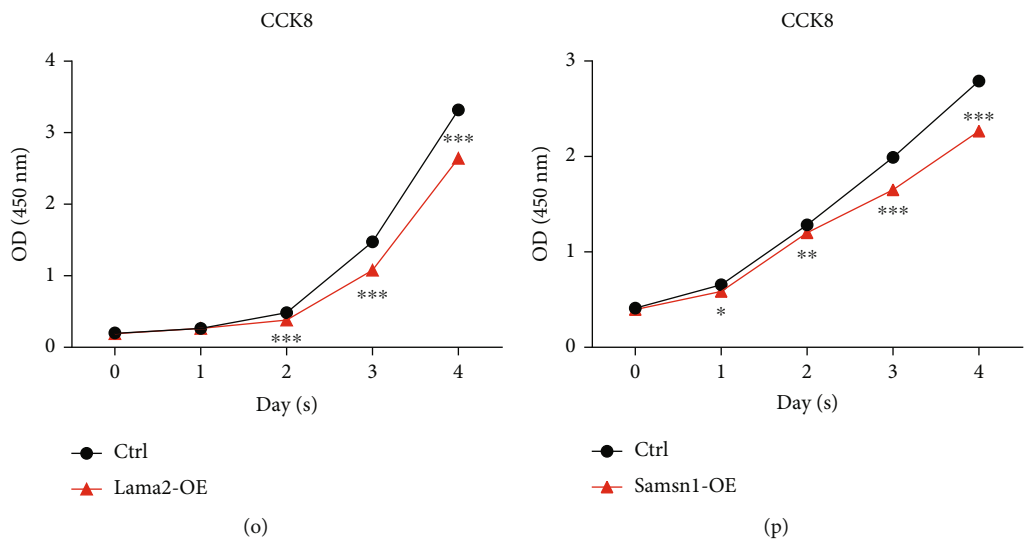

Figure 3: Lama2 activation or Samsn1 overexpression inhibits the proliferation of hippocampal NSCs. (a) Quantification of Lama2 mRNA level normalized to β-actin in the hippocampal NSCs which were transfected with different concentrations of Lama2 CRISPR SAM coactivated plasmid. (b) Quantification of Samsn1 mRNA level normalized to β-actin in the hippocampal NSCs which were infected by Samsn1 overexpression lentivirus. (c) The upper panel is the representative immunoblots of Samsn1 and β-actin after being infected by Samsn1 overexpression lentivirus; the lower panel is the quantification of Samsn1 protein level normalized to β-actin. (d) The upper panel is the representative immunoblots of Lama2 and β-actin after being infected by Lama2 CRISPR SAM coactivated plasmid; the lower panel is the quantification of Lama2 protein level normalized to β-actin. (e, f) Representative EdU-staining in primary hippocampal NSCs. Bar = 20 μm. (g, h) Quantification of EdU-positive cells normalized to Hoechst. (i–k) Representative cell cycle distribution analyzed by flow cytometry in primary hippocampal NSCs after Lama2 activation (i, j) and quantification for NSCs in the different stages of the cell cycle (k). (l–n) Representative cell cycle distribution analyzed by flow cytometry in primary hippocampal NSCs after Samsn1 overexpression (l, m) and quantification for NSCs in the different stages of the cell cycle (n). (o, p) CCK-8 assay in primary hippocampal NSCs 0, 1, 2, 3, 4 days after plasmid transfection or virus infection. Error bars represent the mean ± SEM. $n = 3$. $^{*}P < 0.05$, $^{**}P < 0.01$, $^{***}P < 0.001$. Abbreviations: Ctrl: control; Lama2-OE: Lama2-overexpression; Samsn1-OE: Samsn1-overexpression.

the promoters of Pla2g4a (Figure 2(f)). These results indicated that Brn4 may bind to the promoters of Lama2 and Samsn1 and promote their mRNA expression.

Next, we analyzed the binding sites of Lama2 and Samsn1 promoter regions with Brn4 using the JASPAR website. The top three sites with the highest scores were, respectively, selected as targets (Figure 2(g)), which were deleted simultaneously to construct dual luciferase reporter gene mutation plasmids. The results of the dual luciferase reporter gene experiment showed that the top three sites analyzed by the JASPAR website contained the effective Brn4-bound sites of the Lama2 and Samsn1 promoters (Figures 2(h) and 2(i)). Western blot demonstrated that, consistent with the mRNA, the level of Lama2 and Samsn1 protein also increased significantly after Brn4 overexpression (Figures 2(j)–2(m)). The above results revealed that Brn4 bound to the specific sites of the Lama2 and Samsn1 promoter regions and promoted their expression at the protein level.

3.3. Lama2 And Samsn1 Partially Mediated the Inhibitory Effect of Brn4 on NSC Proliferation. Firstly, we used Lama2 CRISPR SAM coactivated plasmids and Samsn1 overexpression lentiviruses to activate or force their expression. RT-qPCR results showed that the optimal transfection concentration of Lama2 plasmids was 1/3 μg/mL medium (Figure 3(a)). Western blot showed that the level of Lama2 protein was also upregulated after activation using the Lama2 CRISPR SAM coactivated plasmids (1/3 μg/mL medium, Figure 3(d)). Samsn1 overexpression lentivirus also significantly increased its mRNA and protein expression levels (Figures 3(b) and 3(c)). Compared with the control group, the proportion of EdU positive cells decreased significantly after Lama2 activation or Samsn1 overexpression in primary hippocampal NSCs, indicating that the cell proliferation rate was slowed down by Lama2 and Samsn1 forced expresssion (Figures 3(e)–3(h)). Cell cycle analysis by flow cytometry revealed that after Lama2 activation or Samsn1 overexpression, the proportion of cells in the G1 phase increased, while the proportion of cells in the S phase and G2 phase decreased, suggesting that the cell division ability was reduced (Figures 3(i)–3(n)). CCK-8 assay was performed to value the growth of the cells at 0, 1, 2, 3, and 4 days after plasmid transfection or lentivirus infection. The results showed that the value of CCK-8 declined in time-dependent manner after Lama2 activation or Samsn1 overexpression compared with the control group, supporting the above result that Lama2 or Samsn1 could inhibit the proliferation of hippocampal NSCs (Figures 3(o) and 3(p)).

Next, RT-qPCR and Western blot were performed to detect the knockdown efficiency of Lama2 or Samsn1 shRNA lentivirus. The results indicated that shRNA-78 and shRNA-75, one of the three shRNA sequences of Lama2 and Samsn1, respectively, had the best knockdown efficiency

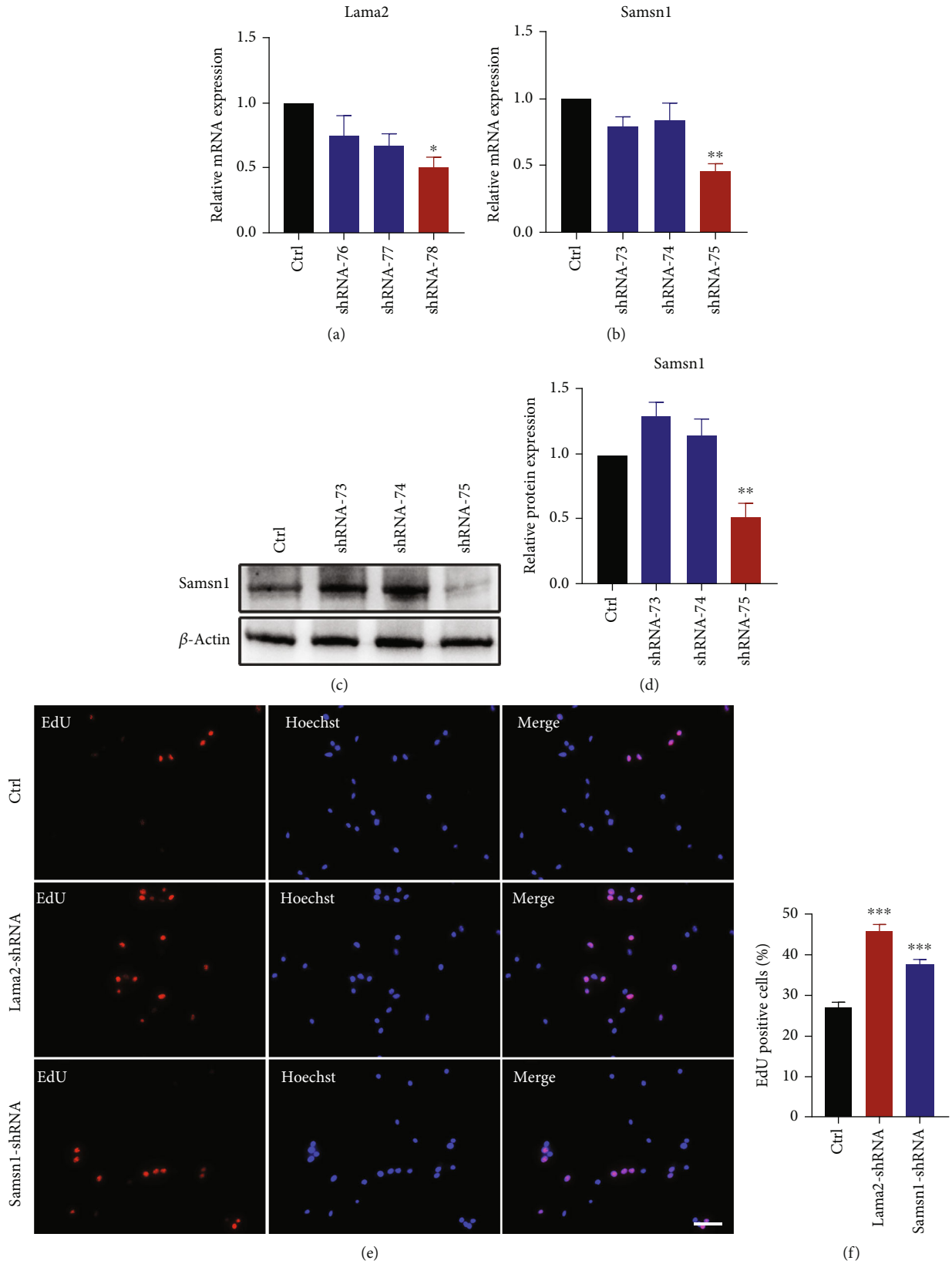

Figure 4: Continued.

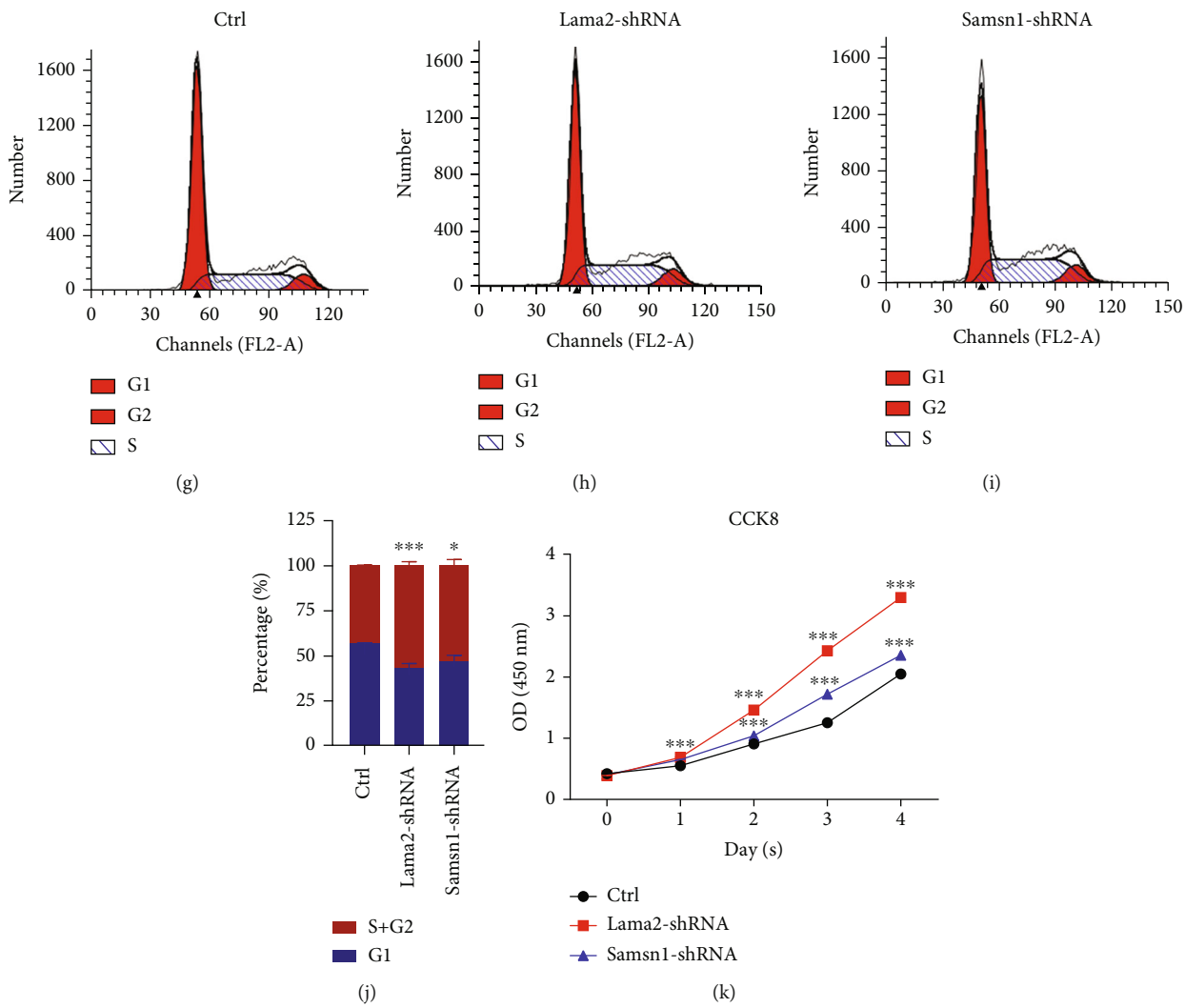

Figure 4: Lama2 or Samsn1 knockdown promotes the proliferation of hippocampal NSCs. (a, b) Quantification of Lama2 and Samsn1 mRNA levels normalized to β-actin in the primary hippocampal NSCs which were infected with Lama2-shRNA lentivirus or Samsn1-shRNA lentivirus. (c, d) Representative immunoblots of Samsn1 and β-actin after being infected by Samsn1-shRNA lentivirus (c) and quantification of Samsn1 protein level normalized to β-actin (d). (e) Representative EdU-staining after Lama2 or Samsn1 knockdown in primary hippocampal NSCs. Bar = 20 μm. (f) Quantification of EdU-positive cells normalized to Hoechst. (g–j) Representative cell cycle distribution analyzed by flow cytometry after Lama2 or Samsn1 knockdown in primary hippocampal NSCs (g–i) and quantification for NSCs in the different stages of the cell cycle (j). (k) CCK-8 assay in primary hippocampal NSCs 0, 1, 2, 3, and 4 days after lentivirus infection. Error bars represent the mean ± SEM. $n = 3$. $^{*}P < 0.05$, $^{**}P < 0.01$, $^{***}P < 0.001$.

(Figures 4(a)–4(d)), which were used and named Lama2-shRNA group or Samsn1-shRNA group in the subsequent experiments. Compared with the control group, the number of EdU positive cells increased significantly after Lama2 or Samsn1 knockdown in primary hippocampal NSCs, suggesting that the cell proliferation rate increased (Figures 4(e) and 4(f)). Flow cytometry cell cycle analysis results revealed that after Lama2 or Samsn1 knockdown, the proportion of cells in the G1 phase decreased, while the proportion of cells in the S phase and G2 phase increased, indicating that the ability of cell division was improved (Figures 4(g)–4(j)). CCK-8 assay showed that the number of living cells increased after Lama2 or Samsn1 knockdown compared with the control group, and this difference became more obvious with time (Figure 4(k)). These results above confirmed that Lama2 and Samsn1 had a negative effect on hippocampal NSCs proliferation.

Then, we investigated the roles of Lama2 and Samsn1 in the Brn4-knockdown NSCs. The results of cell cycle analysis by flow cytometry showed that after Brn4 knockdown, the proportion of cells in the G1 phase decreased, while the proportion of cells in the S phase and G2 phase increased. However, activation of Lama2 and overexpression of Samsn1 reversed the increase of cell proportion in the S phase and G2 phase induced by Brn4 knockdown (Figures 5(a)–5(f)). Similarly, Brn4 knockdown increased the CCK-8 value of NSCs which was partially reversed by Lama2 activation and Samsn1 overexpression (Figure 5(g)). All the above results confirmed that Lama2 activation and Samsn1 overexpression could inhibit the enhancement of cell proliferation

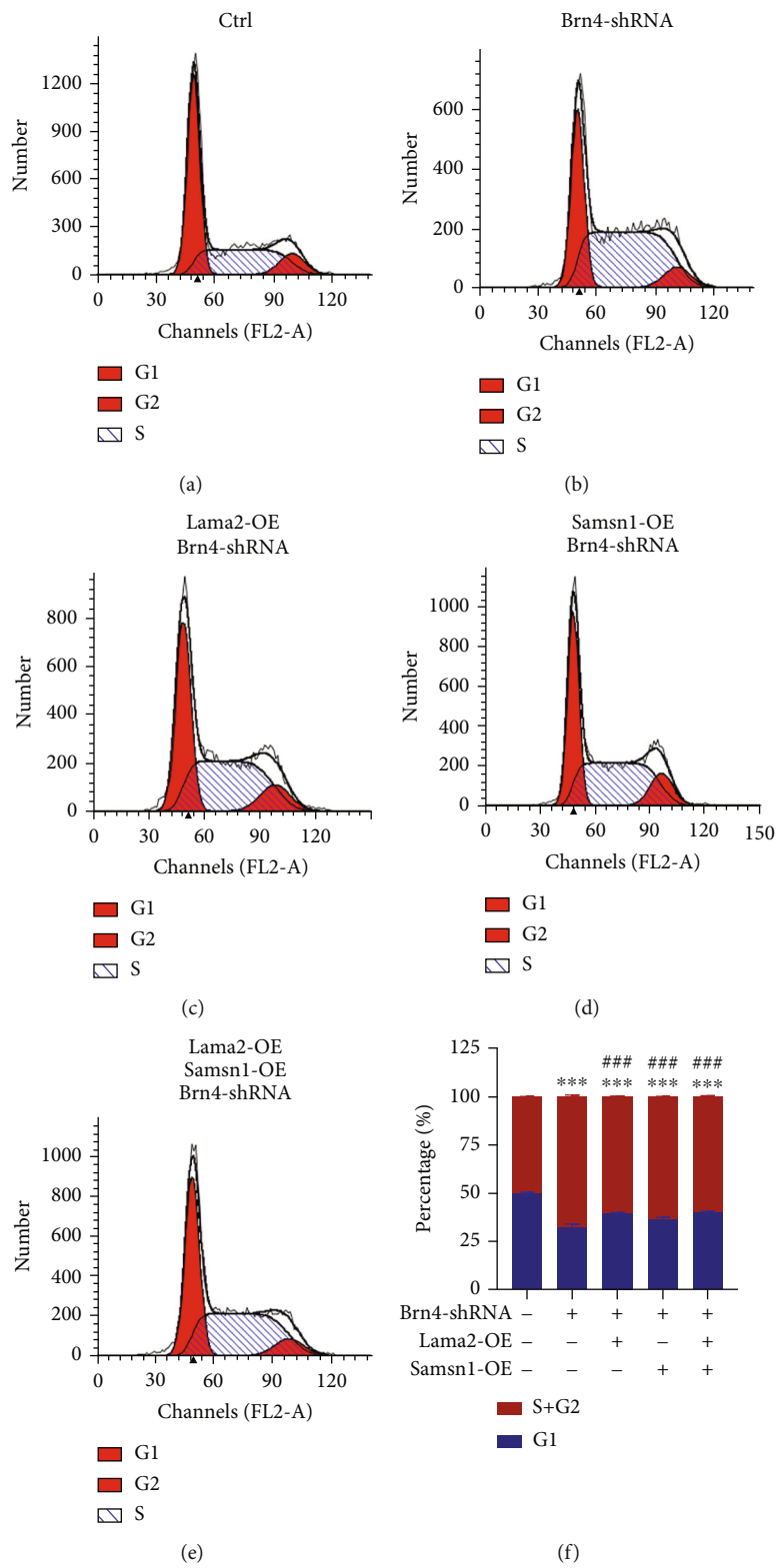

Figure 5: Continued.

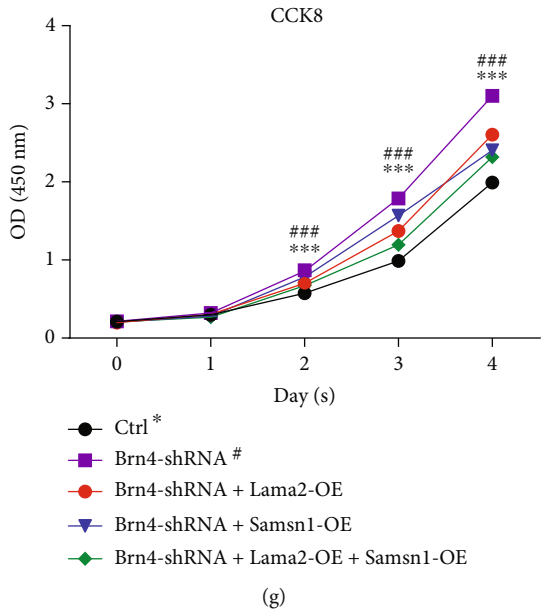

Figure 5: Lama2 and Samsn1 partially reverse the inhibitory effect of Brn4 on NSCs proliferation. (a–f) Representative cell cycle distribution analyzed by flow cytometry for the primary hippocampal NSCs with different treatments at the same time (a–e) and quantification for NSCs in the different stages of the cell cycle (f). (g) CCK-8 assay in primary hippocampal NSCs 0, 1, 2, 3, and 4 days after lentivirus infection or plasmid transfection simultaneously. Error bars represent the mean ± SEM. $n = 3$. $^{***}P < 0.001$ *vs.* Ctrl, $^{###}P < 0.001$ *vs.* Brn4-shRNA.

induced by Brn4 knockdown, which indicated that they partially mediated the negative effect of Brn4 on hippocampal NSCs proliferation.

3.4. Lama2 And Samsn1 Promoting Effect of Brn4 on the Differentiation of NSCs into Neurons. In this study, we used neuron-specific class III beta-tubulin (Tuj1) and microtubule-associated protein 2 (MAP2) as neuron markers, glial fibrillary acidic protein (GFAP), and S100 protein subunit B (S100b) as astrocyte markers. Immunofluorescence staining results showed that the proportion of Tuj1 positive cells in the Lama2 activation or Samsn1 overexpression group was higher, indicating that the number of neurons increased, than that in the control group after NSC differentiation was induced by differentiation medium composed of DMEM/F-12 and 1% FBS (Figures 6(a)–6(d)). Western blot and RT-qPCR also demonstrated that the protein and mRNA levels of Tuj1 and MAP2 elevated, while GFAP and S100b were reduced after Lama2 activation or Samsn1 overexpression (Figures 6(e)–6(n)). These results suggested that Lama2 and Samsn1 could promote the differentiation of hippocampal NSCs into neurons. Oppositely, Lama2 or Samsn1 knockdown induced the decrease in the number of Tuj1 positive cells (Figures 7(a) and 7(b)) and the protein or mRNA levels of Tuj1 and MAP2, and the increase of GFAP and S100b (Figures 7(c)–7(g)), indicating that Lama2 or Samsn1 knockdown could inhibit the differentiation of hippocampal NSCs into neurons, but enhance their ability to differentiate into astrocytes.

The results of Western blot and RT-qPCR also showed that Lama2 and Samsn1 could reverse the expression levels of neuron and astrocyte markers which changed after Brn4 knockdown (Figures 8(a)–8(e)). The above results suggested that Lama2 and Samsn1 partially mediated the promoting effect of Brn4 on the differentiation of hippocampal NSCs into neurons. To explore whether there was some connection between Lama2 and Samsn1, we detected the mRNA level of Lama2 and Samsn1 after another gene activation or overexpression. RT-qPCR results suggested that Samsn1 overexpression could not change Lama2 transcription and vice versa (Figures 8(f) and 8(g)), which indicated that each of them possibly mediated the role of Brn4 in an independent way.

4. Discussion

Transcription factor Brn4 is widely expressed in the neural crest and neuroectoderm at the early stage of embryonic nervous system development, while in the hypothalamus, pituitary, and hippocampus at the middle stage [14]. It plays an essential role in the embryonic development of the nervous system, inner ear, and pancreas [28–30]. Our previous studies (unpublished data) have shown that Brn4 can regulate the proliferation and differentiation of hippocampal NSCs, but its downstream mechanism remains unclear.

To explore its target genes, we performed RNA-seq and ChIP-seq after Brn4 overexpression in N2a cells. N2a cells are derived from mouse neuroblastoma which have similar bioactivities as the NSCs and can also be induced to differentiate into neuron-like cells. At present, this cell line is mainly used as NSC or neural progenitor model for pathological research *in vitro* [31]. In our study, we used N2a cells as a tool cell, just to preliminarily explore the possible downstream genes of Brn4, and then verify them on hippocampal NSCs. After RNA-seq and ChIP-seq, we found 16 genes at the intersection of the two sequencing results. Next, among

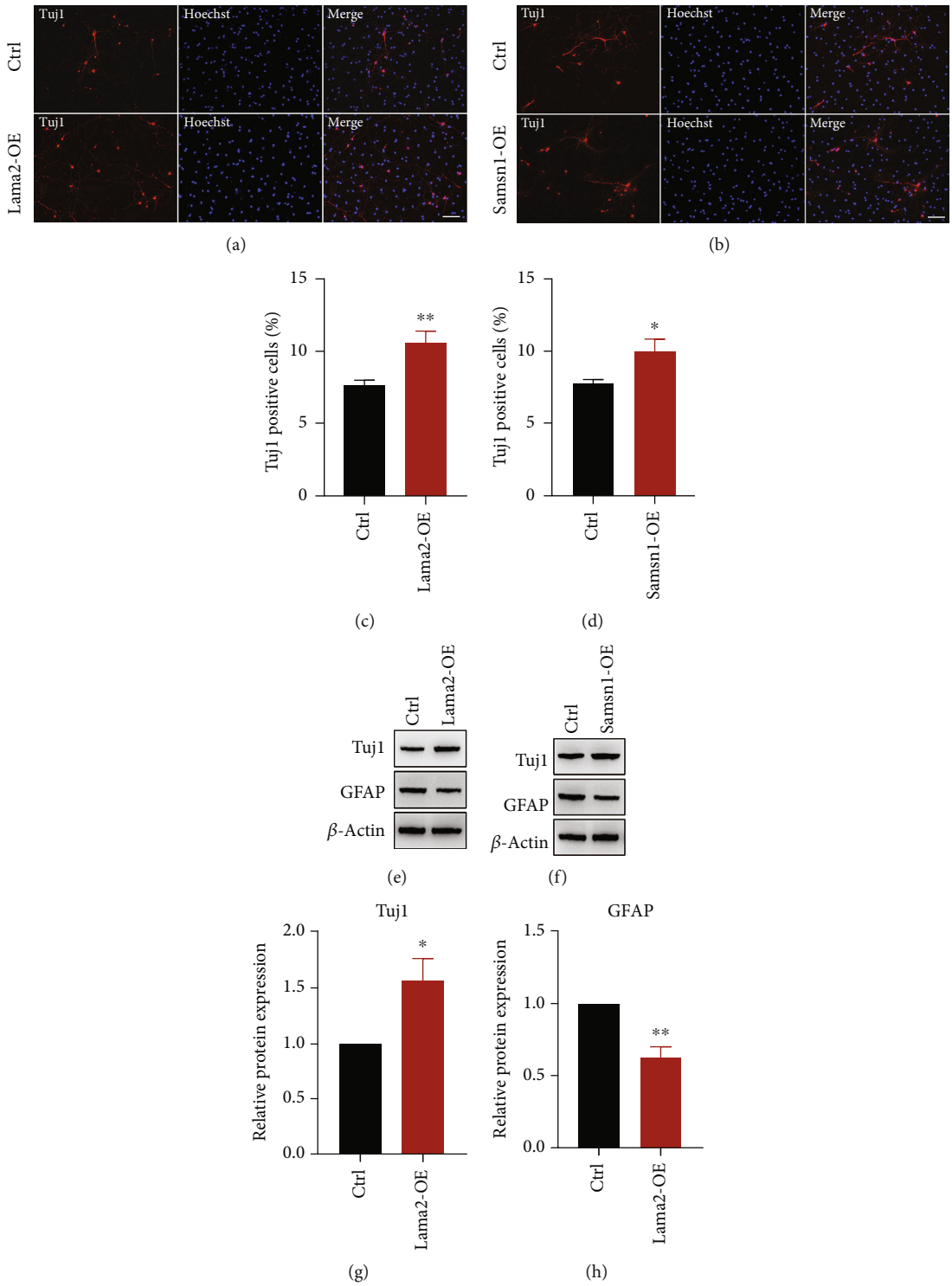

Figure 6: Continued.

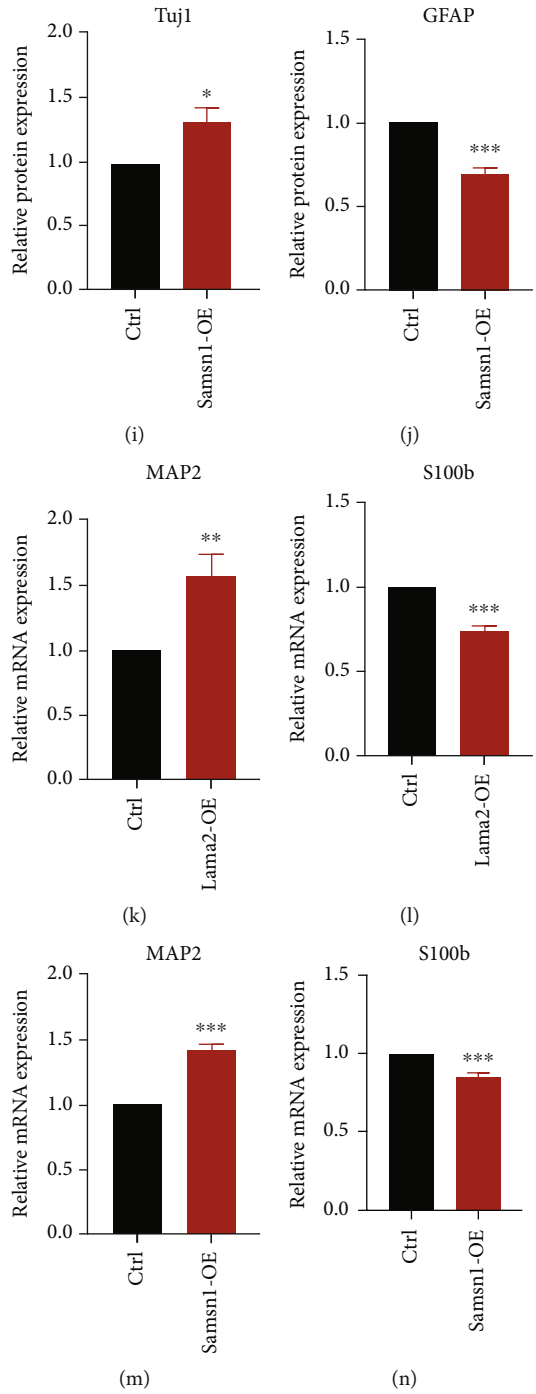

Figure 6: Lama2 activation or Samsn1 overexpression promotes NSCs differentiation into neurons. (a, b) Representative immunostaining for Tuj1 (red) in the primary hippocampal NSCs after induced differentiation for 7 days following plasmid transfection or lentivirus infection. Bar = 50 μm. (c, d) Quantification of Tuj1-positive cells normalized to Hoechst. (e–j) Representative immunoblots of Tuj1, GFAP, and β-actin in the primary hippocampal NSCs after induced differentiation for 7 days following plasmid transfection or lentivirus infection (e, f) and quantification of Tuj1 and GFAP protein levels normalized to β-actin (g–j). (k–n) Quantification of MAP2 and S100b mRNA levels normalized to β-actin after induced differentiation for 7 days following plasmid transfection or lentivirus infection. Error bars represent the mean ± SEM. $n = 3$. $^{*}P < 0.05$, $^{**}P < 0.01$, $^{***}P < 0.001$.

the 16 genes, we verified Brn4 bound to the promoters of Lama2 and Samsn1 and promoted their expression both at mRNA and protein levels using RT-qPCR, ChIP assay, dual luciferase reporter gene experiment, and Western blot. In order to investigate whether Lama2 and Samsn1 regulate the proliferation and differentiation of hippocampal NSCs, we conducted EdU incorporation, cell cycle analysis by flow cytometry, and CCK-8 assay to detect NSC proliferation ability and Tuj1 immunofluorescence staining, RT-qPCR, and Western blot to detect NSCs differentiation ability after

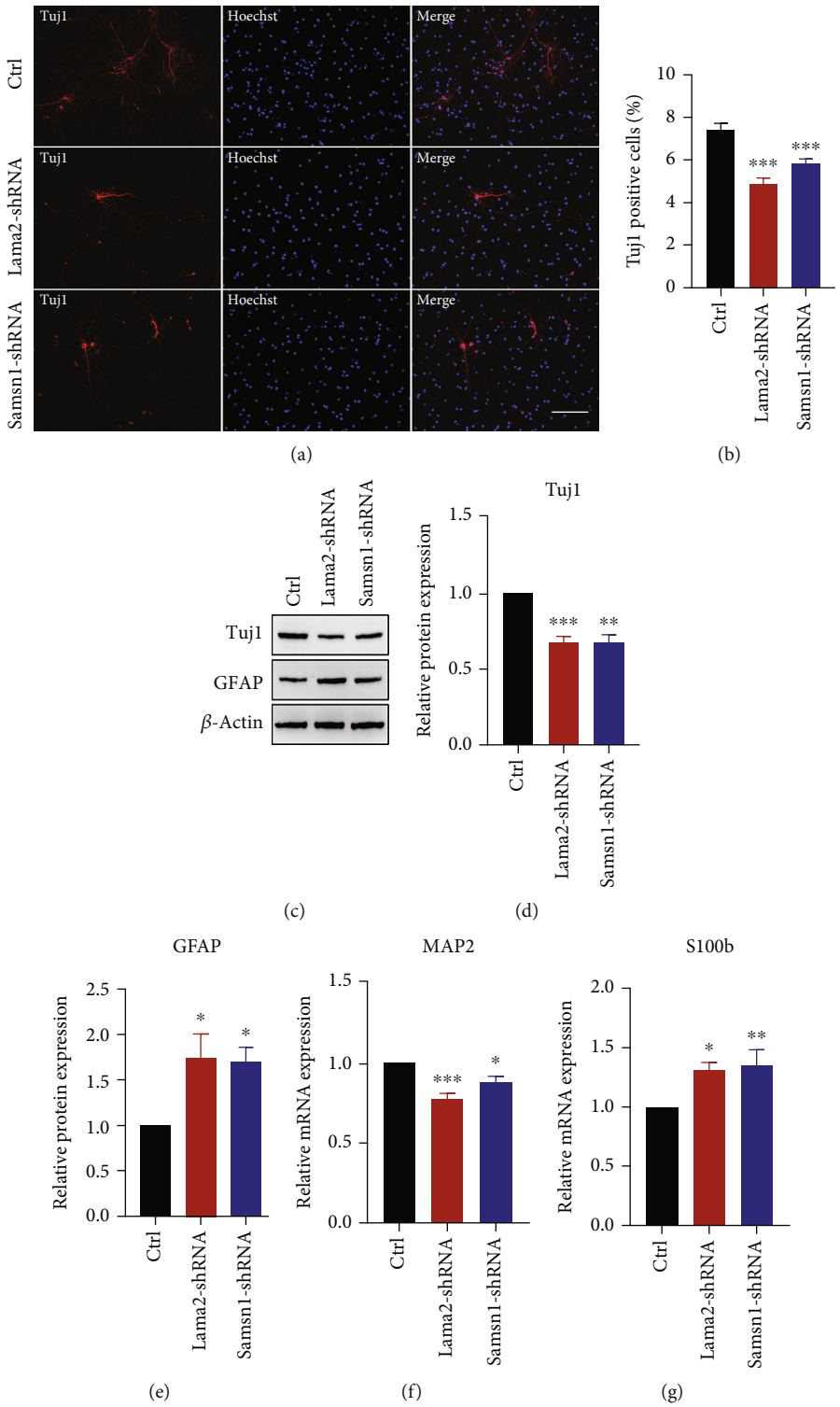

Figure 7: Lama2 or Samsn1 knockdown inhibits NSCs differentiation into neurons. (a) Representative immunostaining for Tuj1 (red) in the primary hippocampal NSCs after induced differentiation for 7 days following lentivirus infection. Bar = 50 μm. (b) Quantification of Tuj1-positive cells normalized to Hoechst. (c–e) Representative immunoblots of Tuj1, GFAP, and β-actin in the primary hippocampal NSCs after induced differentiation for 7 days following lentivirus infection (c) and quantification of Tuj1 and GFAP protein levels normalized to β-actin (d, e). (f, g) Quantification of MAP2 and S100b mRNA levels normalized to β-actin after the NSCs induced differentiation for 7 days following lentivirus infection. Error bars represent the mean ± SEM. $n = 3$. $^{*}P < 0.05$, $^{**}P < 0.01$, $^{***}P < 0.001$.

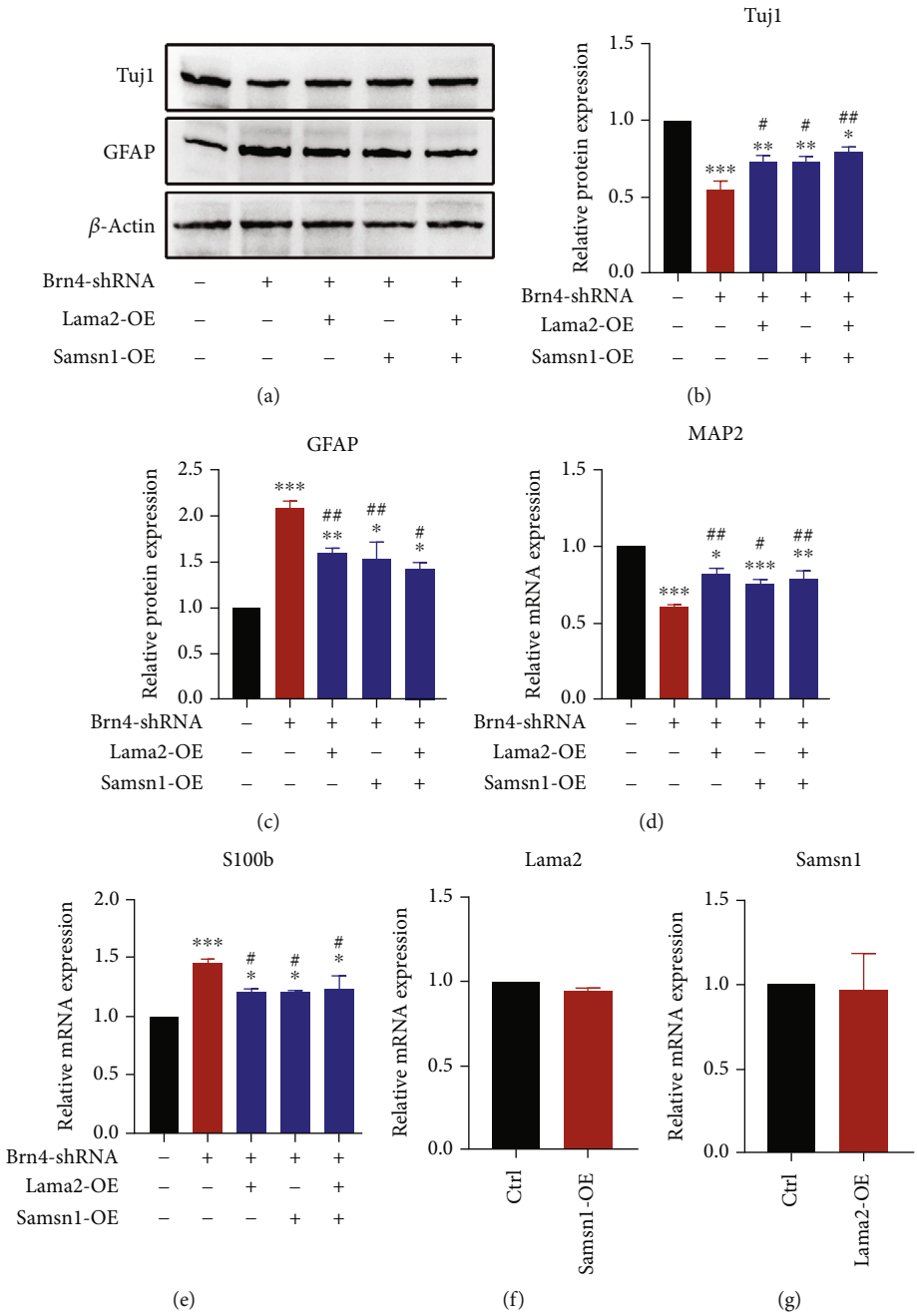

Figure 8: Lama2 and Samsn1 partially reversed the decrease of NSCs differentiation into neurons caused by Brn4 knockdown. (a–c) Representative immunoblots of Tuj1, GFAP, and β-actin in the primary hippocampal NSCs after induced differentiation for 7 days (a) and quantification of Tuj1 and GFAP protein levels normalized to β-actin (b, c). (d, e) Quantification of MAP2 and S100b mRNA levels normalized to β-actin after the NSCs induced differentiation for 7 days. (f, g) Quantification of Lama2 and Samsn1 mRNA levels normalized to β-actin. Error bars represent the mean ± SEM. $n = 3$. $^{*}P < 0.05$, $^{**}P < 0.01$, and $^{***}P < 0.001$ *vs.* Ctrl; $^{\#}P < 0.05$ and $^{\#\#}P < 0.01$ *vs.* Brn4-shRNA.

overexpression or knockdown of Lama2 and Samsn1. The results suggested that Lama2 and Samsn1 not only inhibited hippocampal NSCs proliferation but also enhanced their differentiation into neurons. Based on the similar effects on NSCs, we proposed a hypothesis that Lama2 and Samsn1 mediated the function of Brn4 on the proliferation and differentiation of hippocampal NSCs. Thus, we forced their expression in Brn4 knockdown hippocampal NSCs, and the results showed that Lama2 and Samsn1 reversed the changes occurring after Brn4 knockdown. Interestingly, simultaneous force-expression of Lama2 and Samsn1 did not have a better effect, and Samsn1 overexpression could not change Lama2 transcription and vice versa, which indicated that they mediated the role of Brn4 in different ways.

Lama2 is the protein-coding gene of the extracellular matrix laminin $\alpha 2$ chain [32]. It not only participates in

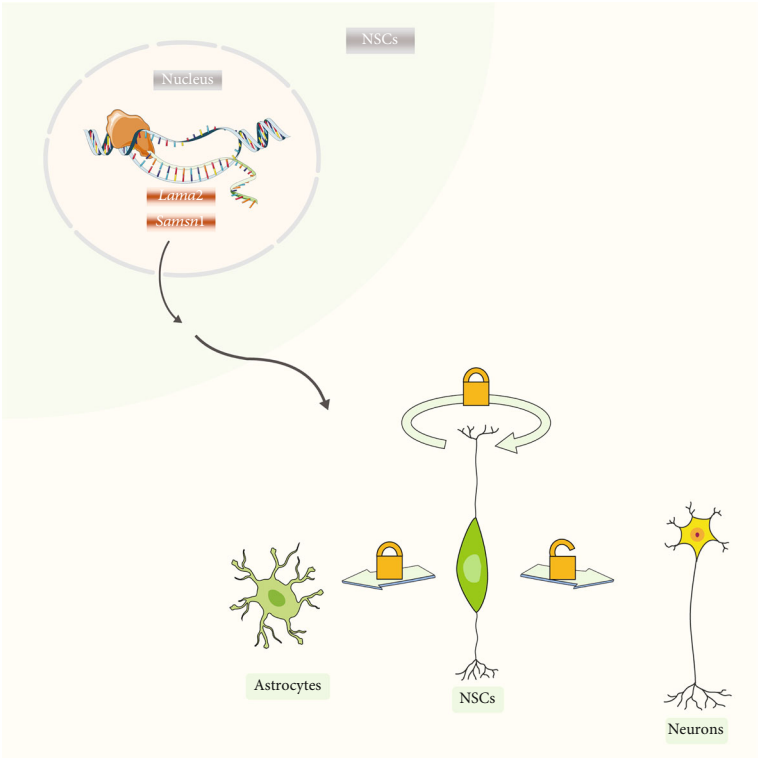

Figure 9: Schematic diagram describing the mechanism of Lama2 and Samsn1-mediated Brn4 effect on differentiation of hippocampal NSCs.

the formation of the glial vascular basement membrane of the blood-brain barrier but also exists in the neurons of the brain, regulating the synaptic function and plasticity of the central nervous system [33]. However, the role of Lama2 in the proliferation and differentiation of hippocampal NSCs has not been reported. Our results show that Lama2 have a negative effect on the proliferation of hippocampal NSCs, keeping consistency with its roles in the malignant progression of lung adenocarcinoma [34], pituitary adenoma [35], hepatocellular carcinoma [36], and colorectal cancer [37]. In addition, De La Fuente et al. [38] believe that Lama2 derived from pericytes can promote the differentiation of oligodendrocyte progenitor cells, which may explain why patients with Lama2-associated muscular dystrophy are often accompanied by myelin dysplasia. It is also proved that Lama2 plays a positive effect on the osteogenic differentiation of mesenchymal stem cells [39] and dental follicle cells [40] and the differentiation of human embryonic stem cells into islet B cells [41]. These studies more or less support our results that Lama2 promoted hippocampal NSC differentiation into neurons.

Samsn1, alias HACS1, NASH1, and SLy2, is mainly expressed in normal hematopoietic tissues and malignant tumors of the hematopoietic system, such as multiple myeloma, lymphoma, etc., and also in gallbladder, heart, lung, brain, and other tissues [42]. The expression of Samsn1 is raised after antigens stimulate B lymphocytes and then regulates the formation of cytoskeleton and membrane folds through Rac1, which in turn mitigates the diffusion and polarization of B cells to maintain the appropriate adaptive immunity [43]. Even supposing that the increased expression of Samsn1 in microglia induced by amyloid β may be involved in the pathogenesis of AD [44], the role of it on hippocampal NSCs remains unclear. Unlike the earlier findings from Yan et al. [45] that Samsn1 high expression is related to the poor prognosis in glioblastoma, our results find that it inhibits the hippocampal NSC proliferation, which is in good agreement with its role, as a tumor suppressor, in gastric cancer, lung cancer, and liver cancer [46–48]. Samsn1 is an adaptor protein, and its protein structure can be divided into three parts: the N-terminal is the nuclear localization signal, the C-terminal is the SAM domain, and the middle link is the SH3 domain which contributes to different proteins combined by Samsn1 acting together in the cytoplasm or nucleus [49]. Thus, this inconsistency may be due to some key molecules in glioblastoma interacting with each other to promote the malignant progression. Besides, our research indicates that Samsn1 promotes hippocampal NSC differentiation into neurons, which compares well with the previous study that Samsn1 knockdown in induced pluripotent stem cells causes the impaired differentiation ability into kidney-like cells [50].

Our previous reports [15–18] and the result in this study indicated that Brn4 regulates the proliferation and neuronal differentiation of hippocampal NSCs. Promoting the transcription of the downstream genes Lama2 and Samsn1 may partially mediate the Brn4 effects on NSCs (as shown in Figure 9). However, the proliferation and differentiation functions of NSCs are detected mainly *in vitro*, and it is still unknown whether the results can be applied *in vivo*. The

valuation of the differentiation function of NSCs is according to the number of newborn neurons and the expression level of related markers, which cannot explain whether the newborn neurons can generate and conduct excitement, form a synaptic connection with the surrounding cells after transplantation, and truly replace the damaged neurons. What is more, the downstream signaling molecules and pathways involved are still unclear, although we confirmed that Lama2 and Samsn1 mediated the regulation of Brn4 on NSCs. The above problems need to be solved urgently, and our further research direction.

5. Conclusion

In conclusion, our study indicated that Brn4 bound to the promoters of Lama2 and Samsn1 which may partially mediate the regulation of Brn4 on the proliferation and differentiation of mouse hippocampal NSCs. Our data provided novel insights for regulating neurogenesis of hippocampal NSCs, which is helpful to solve hippocampal disorders through self-repairing and cell replacement therapy.

Data Availability

The figures and tables data used to support the findings of this study have been deposited in the GIN (G-Node Data Infrastructure Services) repository (https://gin.g-node.org/zhangxinhua/DSC/src/master/For%20Stem%20Cells%20International).

Conflicts of Interest

The authors declare that they have no competing interests.

Authors' Contributions

LZ, XZ, RJ, YJ, YW, XD, ZS, XL, WL, JG, and JW conducted the experiments, collected the data, and drafted the manuscript. XC, JB, and MT assisted with experiment preparation. GJ and LZ revised the final manuscript. LZ and XZ conceived and designed the idea for this paper. All authors read and approved the final manuscript. Lei Zhang and Xunrui Zhang contributed equally to this work.

Acknowledgments

The present study was supported by the National Natural Science Foundation of China (grant no. 31171038), the Jiangsu Natural Science Foundation (grant no. BK2011385), the Jiangsu "333" Program Funding (grant no. BRA2016450), the Application Research Project of Nantong City (grant no. MS12017015-3), and the Training Program of Innovation and Entrepreneurship for Graduates (no. 265, 202210304043Z).

References

[1] F. H. Gage, "Neurogenesis in the adult brain," *The Journal of Neuroscience*, vol. 22, no. 3, pp. 612-613, 2002.

[2] H. van Praag, A. F. Schinder, B. R. Christie, N. Toni, T. D. Palmer, and F. H. Gage, "Functional neurogenesis in the adult hippocampus," *Nature*, vol. 415, no. 6875, pp. 1030–1034, 2002.

[3] J. M. Long and D. M. Holtzman, "Alzheimer disease: an update on pathobiology and treatment strategies," *Cell*, vol. 179, no. 2, pp. 312–339, 2019.

[4] B. De Strooper and E. Karran, "The cellular phase of Alzheimer's disease," *Cell*, vol. 164, no. 4, pp. 603–615, 2016.

[5] T. C. Fung, C. A. Olson, and E. Y. Hsiao, "Interactions between the microbiota, immune and nervous systems in health and disease," *Nature Neuroscience*, vol. 20, no. 2, pp. 145–155, 2017.

[6] E. F. Fang, Y. Hou, K. Palikaras et al., "Mitophagy inhibits amyloid-β and tau pathology and reverses cognitive deficits in models of Alzheimer's disease," *Nature Neuroscience*, vol. 22, no. 3, pp. 401–412, 2019.

[7] J. Sevigny, P. Chiao, T. Bussière et al., "The antibody aducanumab reduces Aβ plaques in Alzheimer's disease," *Nature*, vol. 537, no. 7618, pp. 50–56, 2016.

[8] K. Jin, A. L. Peel, X. O. Mao et al., "Increased hippocampal neurogenesis in Alzheimer's disease," *Proceedings of the National Academy of Sciences of the United States of America*, vol. 101, no. 1, pp. 343–347, 2004.

[9] K. Jin, V. Galvan, L. Xie et al., "Enhanced neurogenesis in Alzheimer's disease transgenic (PDGF-APPSw,Ind) mice," *Proceedings of the National Academy of Sciences of the United States of America*, vol. 101, no. 36, pp. 13363–13367, 2004.

[10] A. Maruszak, A. Pilarski, T. Murphy, N. Branch, and S. Thuret, "Hippocampal neurogenesis in Alzheimer's disease: is there a role for dietary modulation?," *Journal of Alzheimer's Disease*, vol. 38, no. 1, pp. 11–38, 2014.

[11] P. Brundin, O. G. Nilsson, R. E. Strecker, O. Lindvall, B. Astedt, and A. Björklund, "Behavioural effects of human fetal dopamine neurons grafted in a rat model of Parkinson's disease," *Experimental Brain Research*, vol. 65, no. 1, pp. 235–240, 1986.

[12] R. Zietlow, E. L. Lane, S. B. Dunnett, and A. E. Rosser, "Human stem cells for CNS repair," *Cell and Tissue Research*, vol. 331, no. 1, pp. 301–322, 2008.

[13] J. A. Steinbeck and L. Studer, "Moving stem cells to the clinic: potential and limitations for brain repair," *Neuron*, vol. 86, no. 1, pp. 187–206, 2015.

[14] V. Malik, D. Zimmer, and R. Jauch, "Diversity among POU transcription factors in chromatin recognition and cell fate reprogramming," *Cellular and Molecular Life Sciences*, vol. 75, no. 9, pp. 1587–1612, 2018.

[15] X. Zhang, G. Jin, L. Wang et al., "Brn-4 is upregulated in the deafferented hippocampus and promotes neuronal differentiation of neural progenitors in vitro," *Hippocampus*, vol. 19, no. 2, pp. 176–186, 2009.

[16] J. Shi, G. Jin, H. Zhu et al., "The role of Brn-4 in the regulation of neural stem cell differentiation into neurons," *Neuroscience Research*, vol. 67, no. 1, pp. 8–17, 2010.

[17] X. Zhang, L. Zhang, X. Cheng et al., "IGF-1 promotes Brn-4 expression and neuronal differentiation of neural stem cells via the PI3K/Akt pathway," *PLoS One*, vol. 9, no. 12, article e113801, 2014.

[18] X. F. Tan, J.-. B. Qin, G.-. H. Jin et al., "Effects of Brn-4 on the neuronal differentiation of neural stem cells derived from rat midbrain," *Cell Biology International*, vol. 34, no. 9, pp. 877–882, 2010.

[19] Q. Zou, Q. Yan, J. Zhong et al., "Direct conversion of human fibroblasts into neuronal restricted progenitors*," *The Journal of Biological Chemistry*, vol. 289, no. 8, pp. 5250–5260, 2014.

[20] M. B. Potts, J. J. Siu, J. D. Price et al., "Analysis of Mll1 deficiency identifies neurogenic transcriptional modules and Brn4 as a factor for direct astrocyte-to-neuron reprogramming," *Neurosurgery*, vol. 75, no. 4, pp. 472–482, 2014.

[21] T. Vierbuchen, A. Ostermeier, Z. P. Pang, Y. Kokubu, T. C. Südhof, and M. Wernig, "Direct conversion of fibroblasts to functional neurons by defined factors," *Nature*, vol. 463, no. 7284, pp. 1035–1041, 2010.

[22] Q. Yu, J. Chen, W. Deng et al., "Direct reprogramming of mouse fibroblasts into neural cells via Porphyra yezoensis polysaccharide based high efficient gene co-delivery," *Journal of Nanobiotechnology*, vol. 15, no. 1, p. 82, 2017.

[23] J. Guo, X. Cheng, L. Zhang et al., "Exploration of the Brn4-regulated genes enhancing adult hippocampal neurogenesis by RNA sequencing," *Journal of Neuroscience Research*, vol. 95, no. 10, pp. 2071–2079, 2017.

[24] H. He, W. Li, M. Peng et al., "MicroRNA expression profiles of neural stem cells following valproate inducement," *Journal of Cellular Biochemistry*, vol. 119, no. 7, pp. 6204–6215, 2018.

[25] W. Li, S. Wang, H. He et al., "Expression and function of Ndel1 during the differentiation of neural stem cells induced by hippocampal exosomesticle," *Stem Cell Research & Therapy*, vol. 12, no. 1, p. 51, 2021.

[26] Y. Wu, X. Zhang, J. Wang et al., "P4HA2 promotes cell proliferation and migration in glioblastoma," *Oncology Letters*, vol. 22, no. 2, p. 601, 2021.

[27] K. J. Livak and T. D. Schmittgen, "Analysis of relative gene expression data using real-time quantitative PCR and the $2^{-\Delta\Delta C}{}_{\mathrm{T}}$ method," *Methods*, vol. 25, no. 4, pp. 402–408, 2001.

[28] D. Phippard, A. Heydemann, M. Lechner et al., "Changes in the subcellular localization of the Brn4 gene product precede mesenchymal remodeling of the otic capsule," *Hearing Research*, vol. 120, no. 1-2, pp. 77–85, 1998.

[29] P. M. Brooks, K. P. Rose, M. L. MacRae et al., "Pou3f4-expressing otic mesenchyme cells promote spiral ganglion neuron survival in the postnatal mouse cochlea," *The Journal of Comparative Neurology*, vol. 528, no. 12, pp. 1967–1985, 2020.

[30] N. C. Bramswig and K. H. Kaestner, "Transcriptional regulation of α-cell differentiation," *Diabetes, Obesity & Metabolism*, vol. 13, Suppl 1, pp. 13–20, 2011.

[31] L. Song, X. Tian, and R. Schekman, "Extracellular vesicles from neurons promote neural induction of stem cells through cyclin D1," *The Journal of Cell Biology*, vol. 220, no. 9, 2021.

[32] P. Barraza-Flores, C. R. Bates, A. Oliveira-Santos, and D. J. Burkin, "Laminin and integrin in LAMA2-related congenital muscular dystrophy: from disease to therapeutics," *Frontiers in Molecular Neuroscience*, vol. 13, p. 1, 2020.

[33] M. Tian, T. Hagg, N. Denisova, B. Knusel, E. Engvall, and M. Jucker, "Laminin- α 2 chain-like antigens in CNS dendritic spines," *Brain Research*, vol. 764, no. 1-2, pp. 28–38, 1997.

[34] J. Liang, H. Li, J. Han et al., "Mex3a interacts with LAMA2 to promote lung adenocarcinoma metastasis via PI3K/AKT pathway," *Cell Death & Disease*, vol. 11, no. 8, p. 614, 2020.

[35] R. Q. Wang, Y. L. Lan, J. C. Lou et al., "Expression and methylation status of LAMA2 are associated with the invasiveness of nonfunctioning PitNET," *Therapeutic Advances in Endocrinology and Metabolism*, vol. 10, article 2042018818821296, 2019.

[36] S. Jhunjhunwala, Z. Jiang, E. W. Stawiski et al., "Diverse modes of genomic alteration in hepatocellular carcinoma," *Genome Biology*, vol. 15, no. 8, p. 436, 2014.

[37] S. Lee, T. Oh, H. Chung et al., "Identification of GABRA1 and LAMA2 as new DNA methylation markers in colorectal cancer," *International Journal of Oncology*, vol. 40, no. 3, pp. 889–898, 2012.

[38] A. G. De La Fuente, S. Lange, M. E. Silva et al., "Pericytes stimulate oligodendrocyte progenitor cell differentiation during CNS remyelination," *Cell Reports*, vol. 20, no. 8, pp. 1755–1764, 2017.

[39] Y. Zhu, X. Zhang, R. Gu et al., "LAMA2 regulates the fate commitment of mesenchymal stem cells via hedgehog signaling," *Stem Cell Research & Therapy*, vol. 11, no. 1, p. 135, 2020.

[40] S. Viale-Bouroncle, M. Gosau, and C. Morsczeck, "Laminin regulates the osteogenic differentiation of dental follicle cells via integrin-α2/-β1 and the activation of the FAK/ERK signaling pathway," *Cell and Tissue Research*, vol. 357, no. 1, pp. 345–354, 2014.

[41] H. A. Russ, L. Landsman, C. L. Moss et al., "Dynamic proteomic analysis of pancreatic mesenchyme reveals novel factors that enhance human embryonic stem cell to pancreatic cell differentiation," *Stem Cells International*, vol. 2016, Article ID 6183562, 9 pages, 2016.

[42] J. O. Claudio, Y. X. Zhu, S. J. Benn et al., "HACS1 encodes a novel SH3-SAM adaptor protein differentially expressed in normal and malignant hematopoietic cells," *Oncogene*, vol. 20, no. 38, pp. 5373–5377, 2001.

[43] M. von Holleben, A. Gohla, K. P. Janssen, B. M. Iritani, and S. Beer-Hammer, "Immunoinhibitory adapter protein Src homology domain 3 lymphocyte protein 2 (SLy2) regulates actin dynamics and B cell spreading*," *The Journal of Biological Chemistry*, vol. 286, no. 15, pp. 13489–13501, 2011.

[44] A. Sierksma, A. Lu, R. Mancuso et al., "Novel Alzheimer risk genes determine the microglia response to amyloid-β but not to TAU pathology," *EMBO Molecular Medicine*, vol. 12, no. 3, article e10606, 2020.

[45] Y. Yan, L. Zhang, T. Xu et al., "SAMSN1 is highly expressed and associated with a poor survival in glioblastoma multiforme," *PLoS One*, vol. 8, no. 11, article e81905, 2013.

[46] M. Kanda, D. Shimizu, S. Sueoka et al., "Prognostic relevance of SAMSN1 expression in gastric cancer," *Oncology Letters*, vol. 12, no. 6, pp. 4708–4716, 2016.

[47] H. Yamada, K. Yanagisawa, S. Tokumaru et al., "Detailed characterization of a homozygously deleted region corresponding to a candidate tumor suppressor locus at 21q11-21 in human lung cancer," *Genes, Chromosomes & Cancer*, vol. 47, no. 9, pp. 810–818, 2008.

[48] S. Sueoka, M. Kanda, H. Sugimoto et al., "Suppression of *SAMSN1* expression is associated with the malignant phenotype of hepatocellular carcinoma," *Annals of Surgical Oncology*, vol. 22, Supplement 3, pp. S1453–S1460, 2015.

[49] T. Uchida, A. Nakao, N. Nakano et al., "Identification of Nash1, a novel protein containing a nuclear localization signal, a sterile α motif, and an SH3 domain preferentially expressed in mast cells," *Biochemical and Biophysical Research Communications*, vol. 288, no. 1, pp. 137–141, 2001.

[50] J. Huang, S. Zhou, X. Niu et al., "Generation of special autosomal dominant polycystic kidney disease iPSCs with the capability of functional kidney-like cell differentiation," *Stem Cell Research & Therapy*, vol. 8, no. 1, p. 196, 2017.